

Dissertation
submitted to the
Combined Faculty of Natural Sciences and Mathematics
of the Ruperto Carola University Heidelberg, Germany
for the degree of
Doctor of Natural Science

Presented by
M.Sc. Christoph Hangel
born in: Mannheim
Oral examination: 24.10.19

Leptin-mediated downregulation of glutathione peroxidase 4 and iron overload contributing to podocyte ferroptosis in diabetic nephropathy

Referees: Prof. Dr. Markus Hecker
Prof. Dr. Marc Freichel

Table of contents

Abbreviations	8
1.1 Summary	9
1.2. Zusammenfassung	10
2. Introduction	12
2.1 Diabetes mellitus	12
2.1.1 Type 1 diabetes (T1D).....	13
2.1.2 Type 2 diabetes (T2D).....	13
2.2 Obesity	13
2.3 Leptin signaling	14
2.4 Hyperglycemia	15
2.5 Physiology and pathophysiology of the kidney	16
2.5.1 The function of the kidney.....	16
2.5.2 Diabetic nephropathy.....	18
2.6 TGF-β1 signaling	19
2.6.1 TGF- β 1 processing	19
2.6.2 Paracrine TGF- β 1 signalling.....	20
2.7 Redox signaling	21
2.7.1 Reactive oxygen species	21
2.7.2 Glutathione peroxidases (GPx).....	22
2.8 Iron	23
2.8.1 Iron homeostasis.....	23
2.8.2 Ferroptosis in podocytes.....	25
2.9 Feedback loop	26
2.10 Mouse Models of T2D and obesity	27
3.1 Working hypothesis	27
3.2 Aims	30
4. Materials	31
4.1. Cell culture	31
4.1.1. Cell lines and primary cells.....	31
4.1.2 Cytokines, enzymes and inhibitors.....	31
4.1.3 Media	32
4.1.4 Media supplements.....	32
4.2 Protein analysis	32
4.2.1 Inhibitors	33

4.3 Isolation of primary cells.....	33
4.4 ELISA.....	33
4.5 Antibodies.....	34
4.5.1 Western Blot	34
4.5.2 Simple WES.....	34
4.5.3 Histology.....	35
1.6 Buffers.....	35
4.7 Solutions	36
4.8 Chemicals.....	37
4.9 Anesthesia	37
4.10 Additional kits.....	37
4.11 Equipment.....	38
5. Methods	39
5.1 Animals	39
5.2 Isolation of primary podocytes.....	39
5.3 Immunofluorescence	40
5.4 Cell culture.....	41
5.4.1 E11 podocytes.....	41
5.4.2 Primary podocytes	41
5.4.3 CI-muMECS.....	42
5.4.4 Primary glomerular endothelial cells.....	42
5.4.5 Co-culture of CI-muMECs and E11 podocytes	43
5.5 ELISA of CI-muMEC supernatant.....	44
5.6 Bradford Assay.....	44
5.7 SDS–polyacrylamide gel electrophoresis (SDS-PAGE).....	45
5.8 Western Blot.....	45
5.9 BCA Assay (Pierce)	46
5.10 Simple WES analysis of E11 podocytes	47
5.11 Messenger RNA isolation	48
5.12 Copy DNA synthesis	48
5.13 Quantitative real time polymerase chain reaction (q-PCR)	49
5.14 Agarose gel electrophoresis.....	50
5.15 Periodic acid-Schiff (PAS) staining.....	50
5.16 Immunohistochemistry	51
5.17 GPx-4 activity assay.....	52
5.18 Iron staining	52

5.19 Image analysis	52
5.20 Statistics.....	52
6. Results	53
6.1 Validation of the expression of cell-specific markers using immunofluorescence microscopy	53
6.2 Detection of leptin receptor splice variants by realtime PCR	54
6.3 Cell culture.....	56
6.3.1 Endothelial cells	56
6.3.1.1 TGF- β 1 mRNA expression in leptin-stimulated CI-muMECs	56
6.3.1.2 Active TGF- β 1 in the medium of leptin-stimulated CI-muMECS	57
6.3.1.3 Active TGF- β 1 in the medium of leptin-stimulated primary glomerular endothelial cells	57
6.3.2 Podocytes.....	58
6.3.2.1 GPx-1 protein abundance in leptin-stimulated or TGF- β 1-stimulated E11 podocytes	58
6.3.2.2 GPx-4 protein abundance in leptin-stimulated or TGF- β 1-stimulated E11 podocytes	59
6.3.2.2 GPx-4 protein abundance in E11 podocytes exposed to TGF- β 1 and/or iron overload	62
6.3.2.3 GPx-4 protein abundance in E11 podocytes stimulated with TGF- β 1 and iron in high-glucose medium	64
6.3.2.4 GPx-4 activity in E11 podocytes exposed to TGF- β 1 and/or iron in high-glucose medium	65
6.3.3 Co-culture of endothelial cells and podocytes	66
6.3.3.1 GPx-4 expression in E11 podocytes co-cultured with CI-muMECs	66
6.3.3.2 GPx-4 expression in E11 podocytes co-cultured with gECs.....	68
6.3.3.3 GPx-4 expression in primary podocytes co-cultured with gECs.....	69
6.4 Leptin receptor-deficient mice lacking the long leptin receptor splicing variant (Ob-Rb)	71
6.5 <i>Ex vivo</i> data	72
6.5.1 Extracellular matrix expansion in the glomeruli of 32-42 weeks old <i>fpn</i> ^{+/-} and db/db mice.....	72
6.5.2 Iron accumulation in the glomeruli of 32-42 weeks old <i>fpn</i> ^{+/-} mice.....	73
6.5.3 GPx-4 protein reduction in the glomeruli of 32-42 weeks old db/db mice.....	75
6.5.4 GPx-4 protein abundance is not altered in the glomeruli of 23 weeks old ob/ob mice.....	79
7. Discussion.....	82
7.1 The source of reactive oxygen species in T2D	82
7.2. Detection of leptin receptor splice variants.....	83

7.3. Cell culture	84
7.3.1 TGF- β 1 mRNA expression and active TGF- β 1 in the supernatant of leptin-stimulated endothelial cells.....	84
7.3.2. GPx-1 and GPx-4 protein abundance in leptin-stimulated or TGF- β 1-stimulated E11 podocytes.....	85
7.3.3. GPx-4 protein abundance in E11 podocytes exposed to TGF- β 1 and/or iron overload.....	86
7.3.4. GPx-4 protein abundance in E11 podocytes exposed to TGF- β 1 and/or iron overload in high-glucose medium.....	86
7.3.5. GPx-4 expression in podocytes co-cultured with endothelial cells.....	87
7.4. Leptin receptor-deficient mice lacking the long leptin receptor splicing variant (Ob-Rb)	88
7.5. Ex vivo experiments	89
7.5.1. Extracellular matrix expansion in the glomeruli of 32-42 weeks old <i>fpn</i> ^{+/-} and db/db mice.....	89
7.5.2. Iron accumulation in the glomeruli of 32-42 weeks old <i>fpn</i> ^{+/-} mice	89
7.5.3. GPx-4 protein reduction in the glomeruli of 32-42 weeks old db/db mice.....	90
7.6. Outlook	92
7.6.1. <i>In vivo</i> activation of the feedback loop.....	92
7.6.2 Quantification of TGF- β 1 in mouse models of T2D	93
7.6.3 Obesity and overfeeding might drive the pathophysiological changes in the kidney	93
8.1. References	95

Abbreviations

4-HNE	<u>4-hydroxynonenal</u>
AGE	<u>Advanced Glycation End products</u>
CI-muMECs	<u>Conditionally Immortalized murine Microvascular Endothelial Cells</u>
CL	<u>Cardiolipin</u>
DMT1	<u>Divalent Metal Transporter 1</u>
ESRD	<u>End-Stage Renal Disease</u>
FeNTA	<u>Nitrilotriacetic acid Fe (III)</u>
gECs	<u>glomerular Endothelial Cells</u>
GBM	<u>Glomerular Basal Membrane</u>
GFR	<u>Glomerular Filtration Rate</u>
GPx	<u>Glutathione Peroxidase</u>
GSH	reduced glutathione (<u>Glutathione Sulfhydroxyl group</u>)
HbA1c	<u>Hemoglobin A1c</u>
JAK	<u>Janus Kinase</u>
LAP	<u>Latency Associated Peptide</u>
LTBP	<u>Latent TGF-β1 Binding Protein</u>
MDA	<u>Malondialdehyde</u>
NADPH	<u>Nicotinamide Adenine Dinucleotide Phosphate</u>
NOX	<u>NADPH Oxidases</u>
PC	<u>Polyvinylchloramine</u>
PE	<u>Polyvinylethanolamine</u>
RSL-3	<u>Ras Small molecule Like inhibitor 3</u>
ROS	<u>Reactive Oxygen Species</u>
SOD	<u>Superoxide Dismutase</u>
SMAD	<u>Small Mothers Against Decapentaplegic</u>
STAT	transcription factor <u>Signal Transducer and Activator of Transcription</u>
STEAP	<u>Six Transmembrane Epithelial Antigen of the Prostate</u>
T1D	<u>Type 1 Diabetes</u>
T2D	<u>Type 2 Diabetes</u>
TBARS	<u>Thiobarbituric Acid Reactive Substances</u>
TGF- β	<u>Transforming Growth Factor β</u>
ZIP14	<u>Zinc transporter Protein 14</u>

1.1 Summary

For almost two decades the dogma of the unifying hypothesis published by Brownlee defines the major research topics in the field of diabetes research. Unfortunately, normalization of blood glucose levels using insulin treatment can postpone or reduce but cannot prevent diabetic late complications. Factors related to obesity may play an important role and are pivotal for the severity and progression of type 2 diabetes. Therefore, this thesis focuses at three characteristics observed during the progression of diabetic nephropathy, i.e. leptin signaling, iron overload and reduction of GPx-4 protein abundance leading to ferroptosis of podocytes. We assume that even though obesity leads to impaired leptin signaling in neurons of the central nervous system, high leptin signaling takes place in peripheral organs like the kidney, contributing to obesity-related disorders.

The aim of this study was to show that hyperglycemia itself is not the main reason for developing diabetic nephropathy, but rather an epiphenomenon pivotal to induce a self-reinforcing feedback loop driving the inactivation of GPx-4. The resulting detrimental accumulation of lipid hydroperoxides could trigger the novel programmed cell death pathway ferroptosis in podocytes, which might explain the loss of these cells during the progression of the disease.

In the present study we demonstrate that microvascular endothelial cells respond to leptin with an increased release/activation of transforming growth factor (TGF) $\beta 1$ causing downregulation of GPx-4 protein in the nearby podocytes. Moreover, a role of leptin signaling and systemic iron overload was analyzed *ex vivo* by quantifying the amount of GPx-4 protein and iron in the glomeruli of db/db mice, db/db/Fpn^{+/-} mice and leptin-deficient ob/ob mice. GPx-4 protein abundance was slightly reduced in the glomeruli of 32-42 weeks old db/db mice. This decline of GPx-4 protein abundance was augmented in db/db/Fpn^{+/-} mice of the same age. In contrast, the amount of iron was significantly increased in the glomeruli of these mice. Impaired iron homeostasis could influence the activity of GPx-4 in podocytes as we showed that iron accumulates in the glomeruli of Fpn^{+/-} mice. The co-action of both the downregulation of GPx-4 in podocytes induced by leptin signaling in glomerular endothelial cells in combination with the postulated accumulation of iron in the podocytes could thus trigger a negative and self-sustained feedback loop.

Obesity is a major risk factor for the development of type 2 diabetes but so far, its relationship with diabetic kidney disease remained unclear. This thesis may have helped to gain insight into one important aspect of the pathogenesis of obesity-related diabetic nephropathy and to facilitate the development of future therapies.

1.2. Zusammenfassung

Die Diabetesforschung wird seit mehr als zwei Jahrzehnten von der Brownlee-Hypothese der hyperglykämiebedingten Gefäßschädigung dominiert. Leider können durch die Normalisierung der Blutzuckerwerte diabetische Spätschäden nur aufgeschoben, aber nicht verhindert werden. Diese Tatsache führt zur Annahme, dass andere Faktoren, die in Verbindung mit Übergewicht stehen, eine übergeordnete Rolle bei der Entstehung von T2D spielen. Die vorliegende Studie legt daher einen Schwerpunkt auf drei charakteristische Eigenschaften, die mit dem Fortschreiten einer diabetischen Nephropathie einhergehen: Leptin-Signaltransduktion, eine systemische Eisenüberladung, Reduzierung der GPx-4 Proteinmenge in den Podozyten, sowie die daraus resultierende als Ferroptose bekannte Form des Zelltods. Krankhaft übergewichtige Menschen weisen meist eine Leptinresistenz und Störung im Leptin-Signalweg in Neuronen des zentralen Nervensystems auf. Dennoch wird in peripheren Organen wie der Niere eine gesteigerte Leptin-Signalwirkung angenommen, die die Entstehung von Folgeerkrankungen begünstigen.

Das Ziel dieser Studie war es zu zeigen, dass Hyperglykämie eher eine Begleiterscheinung und nicht den Hauptgrund für die Entwicklung einer diabetischen Nephropathie darstellt. Trotzdem ist die Hyperglykämie essenziell für die Einleitung der positiven Rückkopplung, die zu einer Inaktivierung der GPx-4 führt. Eine zellschädigende Akkumulation von Lipidperoxiden löst möglicherweise die programmierte Zelltodform Ferroptose in Podozyten aus und könnte den Verlust dieser Zellen während des Verlaufs einer diabetischen Nephropathie erklären.

In der vorliegenden Studie konnte gezeigt werden, dass mikrovaskuläre Endothelzellen nach Leptin-Stimulation TGF- β 1 freisetzen, was in kokultivierten Podozyten zu einer Reduktion der GPx-4 Proteinmenge führte. Zusätzlich wurde die GPx-4 Proteinmenge und die Eisenmenge in den Glomeruli von db/db Mäusen, Fpn^{+/-} Mäusen, db/db/Fpn^{+/-} Mäusen und Leptin-defizienten ob/ob Mäusen quantifiziert. Im Vergleich zu den Wildtypkontrolltieren war die Reduktion der GPx-4 Proteinmenge in den Glomeruli von 32-42 Wochen alten db/db/Fpn^{+/-} Mäusen deutlich stärker ausgeprägt, als in den db/db Mäusen, bei denen die GPx-4 Proteinmenge nur leicht reduziert war. In den Glomeruli der Fpn^{+/-} Mäuse konnte andererseits eine deutlich höhere Menge an Eisen im Vergleich zu den Kontrolltieren festgestellt werden. Die durch die beeinträchtigte Eisenhomöostase verursachte Eisenüberladung in den Glomeruli der Fpn^{+/-} Mäuse könnte die Aktivität der GPx-4 in den Podozyten negativ beeinflussen. Das Zusammenspiel von einer Leptin-induzierten Reduzierung der GPx-4 Proteinmenge in den glomerulären Endothelzellen und der postulierten Eisenüberladung in den Podozyten könnte eine positive Rückkopplung

auslösen, die zu einer massiven Akkumulation von Lipidperoxiden führt, da diese hauptsächlich von der GPx-4 reduziert werden.

Obwohl Übergewicht als einer der Hauptfaktoren gilt, die zu einer Entwicklung von Typ 2 Diabetes beitragen, ist der kausale Zusammenhang vor allem bei der Entstehung der diabetischen Nephropathie bislang unzureichend geklärt. Mein Projekt liefert erste Daten über mechanistische Zusammenhänge von Adipositas und der Pathogenese einer Leptin-abhängigen diabetischen Nephropathie und trägt somit möglicherweise zu der Entwicklung von Therapiemöglichkeiten bei.

2. Introduction

2.1 Diabetes mellitus

Diabetes mellitus is a chronic metabolic disorder affecting 8.3 % of the population worldwide causing microvascular complications, such as neuropathy, retinopathy or nephropathy. In 2015 415 million people worldwide suffered from diabetes and its complications (Mbanya, Sandow et al. 2017). By 2040 this figure will rise to over 642 million. Among those, 5 million people are dying each year (Mbanya, Sandow et al. 2017). In Germany every tenth adult suffers from diabetic complications (Koster, Huppertz et al. 2011). According to the International Diabetes Federation numbers have doubled over the last 20 years. Moreover, diabetic late complications are the major risk factor for developing macrovascular disease such as heart attack and stroke, which are responsible for the high mortality rate among these patients (Wolf 2004, Mbanya, Sandow et al. 2017). Diabetes is characterized by high levels of blood glucose and the inability of the body to take it up into the cells (de Mello, Orellana et al. 2019). According to the WHO, diabetes is defined as fasting blood glucose levels above 126 mg/dL (7 mM/L) (Alberti and Zimmet 1998). Glucose concentrations in the blood can be easily quantified, either by measuring glucose itself or by analyzing glycosylated hemoglobin (HbA1c). Blood glucose concentrations give only information about the current glucose level, whereas HbA1c represents the average glucose level over the last 12 weeks. After glucose changes its conformation via Amadori rearrangement, it can be non-enzymatically attached to hemoglobin. Moreover, HbA1c in the blood is degraded after 3 months. Thus, the proportion of HbA1c can be used as a reliable readout of the mean glucose level over the last 12 months. Under physiological conditions about 5 % of the total amount of glucose is glycosylated. In people suffering from diabetes more than 6.5 % of the total amount of glucose is glycosylated (HbA1c > 6.5 %) (Alberti and Zimmet 1998). Blood glucose concentrations rise after food intake. In response to high glucose levels β -cells in the pancreas produce the hormone insulin, which is responsible for immediate glucose uptake into the skeletal muscles via activation of insulin-dependent glucose-transporter 4. Glucose can either be consumed or stored as glycogen. Low levels of insulin or insulin resistance are responsible for high blood glucose concentrations (Dupont and Scaramuzzi 2016). Thus, it can be discriminated between people suffering from a low insulin production (type 1 diabetes) and people suffering from insulin resistance (type 2 diabetes) (Alberti and Zimmet 1998).

2.1.1 Type 1 diabetes (T1D)

Ten percent of people suffering from diabetes can be grouped into T1D (Alberti and Zimmet 1998). More than 40 genes could be identified as risk genes to develop T1D. The outbreak of the disease occurs usually early at adolescence (Saberzadeh-Ardestani, Karamzadeh et al. 2018). Patients with the autoimmune disease T1D lose pancreatic β -cells during the progression of the disease (Coward, Welsh et al. 2005). Initially, the remaining β -cells can compensate for this loss by increasing the insulin production per cell. As soon as the critical mass of β -cells reaches a certain threshold, the remaining β -cells can not compensate for the loss anymore, which causes the outbreak of the disease (Saberzadeh-Ardestani, Karamzadeh et al. 2018). As a consequence, glucose uptake into skeletal muscles is no longer sufficient. Thus, the glucose supply can meet the needs, but can no longer sufficiently reach the cells. The surplus glucose contributes to high blood glucose levels.

2.1.2 Type 2 diabetes (T2D)

With 90 % the majority of people suffering from diabetes can be grouped into T2D (Alberti and Zimmet 1998). T2D is not characterized by a loss of β -cells, but rather by insulin resistance (Coward, Welsh et al. 2005). In this case, the β -cells need to produce more insulin to reach the same level of action. This occurs when the β -cells are not capable to further increase insulin production (Dupont and Scaramuzzi 2016). As a consequence, glucose uptake into skeletal muscles is no longer sufficient. The remaining glucose increases the blood glucose levels. Moreover, low levels of insulin increase gluconeogenesis in the liver. Thus, blood glucose levels are further increased. A genetic predisposition as well as environmental factors, e.g. lifestyle, are responsible for the development and progression of the disease (Risérus, Willett et al. 2009). Lifestyle interventions such as reduction of visceral body fat as well as increased physical activity can reduce the severity of T2D (Sjostrom, Lindroos et al. 2004, Maggard, Shugarman et al. 2005, Dintsios, Chernyak et al. 2018).

2.2 Obesity

There is a strong correlation between T2D and obesity. Moreover, it is thought that obesity initiates the transition from a physiological to a pathophysiological state. Obese people have a high risk to develop cardiovascular diseases and T2D, and frequently suffer from metabolic syndrome (Wolf 2004), which is characterized by high blood pressure, hyperglycemia, high

serum triglycerides, low serum levels of high-density lipoprotein, insulin and leptin resistance (Riserus, Willett et al. 2009). In addition, obesity provokes a pro-inflammatory environment in people with T2D (Wolf, Chen et al. 2002). Apart from the genetic background excessive food intake, lack of physical activity, sleep deprivation, drinking and smoking are risk factors for developing an obese phenotype (Riserus, Willett et al. 2009). A subsequent 10 % reduction of visceral fat by lifestyle interactions or surgeries *inter alia* gastric bypass can reverse some of the detrimental effects of the metabolic syndrome and thus some of the detrimental effects of T2D (Sjostrom, Lindroos et al. 2004, Maggard, Shugarman et al. 2005, Disse, Pasquer et al. 2014).

2.3 Leptin signaling

Leptin is a 16 kDa protein expressed in white adipose tissue (Wolf, Chen et al. 2002). Therefore, the level of the hormone leptin correlates with the amount of white adipose tissue (Han, Isono et al. 2001, Goto, Kaneko et al. 2016). Moreover, T2D is associated with obesity (Honda, Ikejima et al. 2002, Dam, Jockers et al. 2015). This suggests that there might be a causal link between obesity and T2D. Six splice variants of the leptin receptor (Ob-Rb, Ob-Ra, Ob-Rc, Ob-Rd, Ob-Re and Ob-Re, *cf.* Figure 1) are known so far (Wolf, Chen et al. 2002, Goto, Kaneko et al. 2016). The extracellular leptin binding domains (C-terminus) of the different leptin receptor splice variants are identical, whereas the intracellular leptin binding domains (N-terminus) differ in their length (Friedman and Halaas 1998, Adya, Tan et al. 2015). In healthy individuals, leptin reaches the hypothalamus (Han, Isono et al. 2001) in the brain via the blood-brain-barrier causing an inhibition of neuropeptide Y and agouti-related peptide and stimulation of pro-opiomelanocortin in two subpopulations of neurons (Fei, Okano et al. 1997, Friedman and Halaas 1998). Leptin induces a feedback loop via binding to the long leptin receptor splice variant Ob-Rb causing reduction of food intake and increase of energy expenditure (Fei, Okano et al. 1997, Friedman and Halaas 1998, Han, Isono et al. 2001). Ob-Rb contains a Janus kinase (JAK)/signal transducer and activator of transcription 3 (STAT3) binding motif in the intracellular domain (Wolf, Chen et al. 2002, Li, Ceccarini et al. 2013). Thus, leptin binding to Ob-Rb induces activation of JAK (Figure 2). Furthermore, activated JAK phosphorylates tyrosine residues of Ob-Rb, leading to phosphorylation of STAT3 (Dam, Jockers et al. 2015). In turn, phosphorylated STAT3 homodimers translocate to the nucleus and activate gene transcription (Fei, Okano et al. 1997, Li, Ceccarini et al. 2013) (Figure 2). This signaling cascade and the resulting feedback loop seems to be impaired in obese patients (Han, Isono et al. 2001, Dam, Jockers et al. 2015, Goto, Kaneko et al. 2016).

In peripheral organs, e.g. the kidneys, the short splicing variants of the leptin receptor Ob-Ra and Ob-Rc are highly abundant (Hoggard, Mercer et al. 1997, Han, Isono et al. 2001, De Matteis, Dashtipour et al. 2007, Li, Ceccarini et al. 2013, Goto, Kaneko et al. 2016). Even though it was long time believed that only the long leptin splice variant Ob-Rb is able to signal via the JAK/STAT signaling pathway, it is more and more accepted that the short splicing variants also play a major role in leptin signaling (De Matteis, Dashtipour et al. 2007, Li, Ceccarini et al. 2013, Goto, Kaneko et al. 2016). The development of leptin resistance remains unclear (Friedman and Halaas 1998, Honda, Ikejima et al. 2002, Dam, Jockers et al. 2015). It is likely that transport via the blood brain barrier is somehow impaired (Friedman and Halaas 1998). In this case, only signaling in the brain, e.g. the described feedback loop, is impaired (Dam, Jockers et al. 2015). Leptin signaling may still be intact in peripheral tissues such as the kidneys and should be increased in a pathophysiological state (De Matteis, Dashtipour et al. 2007, Goto, Kaneko et al. 2016).

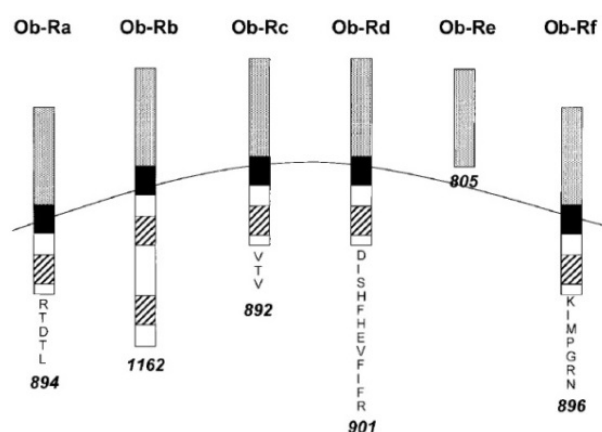


Figure 1: Isoforms of the leptin receptor derived from differential splicing. From Wolf, G. American Journal of Kidney Diseases (2002), 39:1-11

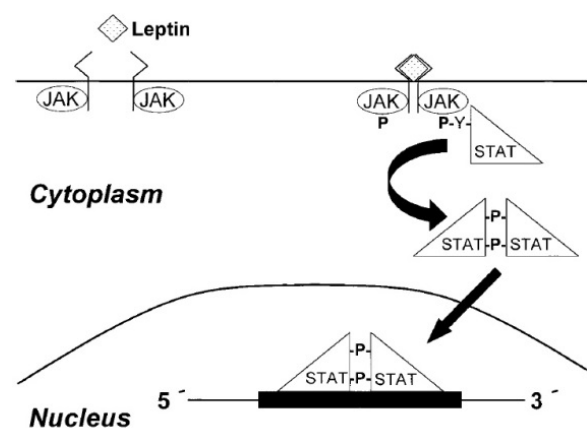


Figure 2: Overview of leptin signaling through the Ob-Rb isoform. From Wolf, G. American Journal of Kidney Diseases (2002), 39:1-11. STAT (transcription factor Signal Transducer and Activator of Transcription), JAK (Janus kinase)

2.4 Hyperglycemia

In both T1D and T2D, insulin substitution is the treatment of choice. Even if glucose levels in patients suffering from diabetes are tightly controlled, they develop diabetic late complications (Martín-Gallán, Carrascosa et al. 2003, Falkevall, Mehlem et al. 2017, Cooper, El-Osta et al. 2018). These complications are postponed but cannot be prevented (UK Prospective Diabetes Study Group 1998, Martín-Gallán, Carrascosa et al. 2003, Falkevall, Mehlem et al. 2017). According to the unifying hypothesis of Brownlee, increased ROS

formation during hyperglycemia inhibits the catalytic enzyme GAPDH, therefore preventing the metabolism of glyceraldehyde-3-phosphate into 1,3 diphosphoglycerate (Brownlee 2001). Thus, alternative metabolic pathways such as the polyol pathway (Giacco and Brownlee 2010), the hexosamine pathway (Brownlee 2005), the protein kinase C pathway (Thallas-Bonke, Thorpe et al. 2008) and the AGE pathway (Makita, Radoff et al. 1991, Nigro, Leone et al. 2017) should be activated. According to Brownlee late diabetic complications can be easily prevented by tight glucose control (Brownlee 2001, Cooper, El-Osta et al. 2018). Nevertheless, patients with diabetes develop late complications even if their glucose levels are tightly controlled (Martín-Gallán, Carrascosa et al. 2003, Falkevall, Mehlem et al. 2017, Cooper, El-Osta et al. 2018). Maybe diabetes is not a disease but rather a phenotype defined by the biomarker glucose.

2.5 Physiology and pathophysiology of the kidney

2.5.1 The function of the kidney

The kidney is the organ responsible for maintaining and regulating water and electrolyte homeostasis. In addition, the two bean-shaped kidneys take part in acid-base homeostasis as well as detoxification processes. The human kidney consists of 1 to 2.5 million glomeruli, in which the ultrafiltration of the blood occurs (Scott and Quaggin 2015). In healthy individuals, large proteins like albumin cannot pass the filtration barrier, which is size and charge selective (Haraldsson, Nystrom et al. 2008). The filtration barrier consists of a monolayer of fenestrated endothelial cells at the luminal side (Ballermann 2007, Hale and Coward 2013), a three-layer basal membrane and a monolayer of podocytes covering the other side of the capillaries in the Bowman's capsule (Figure 3) (Lewko, Bryl et al. 2005). Both cells types are in close proximity only separated by the glomerular basal membrane.

Glomerular endothelial cells (gECs) are microvascular endothelial cells characterized by fenestrations of 60 to 100 nm trans-cellular pores essential for high water permeability (Ballermann 2007, Hale and Coward 2013). They represent the first part of the filtration barrier, withdrawing large proteins such as albumin from the urine. The glomerular endothelial cell surface is covered by a thick glycocalyx, which is responsible for some of the characteristic properties of these cells. The glycocalyx is a negatively charged 200 nm thick layer consisting of proteoglycans and glycoproteins covalently bound to the endothelial cell membrane (Haraldsson and Nystrom 2012). The glomerular basal membrane is mainly built up by type IV collagen, laminin and negatively charged proteoglycans (Deen, Lazzara et al. 2001).

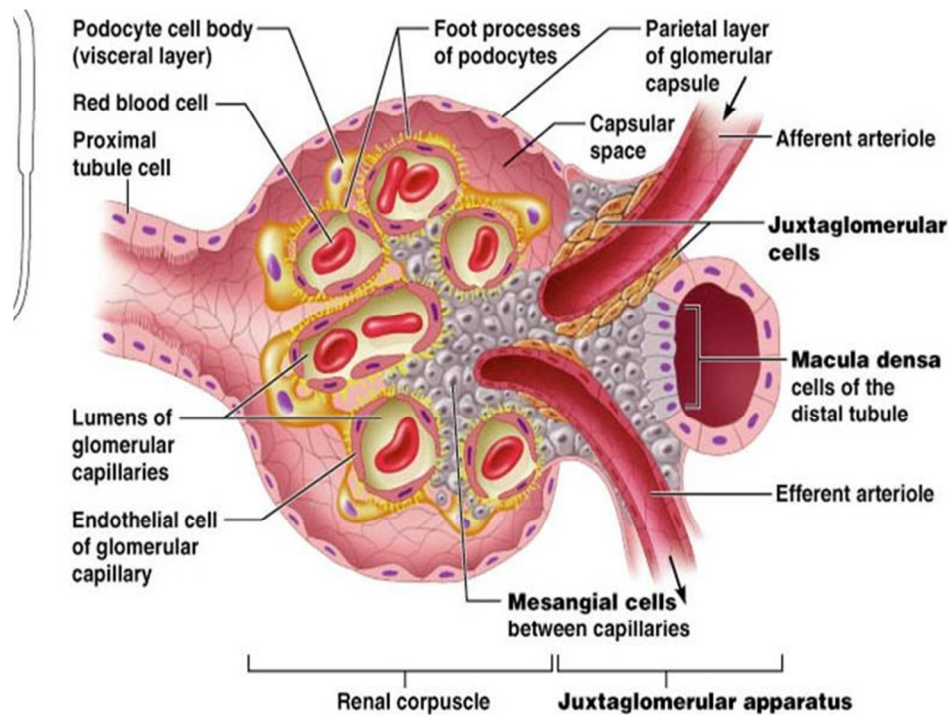


Figure 3: Schematic drawing of a glomerulus. Graph was provided by wbanimalhospital.com

Podocytes represent the last part of the filtration barrier (Figure 3). These epithelial cells are located at the other side of the glomerular basal membrane (GBM) facing towards the Bowman's capsule (Pavenstadt, Kriz et al. 2003, Krttil, Platenik et al. 2007, Ni, Saleem et al. 2012). They consist of a cell body and many foot processes, which connect them to the glomerular basal membrane (Deen, Lazzara et al. 2001, Pavenstadt, Kriz et al. 2003). The foot processes multiply the surface of the tight notched podocytes (Ni, Saleem et al. 2012). Small gaps between the podocyte foot processes are covered by the slit diaphragm (Krttil, Platenik et al. 2007). These slits are 3-5 nm wide and represent a sieve that the ultra-filtrate has to pass (Furukawa, Ohno et al. 1991). Podocytes are post-mitotic cells with a tightly controlled cell cycle (Vallon and Komers 2011, Ni, Saleem et al. 2012). As soon as the podocyte precursor cells differentiate to podocytes, the cell cycle arrests completely, because they express high amounts of the cell cycle inhibitors p27 and p57, which are responsible for the inhibition of cell cycle maintaining cyclin-dependent kinases (Barisoni, Mokrzycki et al. 2000, Pavenstadt, Kriz et al. 2003, Vallon and Komers 2011). At the same time, these cells express markers specific for differentiated podocytes such as podocin, nephrin and synaptopodin (Pavenstadt, Kriz et al. 2003). Once the podocyte monolayer is disrupted through a loss of podocytes, the number of podocytes constantly decreases. Instead of reentering the cell cycle for cell proliferation the remaining podocytes increase their size (hypertrophy) (Pavenstadt, Kriz et al. 2003, Vallon and Komers 2011). Thus, cell hypertrophy is the only mechanism by which podocytes can cope with increased functional

demands, whereas other glomerular cells can adapt by cell proliferation (Barisoni, Mokrzycki et al. 2000).

Besides endothelial cells and podocytes a glomerulus consists of parietal epithelial cells forming the Bowman's capsule as well as mesangial cells (Figure 3). Mesangial cells control the intraglomerular capillary blood flow and contribute to the composition of the extracellular matrix (Vallon and Komers 2011). Both, mesangial cells and extracellular matrix form the mesangium, a scaffold for the glomerular capillaries (Deen, Lazzara et al. 2001, Pavenstadt, Kriz et al. 2003).

2.5.2 Diabetic nephropathy

Diabetic nephropathy is the main reason for end-stage renal disease (ESRD) (Susztak, Raff et al. 2006), characterized by albuminuria (Sharma, McCue et al. 2003), reduced filtration, expansion of the mesangium (Wolf 2004), basal membrane thickening and podocyte loss (Vallon and Komers 2011, Reidy, Kang et al. 2014). Thirty percent of patients with T1D and 30 % of patients with T2D develop diabetic nephropathy (Ritz 2006). As soon as patients have been diagnosed suffering from kidney failure and to be in need of future dialysis the chance to survive is as low as with the most severe types of cancer. The reason why some of the people suffering from diabetes develop diabetic nephropathy and some do not is not well understood (Ritz 2006). At the beginning of diabetic nephropathy, the glomerular filtration rate (GFR) increases from about 100 mL/min to over 150 mL/min (Forbes and Cooper 2013), (Rossing 2015) (Figure 4). This hyperfiltration occurs only in the pre-diabetic phase lasting for about 5 years after the onset of diabetes. The GFR consolidates at 100

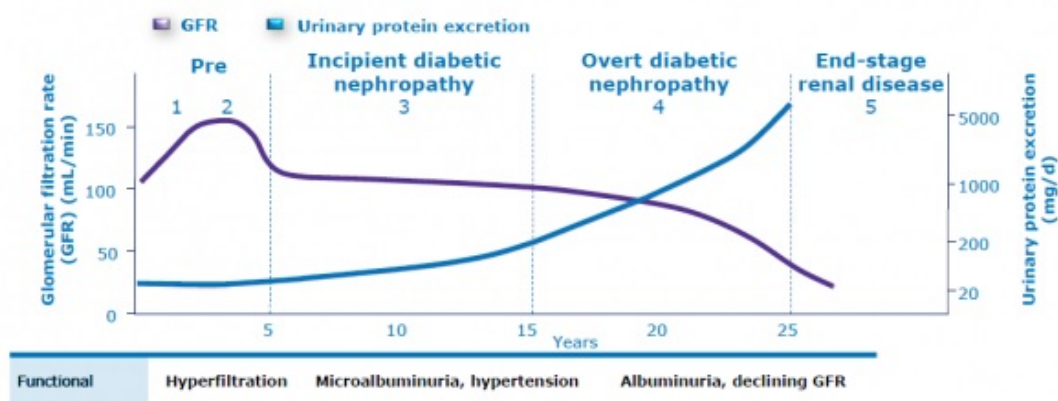


Figure 4: The phases of diabetic nephropathy. From Rossing, P. Clinical pathology of nephropathy [internet]. 2015 Sep 23; Diapedia. GFR (Glomerular Filtration Rate)

mL/min five to fifteen years after the onset of diabetes (Najafian, Alpers et al. 2011). This phase is termed incipient diabetic nephropathy. 15 years after the onset of diabetes the decline of kidney function drops dramatically from around 100 mL/min to less than 50 mL/min (Rossing 2015).

Frequently, kidney damage is diagnosed at the beginning of this phase termed overt diabetic nephropathy. Unfortunately, at this stage the damage is irreversible because the disease lasts already for 15 years (Breyer, Bottinger et al. 2005) (Figure 4). Drug treatment can postpone the next phase to some extent into the future but cannot prevent end-stage renal disease where GFR drops to near zero resulting in total organ failure (Rossing 2015).

Albumin is a large serum protein, which is withdrawn by an intact filtration barrier (Vallon and Komers 2011). Thus, in addition to GFR, the amount of albumin in the urine is an indicator for the integrity of the filtration barrier (Najafian, Alpers et al. 2011). Under physiological conditions (normoalbuminuria) urinary albumin secretion is less than 30 mg per day (Figure 4). Microalbuminuria is defined between 30 mg and 300 mg albumin secreted per day, which successively increases during the first 15 years of the disease (Rossing 2015). Moreover, the kidney is irreversibly damaged if the albumin secretion rate exceeds 300 mg per day, which is defined as macroalbuminuria (Rossing 2015). The reason to develop diabetic nephropathy is multifactorial. Therefore, the progression of the disease and the duration at each phase differs between individuals and cannot be traced back to a single event (Freedman, Bostrom et al. 2007). Kidney biopsies from patients with T2D show a significant reduction of the number of podocytes (Pagtalunan, Miller et al. 1997, Schiffer, Bitzer et al. 2001, Susztak, Raff et al. 2006, Vallon and Komers 2011). It is not known whether podocytes loss occurs early at the stage of microalbuminuria (Susztak, Raff et al. 2006) or late at the stage of macroalbuminuria or even end-stage renal disease.

2.6 TGF- β 1 signaling

2.6.1 TGF- β 1 processing

TGF- β 1 is the most important member of the TGF- β superfamily, as it has the highest affinity to TGF- β type I and II receptors, even though TGF- β 2 and TGF- β 3 can bind to the same receptor. It is synthesized as a precursor protein with a pro-peptide region (Travis and Sheppard 2014). After synthesis, TGF- β homodimers interact with the Latency Associated Peptide (LAP) and form the Small Latent Complex (Figure 5). In addition, the Small Latent

Complex interacts with the Latent TGF- β Binding Protein (LTBP) and forms the Large Latent Complex (Travis and Sheppard 2014). Moreover, the Large Latent Complex is

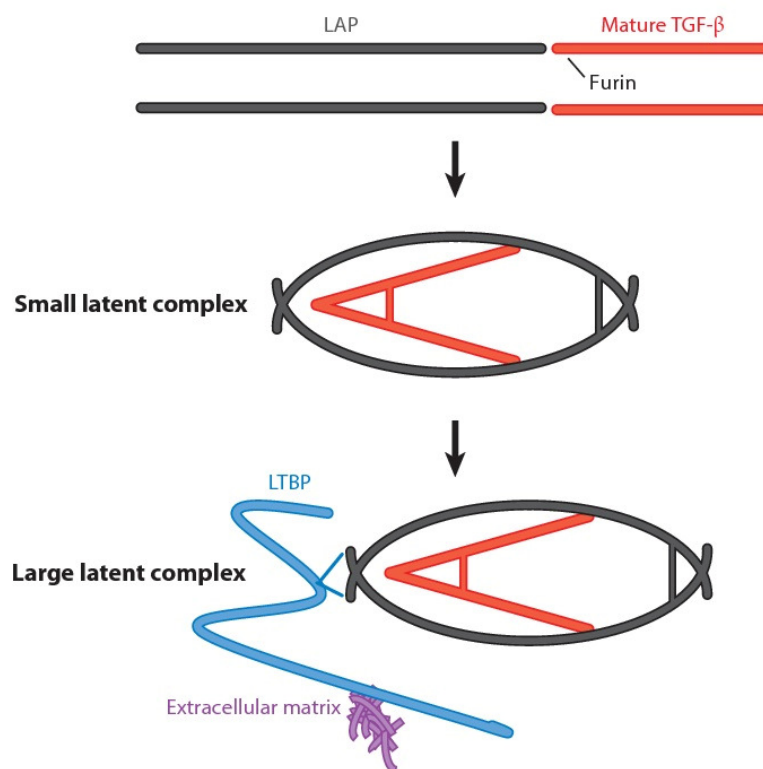


Figure 5: TGF- β activation and function in immunity. From Travis, M. A. Annual review of immunology (2014), 32:51-82. LAP (Latency Associated Peptide), LTBP (Latent TGF- β Binding Protein)

released to the extracellular matrix, where it is bound until it is further released. TGF- β remains inactive as long as it is bound to the complex (Travis and Sheppard 2014). Either the whole complex can be released from the extracellular matrix and remains inactive until it is further cleaved or the disulfide bonds connecting the active TGF- β to the complex can be cleaved directly at the extracellular matrix (Travis and Sheppard 2014). The latter leads to a release of active TGF- β directly from the extracellular matrix. Activation of TGF- β 1 requires the separation of its active form from the complex by proteases or metalloproteases, ROS, thrombospondin-1, alpha 4 containing integrins or even by changes in pH (Travis and Sheppard 2014).

2.6.2 Paracrine TGF- β 1 signalling

It was recently published that glomerular endothelial cells release growth factors after leptin binding (Wolf, Chen et al. 2002, Vallon and Komers 2011, Goto, Kaneko et al. 2016) (Figure

6). Growth factors such as TGF- β 1 affect mesangial cells through paracrine signaling (Wolf, Chen et al. 2002). This was postulated because TGF- β type II receptors are upregulated in mesangial cells after leptin treatment *in vitro*. Thus, endothelial cell-derived TGF- β 1 binds to mesangial TGF- β type II receptors and recruits TGF- β type I receptors followed by an activation of the SMAD (Small Mothers of Decapentaplegic) pathway (Wolf, Chen et al. 2002), (Kanwar, Sun et al. 2011). This paracrine signaling between endothelial and mesangial cells can be applied to endothelial cells and podocytes, as they are localized in close proximity to the endothelial cells in the glomeruli (Figure 6) (Wolf, Chen et al. 2002).

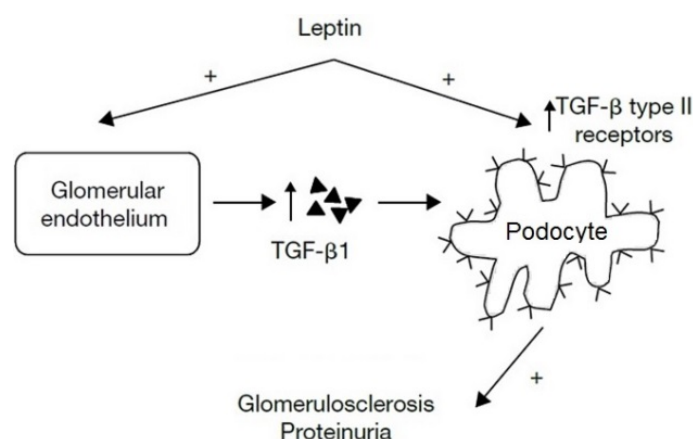


Figure 6: Paracrine TGF- β 1 pathways between glomerular endothelial and podocytes mediated by leptin. Schematic drawing modified from Wolf, G. American Journal of Kidney Diseases (2002), 39:1-11. TGF- β 1 (Transforming growth factor β 1)

2.7 Redox signaling

2.7.1 Reactive oxygen species

Oxidative stress can be described as an imbalance between the production of ROS and their detoxification (Cai and Yan 2013). It is still debated whether enhanced ROS formation (Tang, Luo et al. 2014) or impaired ROS detoxification is responsible for higher ROS levels in T2D (Tavafi 2013, Cooper, El-Osta et al. 2018). Highly reactive ROS such as hydrogen peroxide can reversibly or irreversibly modify cell membranes or proteins via oxidation processes (Moller, Rogowska-Wrzesinska et al. 2011, Ray, Huang et al. 2012). Reversible protein modifications are cysteine-modifications including intramolecular or intermolecular disulfide bond formations (Cai and Yan 2013). Thus, protein function as well as protein stability are changed by such modifications (Brieger, Schiavone et al. 2012). Among all oxidative protein modifications carbonylation is the most common (Cattaruzza and Hecker 2008, Moller, Rogowska-Wrzesinska et al. 2011). Hydrogen peroxide can react with free iron and form hydroxy radicals, which can selectively introduce carbonyl groups into proteins (Cai and Yan

2013). There are two possible ways by which such carbonyl derivatives can emerge. Amino acids can be oxidized directly through an oxidative attack of hydroxy radicals to lysine, arginine, proline or threonine residues at the amino acid side chains or indirectly through secondary reactions of the amino acids lysine, cysteine or histidine (Moller, Rogowska-Wrzesinska et al. 2011). In this case, reactions occur with carbohydrates or AGEs which have been oxidized beforehand (Kalapos 2008).

2.7.2 Glutathione peroxidases (GPx)

Glutathione peroxidases (GPx) are antioxidant defense enzymes expressed in all kinds of tissues that reduce peroxides (Takebe, Yarimizu et al. 2002). They are selenoenzymes, as they contain selenium in their active center (Lubos, Loscalzo et al. 2011, Conrad and Friedmann Angeli 2015). This is a unique feature occurring only in 24 other human proteins (Fang, Goldberg et al. 2010). GPxs are the main detoxifying redox enzymes in the mammalian body which use glutathione as a co-factor (Lubos, Loscalzo et al. 2011). Thus, reduced glutathione is oxidized by enzymes of the GPx family. Moreover, oxidized glutathione is reduced by glutathione reductase utilizing electrons from nicotinamide adenine dinucleotide phosphate (NADPH) back to its reduced state (Takebe, Yarimizu et al. 2002). The ratio of reduced to oxidized glutathione is important for several enzymes such as, e.g. carnosinase 1, which cleaves carnosine (Peters, Schmitt et al. 2017). Three out of eight known isoforms (Brigelius-Flohe and Maiorino 2013) of glutathione peroxidases, GPx-1, GPx-3 and GPx-4 are found in the kidney (Burk, Olson et al. 2011, Wiedenmann, Dietrich et al. 2018).

GPx-1 is expressed ubiquitously in all kinds of tissue and forms homotetramers (Lubos, Loscalzo et al. 2011). Its tertiary structure prevents big proteins from reaching the catalytic center. Therefore, its main function is to reduce small peroxides such as the highly reactive hydrogen peroxide or peroxynitrite in the cytoplasm (Wagner, Kautz et al. 2009, Lubos, Loscalzo et al. 2011, Cozza, Rossetto et al. 2017). In contrast, GPx-4 forms active monomers that are able to detoxify large molecules as there is no steric interference with other subunits. The main substrates of GPx-4 are lipid hydroperoxides (Doll and Conrad 2017, Shah, Shchepinov et al. 2018) such as phospholipid and cholesterol hydroperoxides, but it can also detoxify hydrogen peroxide (Conrad and Friedmann Angeli 2015). GPx-4 is found mainly at cell membranes, but also in the cytoplasm or in the nucleus (Gao, Monian et al. 2016, Cozza, Rossetto et al. 2017). GPx-3 is known as the extracellular GPx but substrate specificity or substrate affinity is still not well understood (Brigelius-Flohe and

Maiorino 2013). As unglycosylated recombinant human GPx-3 mutants expressed in *E. coli* is active as a monomer it might also detoxify large proteins (Song, Yu et al. 2014).

2.8 Iron

2.8.1 Iron homeostasis

Iron is a highly reactive metal in the 8th group of the periodic system (Fanzani and Poli 2017). Free iron is toxic to cells, because ferrous iron (Fe II) can react with hydrogen peroxide to form a hydroxyl radical and a hydroxide ion. In a second step ferric iron (Fe III) is then reduced back to ferrous iron by a second reaction with an additional molecule of hydrogen peroxide (Dixon and Stockwell 2014). During this reaction a hydroperoxyl radical and a proton are formed (Swaminathan, Fonseca et al. 2007). The two-step iron-catalyzed disproportionation of hydrogen peroxide is termed Fenton reaction (Arosio and Levi 2010, Dixon and Stockwell 2014, Doll and Conrad 2017). This occurs because ferrous iron has the ability to donate electrons, whereas ferric iron is an efficient electron acceptor. Thus, excess free iron causes oxidative stress (Enculescu, Metzendorf et al. 2017). For this reason, iron is usually incorporated or bound to molecules (Dixon and Stockwell 2014, Handa, Morgan-Stevenson et al. 2016). Stored iron in cells is bound to ferritin (Arosio and Levi 2010), whereas it is bound to transferrin if it is transported via the blood stream. The vast majority of iron in the human body is bound to hemoglobin (Swaminathan, Fonseca et al. 2007, Dixon and Stockwell 2014).

Systemic iron overload harms the organism (Kemna, Tjalsma et al. 2008, Neves, Leitz et al. 2017) as it changes, e.g. glucose metabolism in a negative way (Handa, Morgan-Stevenson et al. 2016). Studies have shown a relationship between systemic iron overload caused by hemochromatosis and the risk to develop T2D (Altamura, Kopf et al. 2017). It was also monitored that increased iron uptake from nutrients can increase the risk to develop insulin resistance (Swaminathan, Fonseca et al. 2007). In contrast, in vivo treatment with the iron chelator deferoxamine reduced HbA1c levels in diabetic rats (Roza, Slakey et al. 1994). The mechanism how iron induces insulin resistance or how iron contributes to diabetic complications remains to be elucidated. The progression of diabetic nephropathy could be postponed into the future by supplementation of an iron chelator or with a low iron-containing diet.

Iron homeostasis is tightly regulated by the hormone hepcidin, which is produced in the liver (Altamura, Kopf et al. 2017, Enculescu, Metzendorf et al. 2017). Its main function is to bind to the iron exporter ferroportin in the membranes of duodenal enterocytes in the gut or to

iron to its receptor (Liu, Sun et al. 2009, Muckenthaler, Rivella et al. 2017). Therefore, the ferric iron detaches from the iron-transferrin-transferrin-receptor complex (Creighton Mitchell and McClain 2014). Moreover, iron is actively transported via Divalent Metal Transporter 1 (DMT1) after it is reduced to ferrous iron by a Six Transmembrane Epithelial Antigen of the Prostate (STEAP) family member (Kemna, Tjalsma et al. 2008, Bogdan, Miyazawa et al. 2016). The transferrin-transferrin-receptor complex in the vesicle is transported back to the membrane (Bogdan, Miyazawa et al. 2016, Muckenthaler, Rivella et al. 2017). The whole complex is released into the blood stream after fusion of the vesicle with the membrane. The second possibility to take up iron is the direct uptake via Zinc Transporter Protein 14 (ZIP14) or DMT1 (Fanzani and Poli 2017) after it is reduced by a STEAP family member to ferrous iron (Creighton Mitchell and McClain 2014). In both cases, iron is immediately stored into ferritin or incorporated into a molecule (Bogdan, Miyazawa et al. 2016, Muckenthaler, Rivella et al. 2017).

People with T2D have a significant higher transferrin saturation as well as more stored iron in the epithelial cells of the liver (Muckenthaler, Rivella et al. 2017). Systemic iron overload is associated with low hepcidin levels and therefore constitutive active ferroportin in the duodenal enterocytes in the gut and in macrophages (Steinbicker and Muckenthaler 2013). Increased levels of phosphorylated AKT in the liver of db/db mice could inhibit the translation of hepcidin mRNA, thus reducing the amount of hepcidin released from the liver into the blood stream (Altamura, Kopf et al. 2017).

2.8.2 Ferroptosis in podocytes

Ferroptosis is a recently discovered iron-dependent regulated form of cell death (Doll and Conrad 2017, Shah, Shchepinov et al. 2018). It is morphologically and biochemically distinct from other regulated cell death pathways as pyroptosis, necroptosis or autophagy (Latunde-Dada 2017). Ferroptosis is a caspase-independent cell death (Cao and Dixon 2016) and executed by a loss of GPx-4 protein abundance or GPx-4 activity (Figure 8), and a subsequent accumulation of phosphatidylcholine (PC), phosphatidylethanolamine (PE) and cardiolipin (CL) lysoforms (Friedmann Angeli, Schneider et al. 2014, Conrad and Friedmann Angeli 2015, Doll and Conrad 2017). All three lysoforms belong to the group of lipid hydroperoxides and are mainly detoxified by GPx-4 (Friedmann Angeli, Schneider et al. 2014, Cozza, Rossetto et al. 2017). An accumulation of these species changes the fluidity and the permeability of all kind of cell membranes (Doll and Conrad 2017, Latunde-Dada 2017).

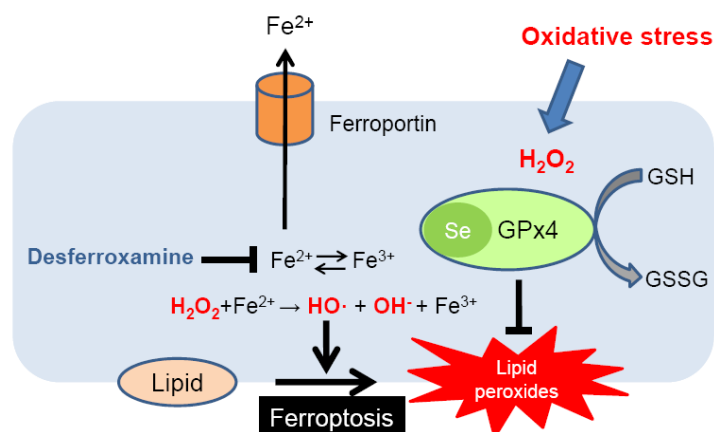


Figure 8: Ferroptosis: Death by Lipid Peroxidation. From Yang WS, Stockwell BR. Trends Cell Biology (2016), 26:165-76. GSH (reduced glutathione), GSSG (oxidized glutathione), GPx-4 (Glutathione peroxidase 4), Fe^{2+} (ferrous iron)

2.9 Feedback loop

GPx-4 protein abundance is significantly reduced in the glomeruli of human kidneys from patients with T2D (Wiedenmann, Dietrich et al. 2018). Moreover, lipid hydroperoxides are detoxified exclusively by GPx-4 (Friedmann Angeli, Schneider et al. 2014, Yang, SriRamaratnam et al. 2014). Thus, lipid hydroperoxides accumulate in the glomeruli of

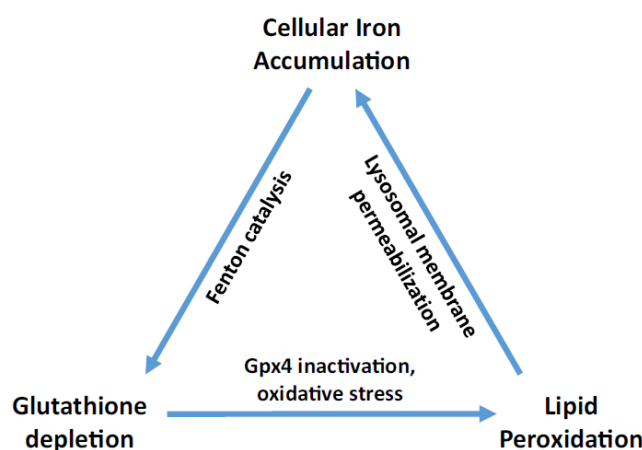


Figure 9: Iron accumulation, glutathione depletion, and lipid peroxidation must occur simultaneously during ferroptosis and are mutually amplifying Events. From Bertrand, R. L. Medical Hypotheses. (2017), February: 69-74.

human kidneys from patients with T2D (Figure 9). Lipid hydroperoxides are highly reactive and change the fluidity and the permeability of the cell membranes inter alia the membranes of vesicles (Dixon and Stockwell 2014, Bertrand 2017, Doll and Conrad 2017). This can be detrimental, because iron import is mainly regulated via transferrin mediated endocytosis. Lysosomal membrane permeabilization leads to an uncontrolled release of transferrin-transferrin-receptor bound iron complexes into the cytoplasm (Doll and Conrad 2017). The

pH shift changes the affinity of the transferrin-iron complex which releases the iron. Excess cellular iron reacts with non-detoxified hydrogen peroxide (Doll and Conrad 2017). Thus, Fenton reaction occurs more often causing glutathione depletion (Bertrand 2017, Latunde-Dada 2017). After reaching a certain threshold, the activity of the glutathione peroxidases gets reduced (Figure 9).

2.10 Mouse Models of T2D and obesity

Leptin (Ob-Rb) receptor-deficient db/db mice develop human type 2 diabetes mellitus (Brosius, Alpers et al. 2009). In db/db mice a point mutation leads to premature termination of translation of the long cellular domain of the Ob-Rb splice variant and loss of its signal transducing function (Lee, Proenca et al. 1996, Han, Isono et al. 2001, Jung, Nam et al. 2016). As already discussed in chapter 3.3 the Ob-Rb isoform is highly abundant in the hypothalamus and contains intracellular motifs required for activation of the JAK/STAT signal transduction pathway, which is responsible for the feedback loop required to reduce food intake. Obese db/db mice are more than two times as heavy as their wild-type counterparts which results in an increased concentration of leptin in the blood. In addition, Ob-Rb deficiency leads to the development of hypertension (UK Prospective Diabetes Study Group 1998). In contrast, the ob/ob mouse model lacks the hormone leptin. Leptin deficiency has the same consequence in the hypothalamus as a point mutation in the long leptin receptor splice variant Ob-Rb. Thus, the absence of activation of the JAK/STAT signal transduction pathway in the hypothalamus, which is responsible for the feedback loop required to reduce food intake, also causes the obese phenotype in these mice. In contrast to the db/db mice, leptin signaling in general is impaired. This includes also leptin signaling in peripheral organs such as the kidney.

3.1 Working hypothesis

For more than a few decades diabetes is defined as the disease with high blood glucose concentrations. The unifying hypothesis published by Brownlee turned the initial observation that normalization of blood glucose levels with insulin treatment can prevent diabetic late complications into a dogma. Unfortunately, insulin treatment can postpone or reduce, but cannot prevent the development of diabetic late complications (Falkevall, Mehlem et al. 2017, Cooper, El-Osta et al. 2018). Thus, we assume diabetes is not a disease, but rather a phenotype defined by the biomarker glucose. Instead, most of the patients suffering from

T2D are obese. We conclude, that factors related to obesity may play a bigger role and are pivotal for the severity and the progression of the disease. The hormone leptin which is expressed by white adipose tissue is one of the suspected candidates. Until today it is unknown, how leptin resistance develops (Friedman and Halaas 1998, Dam, Jockers et al. 2015). Moreover, the action of leptin in peripheral organs is not known as well (Han, Isono et al. 2001, Honda, Ikejima et al. 2002, De Matteis, Dashtipour et al. 2007, Li, Ceccarini et al. 2013, Goto, Kaneko et al. 2016). We assume, that even though leptin resistance occurs in the brain, it is not implemented in peripheral organs. Thus, in obese people high leptin levels provoke high leptin signaling in peripheral organs inter alia the kidney. We also postulate that leptin signaling occurs by binding of the ligand leptin to the short leptin receptor splicing variant Ob-Ra, rather than to the long leptin receptor splicing variant Ob-Rb at the glomerular endothelial cells in the kidney (De Matteis, Dashtipour et al. 2007, Goto, Kaneko et al. 2016). Further, glomerular endothelial cells could respond to leptin binding with the release/activation of TGF- β 1. As glomerular endothelial cells and podocytes are in close proximity, we assume a paracrine TGF- β 1 signaling between these two cell types. Binding of TGF- β 1 to TGF- β type I receptors might recruit TGF- β type II receptors causing an activation of the downstream cascade leading to the downregulation of GPx-4 protein in the podocytes.

In parallel an impaired iron homeostasis could influence the activity of GPx-4 in the podocytes (Doll and Conrad 2017). In patients suffering from T2D hepcidin levels are lower compared to healthy individuals, most likely caused by elevated phosphorylated AKT (Altamura, Kopf et al. 2017). Thus, the iron exporter ferroportin in the duodenal enterocytes of the gut and in the macrophages is constantly active. Therefore, circulating iron levels are high. Iron might accumulate in epithelial cells inter alia podocytes of the kidney.

The co-action of both the downregulation of GPx-4 in podocytes induced by leptin signaling in glomerular endothelial cells and the iron accumulation in podocytes caused by a systemic iron overload might trigger a feedback loop, as lipid hydroperoxides are detoxified exclusively by GPx-4 (Bertrand 2017). Therefore, we assume that lipid hydroperoxides accumulate in the glomeruli of kidneys from patients with T2D. Lipid hydroperoxides are highly reactive and change the fluidity and the permeability of the cell membranes inter alia the membranes of vesicles (Bertrand 2017). This could be detrimental, because iron import is mainly regulated via transferrin mediated endocytosis. Lysosomal membrane permeabilization could lead to an uncontrolled release of transferrin-transferrin-receptor bound iron complexes into the cytoplasm (Doll and Conrad 2017). The change in pH changes the affinity of the transferrin-iron complex which could release the iron. Excess cellular iron might react with non-detoxified hydrogen peroxide (Dixon and Stockwell 2014). Thus, Fenton reaction could occur

more often causing a glutathione depletion (Doll and Conrad 2017). After reaching a certain threshold, the activity of the glutathione peroxidases could be reduced (Bertrand 2017).

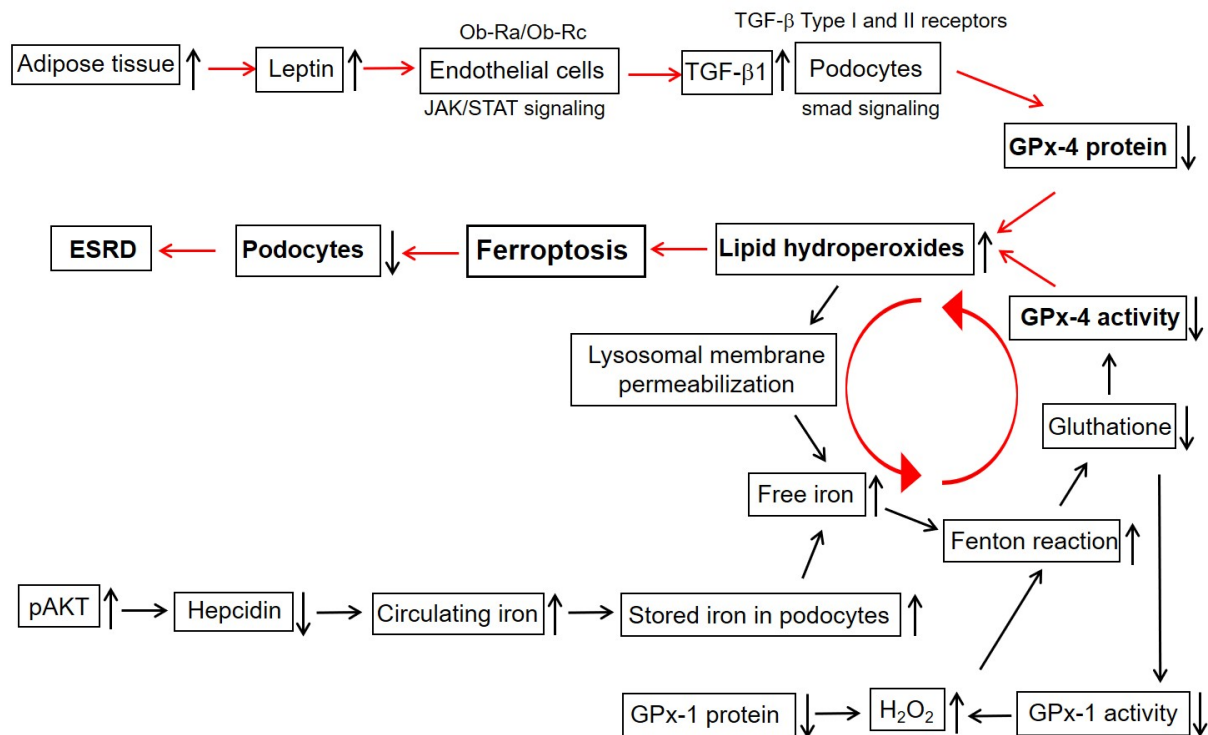


Figure 10: Working hypothesis. Paracrine TGF-β1 signaling between endothelial cells and podocytes leads to downregulation of GPx-4 in these cells. In addition, excess iron derived from a systemic iron overload spurs the feedback loop driving the podocytes into ferroptosis.

In addition, a third trigger could be needed to activate the feedback loop. As hyperglycemia is associated with diabetes, high glucose levels might be able to trigger or enhance the vicious cycle described above (Latunde-Dada 2017). A detrimental accumulation of lipid hydroperoxides could trigger the programmed cell death pathway ferroptosis in podocytes, which possibly explains the loss of these cells during the progression of the disease (Cao and Dixon 2016).

3.2 Aims

The aim of this study was to show that hyperglycemia itself is not the main reason for developing diabetic nephropathy but rather a concomitant phenomenon pivotal to induce a self-reinforcing feedback loop driving the inactivation of GPx-4. Thus, the following aspects were covered in this thesis:

- **Quantification of leptin receptor transcripts in endothelial cells:**

The transcripts of the leptin receptor Ob-Rb, Ob-Ra and Ob-Rc were analyzed in two different microvascular endothelial cell types. The quantification of the leptin receptor splice variants will indicate the contribution to a downstream signaling.

- **Analysis of endothelial cell and podocyte interaction:**

Endothelial cells and their respective supernatant medium were collected after leptin stimulation. The following activation/release of TGF- β 1 seemed to play a major role by reducing GPx-4 protein abundance in podocytes. As both cell types are in close proximity, a possible paracrine TGF- β 1 signaling was analyzed.

- **Quantification of GPx-4 protein abundance and iron accumulation in mouse models of T2D:**

The impact of leptin signaling and systemic iron overload was analyzed *ex vivo* by a quantification of the amount of GPx-4 protein and the amount of iron in the glomeruli of db/db, db/db/*fpr*^{+/-} mice and leptin-deficient ob/ob mice.

4. Materials

4.1. Cell culture

CryoStor® CS10 Freeze Media, PeliBiotech, PB-210102

Gelatin-based coating solution, Cell Biologics, 6950

Falcon 12-well plate, neoLab, 353503

Falcon 6-well plate, neoLab, 353502

Transparent PET Membrane 12 Well 0.4 µm pore size, neolab, 353180

Transparent PET Membrane 6 Well 0.4 µm pore size, neoLab, 353090

4.1.1. Cell lines and primary cells

C57BL/6 Mouse Primary Kidney Glomerular Endothelial Cells, PeliBiotech, PB-C57-6014G

Conditionally immortalized murine microvascular endothelial cells, InSCREENeX, INS- CI-1004

E11 podocytes, Cell line services, 400494

4.1.2 Cytokines, enzymes and inhibitors

0.25 % Trypsin-EDTA, Cell Biologics, 6914

(1S, 3R)-RSL3, Cayman Chemical, 19288

Apo-Transferrin human, Sigma-Aldrich, T1147-100MG

Erastin, Merck Millipore, 329600-5MG

LY2109761, Cayman Chemicals, 700874-71-1

Nitrilotriacetic acid disodium salt, Sigma-Aldrich, N0128-100MG

Recombinant murine leptin, PeproTech, AF-450-31

rm IFN-gamma recombinant mouse protein, Thermo Fischer, PMC4031

TGF-β 1,2,3 antibody, R&D Systems, MAB1835-500

Transferrin, Holo, Human Plasma, Merck Millipore, 616424

Trypsin-EDTA, Thermo Scientific, 25200056

4.1.3 Media

Co-culture medium DMEM (1x) + GlutaMAX, gibco, 21885-025

5 % fetal calf serum (FCS), 35 nM Na₂SeO₃, 1 % NEAAs, 0.5 % ECGS, 0.02 % Fungizone and 1 % Penicillin/Streptomycin

DMEM (1x) + GlutaMAX, gibco, 21885-025

10% fetal calf serum (FCS), 35 nM Na₂SeO₃, 1% NEAAs, 0.5% ECGS, 0.02% Fungizone and 1% Penicillin/Streptomycin

RPMI 1640 Medium (no glucose), Thermo Fischer, 11879-020

10 % fetal calf serum (FCS), 5 mM Glucose, 35 nM Na₂SeO₃, 0.02 % Fungizone and 1 % Penicillin/Streptomycin

Mouse Endothelial Cell Medium, PeloBiotech, PB-M1168

4.1.4 Media supplements

ECGS, Promo Cell, C-30120

FCS, Thermo Scientific, 10500-064, LOT 08G7661K

Fungizone, gibco, 15290-018

Glucose, Merck Millipore, 8337

NEAAs, gibco, 11140-035

Penicillin/Streptomycin, Thermo Fischer, 15140122

4.2 Protein analysis

Bradford-Reagent, Bio-Rad, 500-0006

Cartridge: 12-230 kDa, Biotechné, SM-W004-1

Filter paper, Neolab, 2-4325

Protein-Standard, Bio-Rad, 161-0374

PVDF membrane, Merck Millipore, ISEQ00010

SDS Sample buffer, Carl Roth, K929.1

Standard Pack 1, Bio-Techne, PS-ST01-8

Wes Cartridges, Bio-Techne, SM W004-1

4.2.1 Inhibitors

Dithiothreitol (DTT), Sigma-Aldrich, 10197777001

Halt Protease & Phosphatase cocktail, Thermo Scientific, 78442

Leupeptin hemisulfate salt, Sigma-Aldrich, L5793

Pefabloc, Sigma-Aldrich, 76307

Pepstatin A, Sigma-Aldrich, P5318

4.3 Isolation of primary cells

Collagenase A, Roche Diagnostics, 10103586001

Desoxiribonuclease I, Invitrogen, 18047019

Dynabeads® M-450 Tosylactivated, Thermo Fischer Scientific, 140.13

Ketamin 10 %, MEDISTAR Arzneimittelvertrieb GmbH, 03048734

Xylavet (Xylazin) 20 mg/mL, CP-Pharma, 1205

4.4 ELISA

Amicon Ultra-0.5 Centrifugal Filter-10 K, Merck Millipore, UFC501024

TGF- β 1 ELISA Kit (mouse), PromoKine, PK-EL-63506M

4.5 Antibodies

4.5.1 Western Blot

Primary antibodies

Mouse anti- β -actin antibody, abcam, ab6276, 1:5000 in blocking solution

Rabbit anti-GPx-1 antibody, GeneTex, 116040, 1:1000 in blocking solution

Rabbit anti-GPx-4 antibody, abcam, ab125066, 1:1000 in blocking solution

Secondary antibodies

Anti-mouse- IgG-HRP, Sigma Aldrich, A4416, 1:5.000 in blocking solution

Anti-rabbit- IgG-HRP, Sigma Aldrich, A6154, 1:3.000 in blocking solution

4.5.2 Simple WES

Primary antibodies

Goat anti-GPx-3 antibody, Biotechné, AF4199, 1:60

Mouse anti- β -actin antibody, abcam, ab6276, 1:1000

Rabbit anti-GPx-1 antibody, Biotechné, AF3798, 1:30

Rabbit anti-GPx-4 antibody, abcam, ab125066, 1:75

Secondary antibodies

Anti-rabbit detection Module, Biotechné, DM-001, 1:20

Anti-mouse detection Module, Biotechné, DM-002. 1:20

Anti-rabbit HRP conjugate (20x), Biotechné, 043-426, 1:20

Donkey anti-goat secondary HRP conjugate, Biotechné, 043-522-2, 1:50

4.5.3 Histology

Primary antibodies

Anti-CD 31, Santa Cruz, SC-18916, 1:50

Anti-GPx-4, abcam, ab125066, 1:100

Anti-synaptopodin antibody (P-19), Santa Cruz, sc-21537, 1:100

Secondary antibodies

Donkey anti-goat-Cy2, Dianova, 705-546-147, 1:100

Donkey anti-goat-Cy3, Dianova, 711-166-147, 1:100

Donkey anti-goat-Cy5, Dianova, 711-175-147, 1:100

Donkey anti-rabbit-AlexaFluor488, Dianova, 712-545-153, 1:100

Donkey anti-rabbit-Cy3, Dianova, 711-166-152, 1:100

Donkey anti-rat-Dylight549, Dianova, 712-505-153, 1:100

Additional dyes

4',6-Diamidin-2-Phenylindol (DAPI), Invitrogen, D1306

SYBR Green, Qiagen, 204145

1.6 Buffers

Buffer for the isolation of primary podocytes

Buffer 1: 62.1 mg $\text{NaH}_2\text{PO}_4 \times \text{H}_2\text{O}$, 638.8 mg Na_2HPO_4 , H_2O ad 50 mL, pH 7.4-8.0

Buffer 2: 37.2 mg EDTA, 50 mg BSA, PBS ad 50 mL, pH 7.4

Buffer 3: 1.21 g Tris, 50 mg BSA, H_2O ad 50 mL, pH 8.5

Homobuffer (25 mM Tris-HCL (pH 7.4), 0.55% KCL, 1 mM EDTA, 2.5 mM Glucose, 0.1 mM DTT, 80 µg/mL Pefabloc, 6 µg/mL Pepstatin A and 6 µg/mL Leupeptin)

RIPA buffer, Sigma Aldrich, R0278

Roti^R-Load 1 (4x), Roth, K929.1

Running buffer (24.8 mM Tris-HCL (pH 8.3), 192 mM Glycin, 3.5 mM SDS, H₂O ad 1 L)

TBE buffer (90 mM Tris, 90 mM boric acid, 2 mM EDTA)

TBS (50 mM Tris-HCL (pH 7.5), 150 mM NaCl, H₂O ad 1L)

TBS-T (50 mM Tris-HCL (pH 7.5), 150 mM NaCl, 0.05 % Tween, H₂O ad 1 L)

Transfer buffer (24.8 mM Tris-HCL (pH 8.3), 192 mM Glycin, H₂O ad 800 mL), 20 % methanol

and 0.05 % SDS

WES-RIPA-buffer (25 mM Tris-HCL, pH 7.6, 15 mM NaCl, 1 % NP-40, 1 % sodium deoxycholate, 0.1 % SDS)

PBS was purchased from Thermo Fisher Scientific (10010023).

4.7 Solutions

Acrylamide (Rotiph. / 37, 5:1), 3029.1

Eukitt, Kindler

FeNTA (40 mM Nitrilotriacetic acid disodium salt and 10 mM FeCl₃)

Luminata Classico, Merck Millipore, WBLUC0100

Luminata Forte, Merck Millipore, WBLUF0100

Mowiol, Calbiochem, 475904

Paraformaldehyde (PFA), Sigma Aldrich, P6148

Schiff's reagent, Merck Millipore, 1090340250

4.8 Chemicals

β-Mercaptoethanol, Sigma Aldrich, M6250

Ammoniumpersulfat (APS), Carl Roth, 9592.5

BSA, Carl Roth, 8076.2

EDTA, Applichem, A1103.0250

Natriumselenit, Sigma Aldrich, 214485

SDS, Serva Electrophoresis, 20767

Tetramethylethylendiamin (TEMED), Carl Roth, 2367.1

Tris, Carl Roth, 4855.2

TritonX100, Sigma Aldrich, T8787

Tween20, Carl Roth, 9127.1

4.9 Anesthesia

Xylazin/Ketamin Mix: 560 µl NaCl 0.9%, 150µl Ketamin and 90µl Xylazin

4.10 Additional kits

Omniscript RT Kit, Qiagen, 205111

dNTPs, Bioron, 110011

RNAse inhibitor, Promega, N251B

OligodT primer, Promega, C110A

PerOx (TOS/TOC) Kit, Immundiagnostik, KC5100

PierceTM BCA Protein Assay Kit, ThermoScientific, 23225

RNeasy Mini Kit, Qiagen, 74106

4.11 Equipment

ImageQuant LAS 4000 mini, GE Healthcare

Rotor-Gene Q thermocycler, Qiagen

Microscope, CellSens-Olympus (Ix-3)

Microscope, Xellence (rt) – Olympus (Ix-2)

NanoDrop ND1000, NanoDrop Technologies

Simple WES, Bio-Techne, W82844

Tissue lyser, Retsch, MM301

UP50H Ultrasonic Processor, Hielscher Ultrasonics

4.12 Programs

GraphPad Prism, version 7.02

ImageJ, version 1.4.3.67

QuPat, version 0.1.2

5. Methods

5.1 Animals

All animal experiments were performed with permission of the Regional Council Karlsruhe (G53/17) and in accordance with institutional and governmental guidelines. Kidneys were taken from wild-type (wt) mice or from db/db mice (B6.BKS(D)-Leprdb/J) after the mice had been sacrificed with CO₂, immediately frozen in liquid nitrogen and stored at -80 degrees Celsius until they were used for tissue slides or tissue homogenates. For podocyte isolation kidneys were taken from wt mice after intraperitoneal injection with a Ketamine/Xylazine mix and perfusion with PBS containing tosylactivated dynabeads.

Db/db mice (B6.BKS(D)-Leprdb/J), heterozygous littermates, homozygous *Slc40a1*^{C326S/C326S} mice as well as heterozygous *Slc40a1*^{wt/C326S} on a db/db mouse (B6.BKS(D)-Leprdb/J) background were kindly provided by Prof. Martina Muckenthaler and Dr. Sandro Altamura (University of Heidelberg, Department of Pediatric Hematology, Oncology and Immunology).

Ob/ob mice (BTBR.Cg-*Lep*^{ob}/WiscJ) as well as their homozygous littermates were kindly provided by Prof. Benito Yard (Medical Faculty Mannheim of the University of Heidelberg, Department of Nephrology, Endocrinology and Rheumatology).

5.2 Isolation of primary podocytes

The following method is based on the perfusion of mice with PBS containing tosyl-activated dynabeads, which get stuck in the kidney glomeruli and subsequently isolated after homogenization of the kidney by using a magnetic particle concentrator (Katsuya, Yaoita et al. 2006). Isolated glomeruli are seeded afterwards on gelatin-coated petri dishes in podocyte specific medium. Podocytes grow out of the glomeruli after they have settled and attached to the gelatin-coated petri dish. The podocytes were passaged before the podocyte islands started to touch each other.

Magnetic beads were prepared one day before the isolation. Therefore 200 µl beads per mouse were washed with 1 mL buffer for 1 min in the magnetic particle concentrator. The beads were resuspended in 200 µl buffer 1 and washed again. In the next step, beads were washed twice with 200 µl buffer 2 for 5 min on ice. Finally, beads were incubated in 200 µl buffer 3 for 24 hours at room temperature on a rotating platform.

On the next day beads were washed once in 200 µl buffer 2 for 5 min on ice, resuspended in 200 µl buffer 2 and kept on ice until they were utilized. Before they were added to the PBS the beads were resuspended thoroughly. Mice were anaesthetized by intraperitoneal

injection of xylazin/ketamin mix (200 µl for 30 g wt or 600 µl for 65 g db/db mice). The thorax was opened while the diaphragm was detached from the ribs. The costal arch was opened, and the liver was cut several times before perfusion. The mouse was perfused through the left ventricle with 20 mL PBS containing 8×10^7 tosylactivated dynabeads at a speed of 600 mL per hour. The dynabeads got caught in the kidney glomeruli. The kidneys were removed, transferred into an ice-cold PBS-containing tube and minced into 1 mm³ pieces by pressing them gently through a 100 µm cell strainer. In the next step the kidney homogenate was digested in 20 mL collagenase A in PBS (1 mg/mL Collagenase) at 37 degrees Celsius for 30 min with DNase (100 U/ µl). After the first digestion the kidney homogenate was pressed through a 40 µm cell strainer and centrifuged at 200 g for 5 min. The pellet was resuspended in 1.8 mL of PBS in an Eppendorf tube, placed later on in a magnetic particle concentrator for at least 2 min to gather the glomeruli containing dynabeads. After three washing steps the homogenate was digested in 2 mL collagenase A (1mg/mL) for 30 min at 37 degrees Celsius and centrifuged at 1000 rpm for 5 min at 5 degrees Celsius. The pellet was resuspended in 1 mL of RPMI medium and plated on gelatin-coated petri dishes (2% gelatin).

5.3 Immunofluorescence

To assure the purity of the respective cell populations and the degree of their differentiation, their specific marker expression was determined and visualized with an antibody coupled to a fluorescent dye. The integral membrane glycoprotein CD31, also known as platelet endothelial cell adhesion molecule-1 (PECAM-1), was chosen as an endothelial cell specific marker. Differentiated E11 podocytes and primary podocytes express synaptopodin at their foot processes which was selected as podocyte specific marker.

E11 podocytes or primary podocytes were cultivated in 12 well plates and washed two times with PBS before they were fixated for 30 min with 2 % paraformaldehyde. After an additional washing step, cell membranes were permeabilized for 5 min with 0.3 % TritonX100 in PBS and washed again with PBS. Primary glomerular endothelial cells (PeloBiotech) and CI-muMECS were cultivated in 96 well plates and washed twice with PBS before they were fixated with ice cold methanol for 10 min. After the fixation step they were washed again with PBS. The respective cells were incubated for 1 hour with 5 % bovine calf albumin (BCA) independent of the fixation method to block unspecific antibody binding sides. Podocytes were stained subsequently in a wet chamber for synaptopodin and endothelial cells for CD31 for 1 hour at room temperature. After an additional washing step (with PBS) cells were incubated for 1 hour with the secondary antibody coupled to a fluorescent dye. The cells were stained with DAPI for 8 min in order to visualize the nuclei. After the last washing step

(with PBS) cells were embedded in mowiol, covered with a cover slip and dried over night at 4 degrees Celsius. On the next day marker expression was determined using the fluorescence microscope (CellSens-Olympus). First and secondary antibodies were diluted in blocking solution as described above.

5.4 Cell culture

5.4.1 E11 podocytes

For cell culture experiments the murine kidney podocyte cell line E11 was proliferated at 33 degrees Celsius with 50 U/mL IFN- γ added into the medium (RPMI). The E11 podocytes contain a temperature sensitive variant of the SV40T-antigen with an IFN- γ inducible promoter. Under differentiation conditions, i.e. incubation of non-confluent cultures at 37°C without IFN- γ , cell proliferation ceases within the first two weeks. After 14 days of differentiation E11 cells were used for further experiments.

To determine the amount of GPx-1 and GPx-4 protein in E11 podocytes, these cells were incubated with different leptin concentrations (5 to 200 ng/mL) as well as different TGF- β 1 concentrations (1 to 50 ng/mL) and harvested after 5 days of treatment. In order to quantify GPx-4 protein abundance in a time dependent manner, E11 podocytes were stimulated for 5 days with 30 ng/mL recombinant TGF- β 1 and harvested every 24 hours. On day 3 the old medium was removed and replaced by new medium (with TGF- β 1). To test the influence of iron apotransferrin (30 μ M), holotransferrin (30 μ M) or FeNTA (10 mM iron) was added into the medium of E11 podocytes and into the medium of E11 podocytes stimulated with 30 ng/mL recombinant TGF- β 1 for 5 days. To inhibit GPx-4 activity E11 podocytes were stimulated with 10 μ M erastin or 25 μ M RSL-3 for 3 days.

5.4.2 Primary podocytes

Isolated glomeruli have settled for 48 hours on gelatine-coated petri dishes (3 cm). RPMI-medium was gently removed and replaced by new medium. 9 - 11 days post isolation primary podocytes (p0) were trypsinized. Primary podocytes adhere firmly to the gelatine-coated petri dish, therefore 2 mL trypsin EDTA was added after washing two times with -/- PBS. Trypsin EDTA was quickly removed before primary podocytes were incubated with new 2 mL trypsin EDTA for 30 min. The enzymatic reaction was stopped by adding medium to the

cells. Subsequently the cell suspension was centrifuged at 200 g for 5 min. The pellet was resuspended in new medium and plated on gelatine coated petri dishes (10 cm). 20 - 25 days post isolation primary podocytes (p1) were trypsinized again as described above. The cell suspension was plated on non-gelatine-coated 6 well plates or 12 well plates. 30 - 35 days post isolation primary podocytes (p2) were taken for experiments. In order to quantify GPx-4 protein abundance in a time dependent manner, primary podocytes were stimulated for 5 days with 30 ng/mL recombinant TGF- β 1 and harvested every 24 hours. On day 3 the old medium was removed and replaced by new medium (with TGF- β 1).

5.4.3 CI-muMECS

Conditionally immortalized murine microvascular lung endothelial cells (CI-muMECS (INS-CI-1004) were provided by InSCREENeX GmbH (Braunschweig, Germany). These cells retain many characteristic features of native ECs such as shear stress-induced up-regulation of NOS3 and down-regulation of GPx1 expression as well as NO production measured as nitrate in the medium/supernatant (Sachdeva, Fleming et al. 2019). CI-muMECS were cultivated in DMEM in gelatin-coated flasks. Every 2 - 3 days cells were split in a ratio 1:3 to 1:5.

In order to measure the amount of TGF- β 1 mRNA and to quantify active TGF- β 1 in the supernatant of CI-muMECS, these cells were cultured in 5 % DMEM in 12 well plates until they reached 100 % confluence and were stimulated with different concentrations of leptin (10-1000 ng/mL leptin) for 24 hours. The cells were lysed with RLT-buffer containing 1 % β -mercaptoethanol, whereas the supernatant was collected and spent for a TGF- β 1 ELISA. To determine the expression of the different leptin splice variants, CI-muMECS were cultured in 5 % DMEM in T75 flasks until they reached 100 % confluence and were lysed with RLT-buffer containing 1 % β -mercaptoethanol.

5.4.4 Primary glomerular endothelial cells

Primary glomerular endothelial cells purchased from PelloBiotech were cultivated in mouse endothelial cell medium in pre-coated T25 flasks until they reached 80 - 90 % confluence. Cells were washed 2 - 3 times with +/- PBS and incubated with 2 mL warm 0.25 % Trypsin-EDTA solution for 4 min. As soon as cells detached from the flask, 8 mL medium were added to the trypsinized cells, gently resuspended and immediately plated on fresh flasks pre-

coated with gelatin-based coating solution. Primary glomerular endothelial cells were always splitted 1:2. On the next day the medium was gently replaced by new medium. After additional 24 hours the cells were washed with PBS and new medium was added to the cells. Medium was replaced every two days until cells reached a density of 70 %. Medium of primary glomerular endothelial cells between 70 and 90 % confluence was replaced on a daily basis. Primary glomerular endothelial cells were used not later than passage 9. Low cell passages were frozen in Cryostor at -80 degrees Celsius. Cells were grown until they were 100 %% confluent and then used for further experiments.

5.4.5 Co-culture of CI-muMECs and E11 podocytes

In order to establish the co-culture system CI-muMECs were co-cultured with E11 podocytes. At later time points primary glomerular endothelial cells were either co-cultured with E11 podocytes or with primary podocytes.

Thus, E11 podocytes were plated in 6-well plates and cultivated in RPMI 5 days before the experiment started. CI-muMECS on the other hand have been plated on coated 6-well inserts 24 hours before the co-culture experiment started. As podocytes, endothelial cells were also grown in their respective medium. E11 podocytes and CI-muMECs were co-cultured 5 days in co-culture medium as shown in figure 11. At experimental day 3, inserts with endothelial cells were replaced by new ones. In addition, medium of the inserts (1 mL), but not of the wells (2 mL), was changed. Endothelial cells were stimulated with 100 ng/mL leptin or with 30 ng/mL TGF- β 1 as a reference stimulus. Primary podocytes were plated in 12-well plates and cultivated in RPMI 9 days before the experiment started. Glomerular

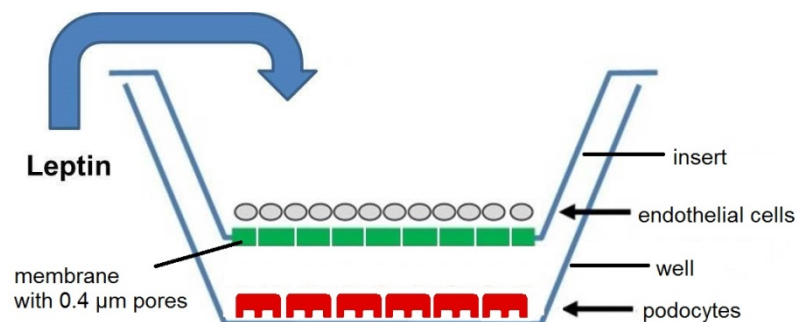


Figure 11: Transwell co-culture system modified from Kumar et al. Vascular Cell (2011), 3:27.

endothelial cells on the other hand have been plated on coated 12-well inserts 7 days before the experiment started and were grown in their respective medium. Primary podocytes and primary glomerular endothelial cells were subsequently co-cultured 5 days in co-culture

medium. Endothelial cells were stimulated with 100 ng/mL leptin or with 30 ng/mL TGF- β 1 as a reference stimulus.

5.5 ELISA of CI-muMEC supernatant

The enzyme-linked immunosorbent assay (ELISA) is an analytical biochemistry assay applied to detect the presence of active TGF- β 1 in the media of cultured endothelial cells. The assay resulted in the formation of a colored product, which was formed proportionally to the amount of TGF- β 1 present in the sample.

Endothelial cells (cell line CI-muMECs) were cultured in 5 % DMEM in 12 well plates until they reached 100 % confluence and were stimulated with different concentrations of leptin (10-1000 ng/mL leptin) for 24 hours. Medium (500 μ l volume) was collected and concentrated with amicon ultra centrifugal filters (MWCO 10 kDa). 20 μ l out of 40 μ l concentrate were spent for a TGF- β 1 ELISA according to the manual of the manufacturer. The assay used a TGF- β 1 antibody coated surface to capture active TGF- β 1 present in the media. In the next step a biotin-conjugated anti-mouse TGF- β 1 antibody was added and bound to mouse TGF- β 1 attached to the first antibody. After a washing step streptavidin-HRP was added and bound to the biotin-conjugated anti-mouse TGF- β 1 antibody. Before substrate solution reactive with HRP was added to the wells an additional washing step was applied. The wells were incubated with TMB substrate in the dark for exact 40 min and stopped by quickly pipetting acid to the respective wells. The absorbance at a wave length of 450 nm was measured immediately at 450 nm. The absorbance at a wave length of 620 nm was used as the reference wave length. Data with significant different values at 620 nm were excluded. TGF- β 1 concentration was determined by the implementation of a standard curve.

5.6 Bradford Assay

To determine the protein concentration the colorimetric protein assay Bradford was performed. This assay is based on the absorbance shift of the dye Coomassie Brilliant Blue from 465 nm to 595 nm by binding specifically to aromatic and basic aminoacids, e.g. arginin, in the sample. The amount of light absorption is proportional to the amount of proteins in the sample.

To measure the protein concentration podocytes (cell line E11) were harvested with a cell scraper in 1 mL PBS and centrifuged at 1.100 g for 5 min. Subsequently pellets were resuspended in 70 μ l homobuffer and sonicated 3 times for 10 sec. Cell suspensions were

cooled on ice between sonification steps. Lysed cells were centrifuged at $1.100 \times g$ for 5 min and supernatant was transferred immediately into a new Eppendorf tube. The samples were diluted 1:25 to 1:100. 80 μ l of the diluted protein homogenate was mixed with 200 μ l Bradford reagent. The absorption at 595 nm was measured with a photometer. The exact protein concentration was determined based on a protein standard concentration row of BSA (5, 10, 15, 20 und 30 μ g/mL).

5.7 SDS–polyacrylamide gel electrophoresis (SDS-PAGE)

SDS-PAGE is a standard method to separate proteins in an electric field by size. SDS is highly negatively charged, binds to the denatured proteins and forms negatively charged SDS-protein complexes. This guarantees a separation only by size and not by any protein specific characteristic properties, e.g. tertiary structure. The proteins were translocated in the electric field of the acrylamide gel matrix. The velocity of the proteins is proportional to their respective size. Bigger proteins get stuck in the matrix and take longer to translocate to the anode, whereas smaller proteins can move faster through the gel matrix.

For this purpose, 15 μ g protein were denatured with sodium dodecyl sulfate (SDS) and beta-mercaptoethanol for 5 min at 95 degrees Celsius and separated in a discontinuous electrophoresis system. A 4 % stacking gel (Millipore water, 0.5 M TRIS-HCL, pH 6.8, 0.3 % Acrylamide, 10 % SDS, 10 % APS, TEMED) ensured the formation of protein stacks according to the principle of isotachopheresis. The separation itself occurred on the 12% running gel (Millipore water, 1.5 M TRIS-HCL, pH 8.8, 0.1 % Acrylamide, 0.1 % SDS, 0.1 % APS, 0.1% TEMED). Both gels differ in their pH, ion strength and pore size. To identify the exact size of the protein the above-mentioned protein standard was loaded next to the samples. For protein stacking 80 volts were applied for 30 min, whereas 120 volts were applied for 90 min to separate the proteins by their respective size in a gel chamber filled with running buffer.

5.8 Western Blot

In order to visualize and quantify the respective proteins they had to be transferred from the SDS PAGE gel (1.5 mm) onto a polyvinylidene difluoride (PVDF) membrane (0.2 μ m pore size). A wet electroblotting (Tank transfer) chamber was chosen to transfer the proteins. As soon as the proteins were immobilized onto the PVDF membrane they were accessible to antibody detection visualized via luminescence reaction.

At first, the PVDF membrane was activated with methanol for 10 min, washed three times with millipore water and equilibrated in transfer buffer. The gel was then placed as a sandwich (filter paper-gel-membrane-filter paper) between platinum wire electrodes in a tank filled with transfer buffer for 40 min at 350 mA. After blotting the PVDF membrane was washed with Millipore water and dried for at least 1 hour at 50 degrees Celsius. The PVDF membrane was reactivated with methanol for 10 min, washed three times with millipore water and blocked for 1 hour with 5 % Blotto in 1x TBS to block unspecific antibody binding sites. Subsequently they were incubated with the first antibodies (GPx-1, GPx-4 and β -actin) in blocking solution over night at 4 degrees Celsius. At the next day the membranes were washed 3 times with TBST and incubated for 1 hour with the horseradish peroxidase (HRP)-conjugated secondary antibodies. After additional 2 washing steps with TBST and a washing step with TBS the membranes were incubated with the respective HRP-substrates. For β -actin Luminata Classico and for GPx Luminata Forte was added to the PVDF membranes to visualize specific antibody bound proteins via a luminescence detection system. The size of the protein bands were quantified with the open-source program ImageJ, whereas the amount of GPx-1 and GPx-4 protein was normalized with the amount of β -actin protein.

5.9 BCA Assay (Pierce)

To determine the exact protein concentration for the simple WES protein detection and quantification method the colorimetric two-component, high-precision BCA Protein Assay was performed. It combines the well-known reduction of Cu^{2+} to Cu^+ by protein in an alkaline medium with the highly sensitive and selective colorimetric detection of the cuprous cation (Cu^+) by bicinchoninic acid.

Podocytes (cell line E11) grown in a 12 well plate were therefore harvested with a cell scraper in 1 mL PBS, centrifuged at 1.100 g for 5 min and frozen at -80 degrees Celsius. On the next day pellets were thawed on ice and resuspended in 25 μL WES-RIPA buffer (with protease and phosphatase inhibitors) and vortexed vigorously. After 15 min incubation on ice samples were vortexed every 2 min for additional 15 minutes on ice. In the next step samples were centrifuged at 1.100 g for 5 min at 4 degrees Celsius. The supernatant was transferred into a new eppendorf tube and centrifuged a second time at 5.133 x g for 10 min at 4 degrees Celsius. The supernatant was transferred again into a new eppendorf tube and was frozen at -80 degrees Celsius. On the next day samples as well as standards (25, 125, 250, 500, 750, 1000, 1500, 2000 $\mu\text{g/mL}$) were thawed on ice and vortexed. WES-RIPA-buffer was used to blank the system. The working reagent was prepared according to the manufacture's protocol. Protein samples were diluted in a dilution series (1.5, 1:7 and 1:10)

in WES-RIPA-buffer. Subsequently 25 µl of each sample and each standard were pipetted in two rows onto a 96-well plate. 200 µl working reagent was added to each well and resuspended thoroughly. The higher the amount of protein in the sample the darker the purple in the respective well. After 30 min at 37°C the absorption at 562 nm was measured with a photometer.

5.10 Simple WES analysis of E11 podocytes

The simple WES is a gel-free capillary-based immunoassay to separate and analyse low amounts of proteins. 3 µl starting material is enough to separate proteins by size from 2-440 kDa. For this reason the simple WES approach was applied for podocyte protein analysis derived from co-culture experiments in 12 well plates. Up to 25 samples could run at a time and be quantified afterwards.

At the beginning 10x sample buffer was diluted 1:100 in RNAase free water. In order to prepare 400 mM DTT solution, 40 µl of deionized water was pipetted into the DTT containing tube provided by the manufacturer. 20 µl of the 400 mM DTT solution was added into the fluorescent 5x master mix tube also provided by the manufacturer together with 20 µl 10x sample buffer. The ladder was prepared by pipetting 20 µl of deionized water to the biotinylated ladder containing tube also provided by the manufacturer. For each capillary a total volume of 10 µl of the respective primary antibody dilution as well as a total volume of 10 µl of the respective secondary antibody dilution was prepared. Diluted antibodies were kept on ice until they have been used. Protein samples suspended in WES-RIPA-buffer were carefully thawed on ice. The concentrations of the different protein samples were adjusted with WES-RIPA-buffer to a temporary working concentration between 0.2 and 2 µg/µl protein. The temporary working dilution was then further diluted with the same volume of 0.1x sample buffer. Subsequently 5 µl of diluted protein suspension were spent for each capillary with a final protein concentration between 0.2 and 0.8 µg/µl. Therefore 5 µl of the diluted protein suspension were mixed with 1.2 µl of fluorescent master mix, transferred into a new eppendorf tube, vortexed thoroughly and boiled for 5 min at 95 degrees Celsius. After cooling on ice samples were vortexed vigorously and centrifuged for a few seconds. Finally, samples were vortexed gently and could be pipetted onto the WES plate according to the manufacture's protocol. We used 4 µl instead of 3 µl prepared samples, 9 µl instead of 10 µl primary antibody and 9 µl instead of 10 µl secondary HRP conjugate. Before pipetting row E, 200 µl luminol and 200 µl peroxide were mixed and used immediately, because luminol-peroxide mix is prone to activity loss starting after 15 min of mixture. In the next step the WES plate was centrifuged at 1,100 g for 5 min. 500 µl wash buffer was added to the first

three rows. The WES plate was placed into the WES reader with the following setting (Table 1).

Separation time	25 min
Separation voltage	375 volts
Antibody diluent time	5 min
Primary antibody time	90 min
Secondary antibody time	30 min

Table 1: WES program to separate and analyze proteins

5.11 Messenger RNA isolation

For mRNA extraction the RNeasy Mini Kit was applied as a purification method to isolate purify mRNA from either cells (E11 podocytes, CI-muMECs or primary glomerular endothelial cells) or from tissue obtained from wildtype or db/db mice.

Tissue was lysed in 750 µl RLT-buffer containing 1 % β-mercaptoethanol and homogenized for 90 sec at 30 Hz with a tissue lyser. Lysed whole kidney homogenate was mixed with the same volume 70 % ethanol and loaded onto the RNA columns. The cultivated cells were washed with PBS and lysed in 500 µl RLT-buffer containing 1 % β-mercaptoethanol per well. Lysed cells were mixed with the same volume 70 % ethanol, harvested using a cell scraper and also loaded onto the RNA columns. The RNA was purified according to the protocol of the manufacturer. The purified RNA was eluted in 20 µl RNase free water and stored at -80 degrees Celsius.

5.12 Copy DNA synthesis

For the synthesis of DNA the single stranded RNA purified with the RNeasy Mini Kit had to be reversely transcribed into complementary DNA (cDNA). Oligo(dT) primers amplify mRNAs containing a poly(A) tail at the 3' end, since that is where the primer binds to promote reverse transcription by the reverse transcriptase

Before cDNA synthesis the concentration of the RNA was determined with a photometrical method using a NanoDrop spectrophotometer. 1 µg RNA was transcribed into cDNA by adding OligodT primer, dNTPs, RNase inhibitors and und reverse transcriptase according to the protocol of the Omniscript RT Kit. After incubation for 1 hour at 37 degrees Celsius samples were stored at -20 degrees Celsius.

5.13 Quantitative real time polymerase chain reaction (q-PCR)

The combination of reverse transcription of a RNA template and quantitative real time polymerase chain reaction improves the capability to detect low abundance RNAs in the samples. The qRT-PCR approach is a method to compare the amount of cDNA between different samples. It is a semi quantitative method, because only the relative change between the samples and not the absolute values are compared. SYBR Green binds specific to double stranded DNA. After binding to double stranded DNA the resulting complex emits green light, which can be measured and quantified. The amount of double stranded DNA duplicates after each cycle, thus the green light emission. The cycle threshold (ct) is determined manually after the run. It describes the number of cycles needed to exceed from the background at the start of the exponential phase of the curve. The cycle number is important to quantify the relative amount of cDNA between the samples. The higher the amount of cDNA in the sample the lower the ct value and vice versa.

In order to calculate the relative fold change the delta-delta ct method was applied. Therefore, the difference between ct values of stimulated and non- stimulated endothelial cells or between db/db and wt mice was calculated and defined as Δct . In the next step the difference between ct values of the housekeeping gene RPL of the respective samples was calculated and defined as Δct housekeeping gene. The comparison with a housekeeping gene was necessary, because it excluded the possibility that a different amount cDNA was utilized at the beginning of the PCR. In order to compare Δct values with Δct housekeeping gene values the formula $2^{-\Delta\Delta ct}$ was applied.

The relative occurrence of mRNA of leptin receptor splicing variant ObRb, ObRa and ObRc was compared between CI-muMECs and glomerular endothelial cells as well as between whole kidneys from wt and db/db mice. TGF- β 1 mRNA was compared between leptin-stimulated and non-stimulated CI-muMECs. Therefore 50 ng cDNA were mixed with 2x SYBR green, forward and reverse primer (Table 2.) as duplicates and measured with a thermocycler with the following settings (Table 3.)

duration	temperature
15 min	95°C
20 sec	95°C
30 sec	50°C
20 sec	72°C

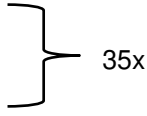


Table 2: qRT-PCR program to multiply cDNA of leptin receptor splice variants

duration	temperature
15 min	95°C
15 sec	95°C
25 sec	60°C
20 sec	72°C

} 35x

Table 3: qRT-PCR program to multiply RPL cDNA

Primer	Sequence (5' to 3')	Final concentration
RPL forward	GGGAGCAACAAGAAAACCAA	1 pmol/μl
RPL reverse	ATTGTGGACCAGGAACCTTGC	1 pmol/μl
ObRb forward	TAACAGTGCTAACTTCTC	1 pmol/μl
ObRb reverse	TGACAGGACTATGGATAA	1 pmol/μl
ObRa forward	GCACAAGGACTGAATTTC	1 pmol/μl
ObRa reverse	GAGAACATGAACACAACAA	1 pmol/μl
ObRc forward	TTGTTTTGGGACGATGTT	1 pmol/μl
ObRc reverse	CAAAGAGTGTCCGTTCTC	1 pmol/μl
TGF-β1 forward	CGCCATCTATGAGAAAACC	1 pmol/μl
TGF-β1 reverse	GTAACGCCAGGAATTGT	1 pmol/μl

Table 4: Primer used for qRT-PCR

5.14 Agarose gel electrophoresis

Agarose gel electrophoresis is a method to separate DNA and RNA fragments in a matrix of agarose. PCR products were separated by length in a 2 % agarose gel for 1 hour at 120 V in 0.5 TBE. 3 - 4 μl ethidium bromide were added to the gel before it started to change from a liquid state to a solid state. 4 μl low range marker were loaded onto the gel as a reference. The gel was scanned after the run and analyzed qualitatively.

5.15 Periodic acid-Schiff (PAS) staining

Periodic acid-Schiff (PAS) is a staining method to detect glycoproteins in tissues. The reaction of periodic acid exclusively oxidizes the vicinal diols in these sugars resulting in the formation of aldehydes, which then react with the Schiff reagent. The reaction turns the respective regions into a purple-magenta color. Diabetic nephropathy is characterized inter alia by the expansion of the extracellular matrix. The PAS-reaction was therefore implemented to show differences in the size of the mentioned extracellular matrix, where glycoproteins found to be highly abundant. Thus, the intensity of the color as well as the size of the stained area can be used as a marker for the degree of kidney damage.

First kidney slices of 5 μm were cut with a cryostat from frozen tissue embedded in tissue tek and dried on air for 4 - 7 days. After kidney slices were washed with millipore water they were incubated with 0.5 % PAS solution for 5 min. After the PAS-reaction the kidney slices were washed for 3 min in running water at the sink followed by a washing step with millipore water. By adding Schiff's reagent for 15 min the aldehydes react with the reagent and change their color to purple-magenta. The slices were washed with millipore water before the nuclei were counterstained for 2 min with hematoxylin. The slices were washed again for 3 min in running water at the sink before dehydration of the tissue started with an increasing alcohol-series. At the end slices were covered with Eukitt and a cover slip and analyzed.

5.16 Immunohistochemistry

Immunohistochemistry is a popular application of immunostaining. Therefore, tissue slices are incubated with antibodies against a specific antigen. After removing excess antibodies, the tissue is incubated with a secondary antibody coupled to a fluorophore which detects the epitope of the first antibody. Thus, it will bind only to first antibodies, which are already bound to the antigen of interest.

In order to quantify GPx-4 protein abundance in kidney slices of db/db mice, *fpn*^{+/-} mice and db/db/*fpn*^{+/-} mice, as well as their respective controls, kidneys were cryoconserved in Tissue-Tek, cut into 5 μm slices with a cryostat and frozen at -80 degrees Celsius until they were utilized. On the first day of immunostaining cryosections were thawed for 10 min at room temperature. Kidney slides were then fixated with 4 % PFA for 20 min at room temperature washed 3 times with PBS and had been permeabilized for 5 min with 0.3 % Triton-X-100 in PBS. Slides were washed again 3 times with PBS and were blocked with blocking solution (50 mM Tris-HCL, pH 7.4, 0.1 % BSA, 0.25 % casein and 15 mM sodium acetate) for 1 hour at room temperature. Subsequently slides were incubated in a wet chamber over night at 4 degrees Celsius with the first antibodies anti-GPx-4 and anti-synaptopodin diluted in blocking solution as mentioned above. On the next day slides were washed 3 times with PBS and incubated with the secondary antibody for 1 hour at room temperature diluted in blocking solution as mentioned above. The slides were washed again 3 times and stained with DAPI for 8 min in order to visualize the nuclei. After the last two washing steps (with PBS) slides were embedded in mowiol, covered with a cover slip and dried over night at 4 degrees Celsius. On the next day marker expression was visualized by using the fluorescence microscope (Xellence (rt) - Olympus).

5.17 GPx-4 activity assay

GPx-4 specific activity was measured in cell lysates of TGF- β 1 and iron stimulated podocytes or of RSL-3 stimulated podocytes cultured in high glucose medium by our cooperation partner Fulvio Ursini (University of Padova, Department of Molecular medicine) using the GPx-4 specific substrate soybean PC as published (Ursini, Maiorino et al. 1985).

5.18 Iron staining

Kidney slices were stained by our cooperation partner Dr. Altamura (University Hospital Heidelberg, Department of Pediatric Hematology, Oncology and Immunology) using DAB advanced Pearls staining. Therefore, kidney slices of 3 μ m on polylysine slides were treated for 20 min with Prussian blue followed by a 20 min incubation of DAB after tissue has been fixed for 24 hours in 10 % neutral buffer formalin, dehydrated and paraffin embedded. In addition, slices were counterstained with Meyer's hematoxylin (Altamura, Kopf et al. 2017).

5.19 Image analysis

The light emission of the excited secondary antibodies was analyzed with the open source program QuPath. In order to find the region of interest the outer edge of the glomerulus defined by synaptopodin positive cells were encircled with the polygon selection tool. Subsequently, the mean of a region of interest was evaluated and divided by the size of the respective area.

5.20 Statistics

The program GraphPad Prism was utilized for statistical analysis. Parametric unpaired student's t-test was used for two-group comparisons and one sample t-test for values expressed as relative to a control sample. For data encompassing three groups or more, one-way ANOVA with Tukey's multiple comparisons test was employed. The results are shown as means \pm SD. P-values < 0.05 were considered statistically significant.

6. Results

6.1 Validation of the expression of cell-specific markers using immunofluorescence microscopy

First, the type of cell lines used for the *in vitro* experiments as well as their purity was validated by immunofluorescence analysis.

To this end, E11 podocytes were differentiated as described in MM 5.4.2. Differentiated E11 podocytes express the podocyte-specific marker synaptopodin (Shankland, Pippin et al. 2007). As shown (Figure 12), the E11 podocytes used for the following experiments were fully differentiated without any other contaminating cell species.

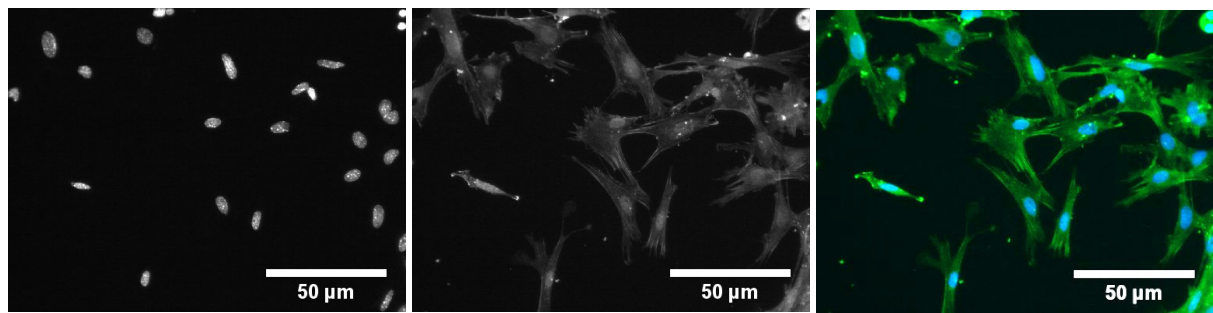


Figure 12: Validation of the expression of the podocyte specific marker synaptopodin in E11 podocytes. Exemplary pictures showing differentiated E11 podocytes. E11 podocytes were proliferated at 33°C with 50 U/mL Interferon- γ (IFN- γ). After 14 days of differentiation at 37°C without IFN- γ podocytes express the podocyte-specific marker synaptopodin. The expression of synaptopodin was visualized by immunofluorescence analysis.

The identity and the purity of the pulmonary microvascular endothelial cell line CI-muMECS were confirmed by a positive CD31 immunofluorescence staining (Figure 13).

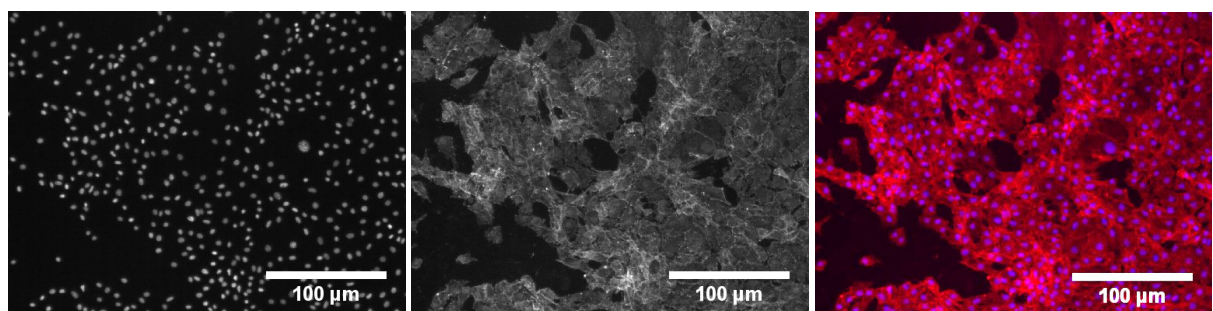


Figure 13: Validation of the expression of the endothelial cell specific marker CD31 in CI-muMECS. Exemplary pictures showing a confluent monolayer of CI-muMECS. CI-muMECS express the endothelial cell specific marker CD31. The expression of the membrane bound CD31 was visualized by immunofluorescence analysis.

Primary podocytes used for the *in vitro* experiments as well as their purity were validated by positive synaptopodin immunofluorescence (Figure 14). To this end, outgrowing cells from isolated glomeruli as described in MM 5.4.2 were stained after 4-week cultivation.

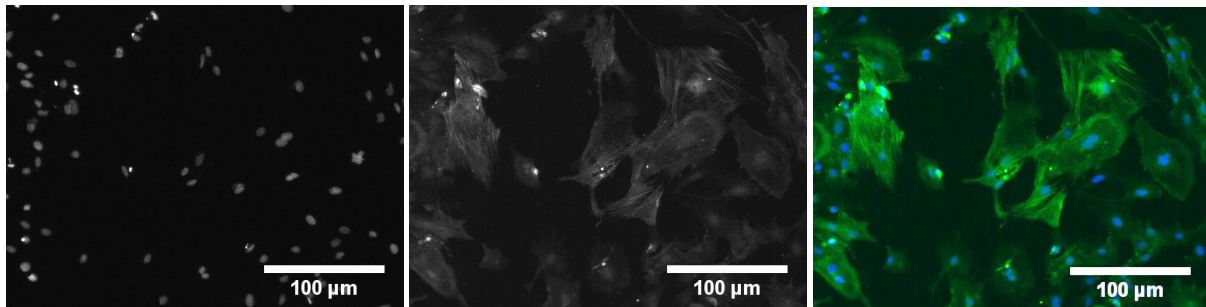


Figure 14: Validation of expression of the podocyte specific marker synaptopodin in primary podocytes. Exemplary pictures showing primary podocytes isolated from wildtype mice and express the podocyte specific marker synaptopodin. The expression of synaptopodin was visualized by immunofluorescence stainings.

Primary mouse glomerular endothelial cells (PeloBiotech) were stained. As shown in Figure 15, the primary mouse glomerular endothelial cells used for the following experiments were endothelial cells based on their morphology and the respective staining (Rops, van der Vlag et al. 2004).

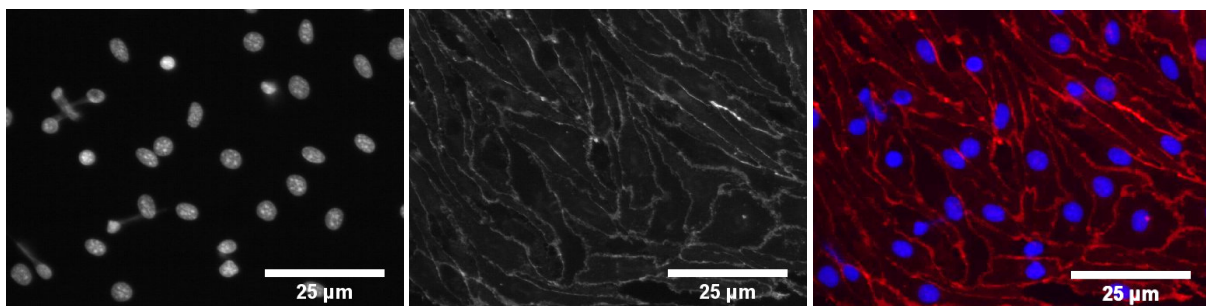


Figure 15: Validation of the expression of the endothelial cell specific marker CD31 in primary mouse glomerular endothelial cells. Exemplary pictures showing primary mouse glomerular endothelial cells (PeloBiotech) expressing the endothelial cell specific marker CD31. The expression of CD31 was visualized by immunofluorescence stainings.

6.2 Detection of leptin receptor splice variants by realtime PCR

As a next step the long leptin receptor splice variant 1 (ObRb), the short variant 2 (ObRa) and variant 3 (ObRc) were compared qualitatively and quantitatively between CI-muMECs and primary glomerular endothelial cells or within the respective cell species using realtime PCR.

First, the different leptin receptor splicing variant transcripts were compared within the cell species. In CI-muMECs the amount of transcript ObRa is 3.3-fold increased compared to

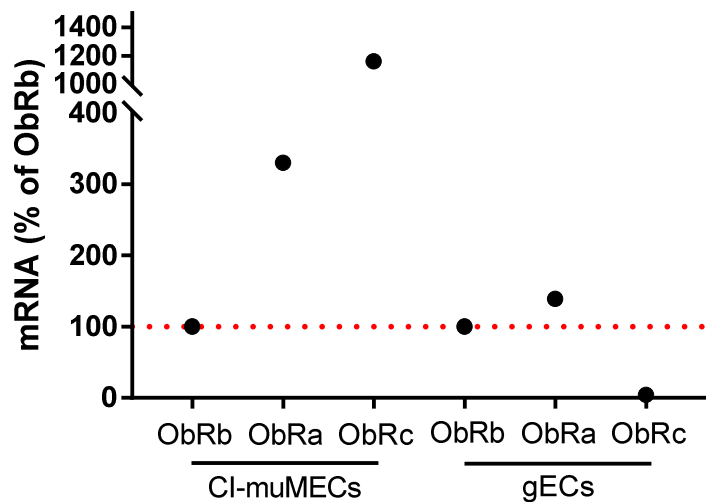


Figure 16: Quantification of the amount of leptin receptor splice variants ObRb, ObRa and ObRc transcripts in CI-muMECs and in gECs. Exemplary graph showing the amount of ObRa and ObRc mRNA in CI-muMECs and gECs compared to the long leptin receptor splicing variant ObRb in the respective cell type. The values were obtained by real time PCR from 3 replicates by using the $\Delta\Delta\text{ct}$ method.

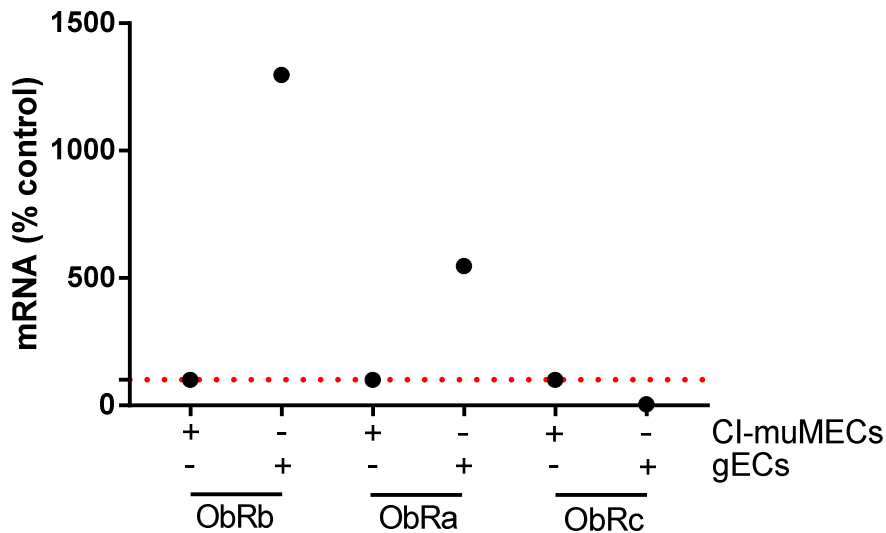


Figure 17: Quantification of the amount of leptin receptor splice variants ObRb, ObRa and ObRc transcripts between gECs and CI-muMECs. Exemplary graph showing the amount of ObRb, ObRa and ObRc mRNA in gECs compared to the respective amount of ObRb, ObRa and ObRc mRNA in CI-muMECs. The values were obtained by real time PCR from 3 replicates by using the $\Delta\Delta\text{ct}$ method.

transcript ObRb. Moreover, transcript ObRc is 11.6-fold more abundant compared to transcript ObRb (Figure 16).

A comparison of the respective leptin receptor splice variant transcripts between CI-muMECS and primary glomerular endothelial cells showed that the amount of the transcript of the long leptin receptor splice variant ObRb is more than 13-fold higher in primary glomerular endothelial cells compared to the CI-muMECs (Figure 17). The amount of the short leptin receptor splice variant transcript ObRa is more than 5.5-fold increased in primary glomerular endothelial cells compared to the CI-muMECs, whereas the amount of the short leptin receptor splice variant transcript ObRc was negligibly low (0.048).

6.3 Cell culture

6.3.1 Endothelial cells

6.3.1.1 TGF- β 1 mRNA expression in leptin-stimulated CI-muMECs

In order to elucidate the effects of leptin on TGF- β 1 mRNA expression CI-muMECs were stimulated for 24 hours with 10 and 100 ng/mL murine recombinant leptin. There was no increase in TGF- β 1 mRNA expression in leptin-stimulated compared to the non-stimulated control cells detectable (Figure 18).

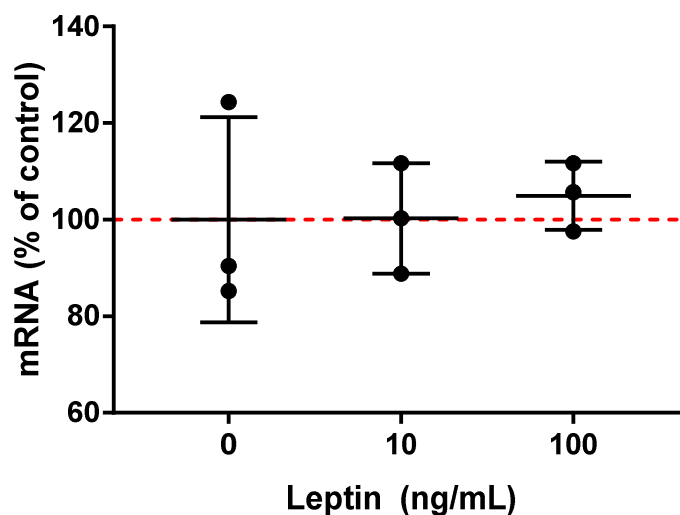


Figure 18: Effect of leptin on TGF- β 1 mRNA levels in CI-muMECs. CI-muMECs were stimulated for 24 hours with 10 and 100 ng/mL murine recombinant leptin. Messenger RNA levels were compared between the groups and shown as a relative fold change in percent of control. The results are shown as means \pm SD with n=3 per group.

6.3.1.2 Active TGF- β 1 in the medium of leptin-stimulated CI-muMECS

As there was no difference detectable at the transcriptional level, it was likely that TGF- β 1 was processed post translationally. As mentioned above the non-active latent TGF- β 1 needs to be released from the extracellular matrix and cleaved by metalloproteases in order to be activated. Activated TGF- β 1 was detected in medium supernatants of CI-muMECs stimulated with 10 or 100 ng/mL leptin using an appropriate ELISA. The active TGF- β 1 concentration was significantly increased in CI-muMECS stimulated with 10 ng/mL leptin (1.36-fold) or 100 ng/mL leptin (1.66-fold) as compared to non-stimulated control cells (Figure 19).

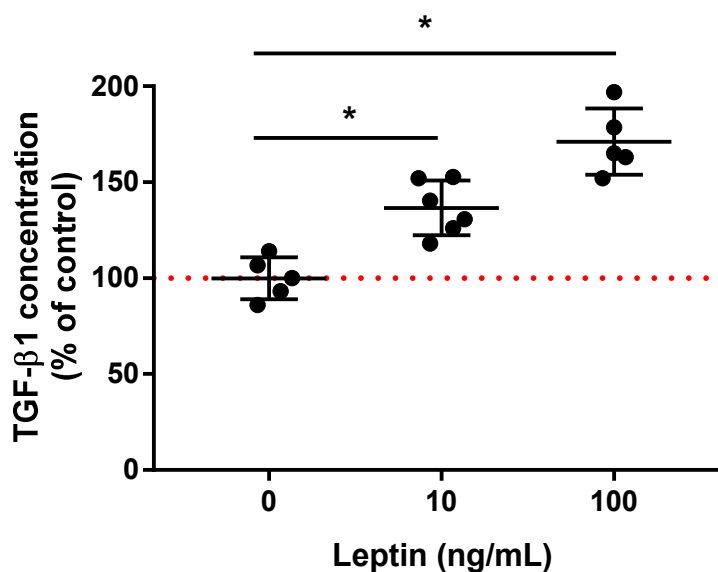


Figure 19: Effect of leptin on TGF- β 1 release/activation in CI-muMECs. CI-muMECs were stimulated for 24 hours with 10 and 100 ng/mL murine recombinant leptin. Active TGF- β 1 concentrations were compared between the groups and are shown as a relative fold change in percent of the unstimulated control. The results are shown as means \pm SD with n=5-6 per group. *p<0.05 as indicated

6.3.1.3 Active TGF- β 1 in the medium of leptin-stimulated primary glomerular endothelial cells

Primary mouse glomerular endothelial cells purchased from PelloBiotech were stimulated the same way as the CI-muMECs for 24 hours with 10 and 100 ng/mL murine recombinant leptin. No effect on TGF- β 1 mRNA expression in leptin-stimulated compared to the non-stimulated control cells was observed. The active TGF- β 1 concentration was not changed in primary glomerular endothelial cells stimulated with 10 ng/mL leptin and significantly

increased (1.24-fold) in primary glomerular endothelial cells stimulated with 100 ng/mL leptin compared to the control group (Figure 20). When compared to the CI-muMECs, the magnitude of the effect of leptin on TGF- β 1 release seemed less pronounced, which was due to the fact that baseline release of TGF- β 1 from these cells was significantly higher than from the CI-muMECs (not shown).

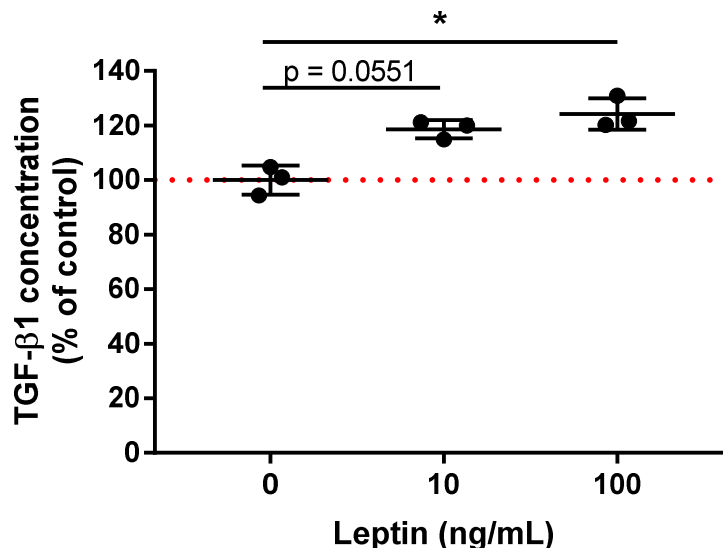


Figure 20: Effect of leptin on TGF- β 1 release in primary murine glomerular endothelial cells. Primary murine glomerular endothelial cells (PeloBiotech) were stimulated for 24 hours with 10 and 100 ng/mL murine recombinant leptin. Active TGF- β 1 concentrations were compared between the groups and are shown as a relative fold change in percent of the unstimulated control. The results are shown as means \pm SD with $n=3$ per group. * $p<0.05$ as indicated

6.3.2 Podocytes

6.3.2.1 GPx-1 protein abundance in leptin-stimulated or TGF- β 1-stimulated E11 podocytes

Next E11 podocytes were stimulated for 5 days with different concentrations (5-200 ng/mL) of murine recombinant leptin or different concentrations of murine recombinant TGF- β 1 (2-50 ng/mL) to investigate whether it affects the abundance of GPx-1 protein or not. Neither E11 podocytes stimulated with low concentrations of leptin (5 and 15 ng/mL) nor E11 podocytes stimulated with high concentrations of leptin (50, 100 or 200 ng/mL) responded to the respective stimulus with a change in their GPx-1 protein content (Figure 21 a). Moreover, there was no change in the amount of GPx-1 protein detectable in the TGF- β 1-stimulated E11 podocytes independent of the dose used for stimulating the cells (Figure 21 b).

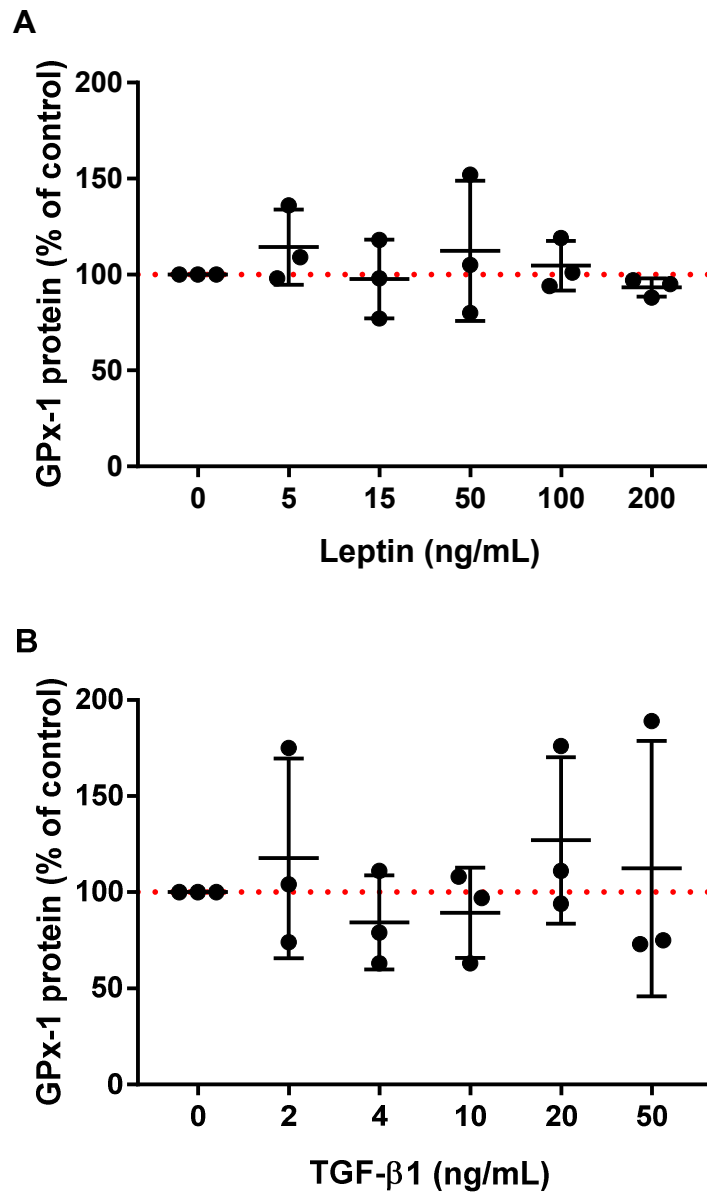


Figure 21: Effect of leptin-stimulated or TGF-β1-stimulated E11 podocytes on GPx-1 protein abundance. GPx-1 protein abundance was determined in E11 podocytes stimulated with different concentrations (5-200 ng/mL) of murine recombinant leptin (a) or different concentrations (2-50 ng/mL) of murine recombinant TGF-β1 (b). The amount of protein per sample was normalized with β-actin. GPx-1 protein abundance was compared between groups and shown as a relative fold change in percent of their respective control. The results are shown as means ± SD with n=3 per group. *p<0.05 as indicated

6.3.2.2 GPx-4 protein abundance in leptin-stimulated or TGF-β1-stimulated E11 podocytes

E11 podocytes were stimulated for 5 days with different concentrations (5-200 ng/mL) of murine recombinant leptin or different concentrations of murine recombinant TGF-β1 (2-50

ng/mL). Neither E11 podocytes stimulated with low concentrations of leptin (5 and 15 ng/mL) nor E11 podocytes stimulated with high concentrations of leptin (50, 100 or 200 ng/mL) responded to the respective stimulus with a change in their GPx-4 protein content (Figure 22 a). In contrast, GPx-4 protein abundance was 24 % lower in E11 podocytes stimulated with 2

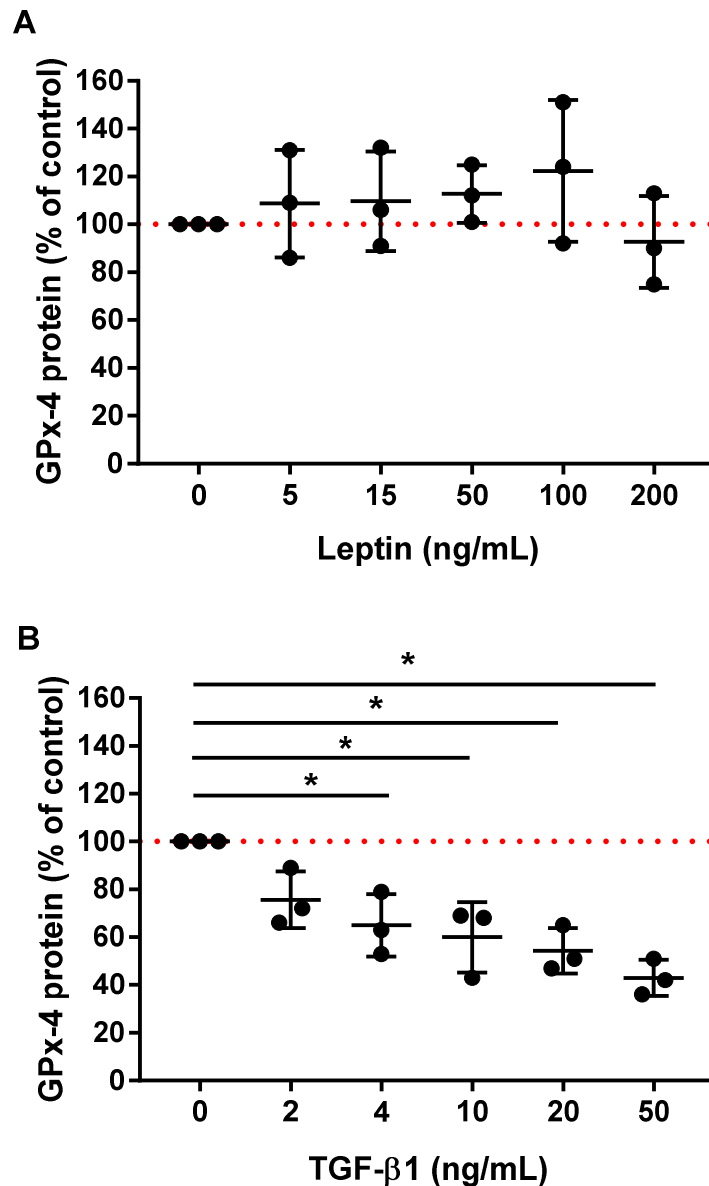


Figure 22: Effect of leptin-stimulated or TGF-β1-stimulated E11 podocytes on GPx-4 protein abundance in a dose-dependent manner. GPx-4 protein abundance was determined in E11 podocytes stimulated with different concentrations (5-200 ng/mL) of murine recombinant leptin (a) or different concentrations (2-50 ng/mL) of murine recombinant TGF-β1 (b). The amount of protein per sample was normalized with β-actin. GPx-4 protein abundance was compared between groups and shown as a relative fold change in percent of their respective control. The results are shown as means ± SD with n=3 per group. *p<0.05 as indicated

ng/mL TGF- β 1 and already significantly reduced (35 %) in cells stimulated with 4 ng/mL TGF- β 1. This decline in GPx-4 protein abundance was augmented in a concentration-dependent manner (Figure 22 b).

E11 podocytes were stimulated for 5 days with 30 ng/mL murine recombinant TGF- β 1. As shown (Figure 19) this concentration equals the concentration of released/activated TGF- β 1 measured by ELISA of the leptin-stimulated CI-muMECs. E11 podocytes were harvested every 24 hours to visualize the kinetic properties of the GPx-4 protein decline. After 24 hours GPx-4 protein abundance was reduced by 27 %, and this inhibitory effect reached significance at 48 hours of TGF- β 1-stimulation (Figure 23).

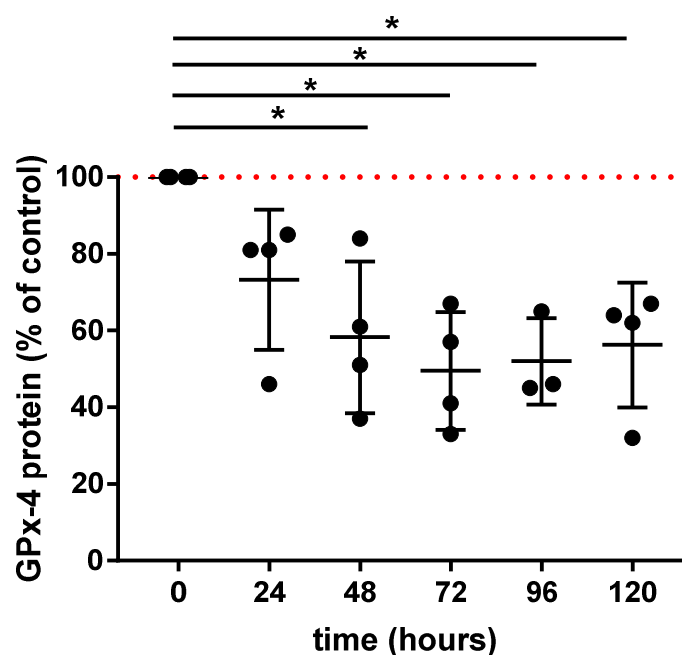


Figure 23: Effect of TGF- β 1-stimulated E11 podocytes on GPx-4 protein abundance in a time-dependent manner. GPx-4 protein abundance was determined in E11 podocytes stimulated with 30 ng/mL of murine recombinant TGF- β 1. The amount of protein per sample was normalized with β -actin. GPx-4 protein abundance was compared between groups and shown as a relative fold change in percent of their respective control. The results are shown as means \pm SD with n=3-4 per group. *p<0.05 as indicated

To compare possible differences in the kinetic properties of the amount of GPx-4 protein in E11 podocytes and primary podocytes, primary podocytes were cultivated the same way as E11 podocytes, and then stimulated for 5 days with 30 ng/mL murine recombinant TGF- β 1. Moreover, they were harvested every 24 hours to visualize the kinetic properties of the presumed inhibitory effect on GPx-4 protein abundance. Surprisingly the primary podocytes responded to TGF- β 1 stimulation with a temporal but not significant increase rather than decrease in GPx-4 protein abundance (Figure 24).

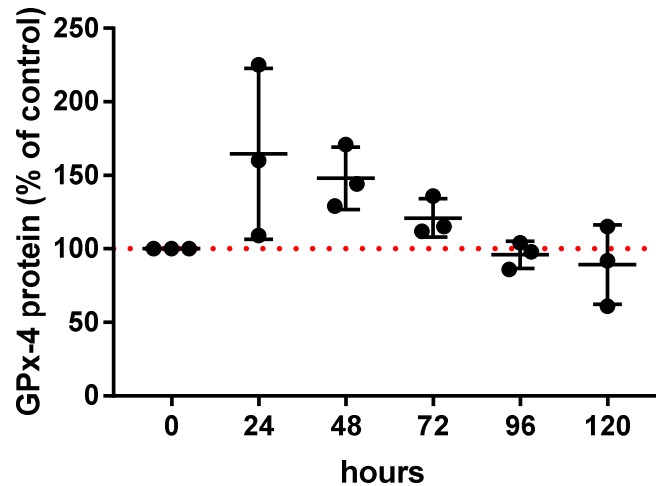


Figure 24: Effect of TGF- β 1-stimulated primary podocytes on GPx-4 protein abundance in a time-dependent manner. GPx-4 protein abundance was determined in primary podocytes stimulated with 30 ng/mL of murine recombinant TGF- β 1. The amount of protein per sample was not normalized with β -actin. GPx-4 protein abundance was compared between groups and shown as a relative fold change in percent of their respective control. The results are shown as means \pm SD with n=3 per group. *p<0.05 as indicated

6.3.2.2 GPx-4 protein abundance in E11 podocytes exposed to TGF- β 1 and/or iron overload

We further investigated whether iron imported into the cell via the transferrin receptor has an additional effect on GPx-4 protein content of E11 podocytes. Accordingly, E11 podocytes were stimulated for 5 days with 30 ng/mL murine recombinant TGF- β 1, 30 μ M transferrin (apotransferrin or holotransferrin) as an iron donor or with a combination of both. Apotransferrin is the non-loaded transferrin form and should be loaded with iron from the iron pool available in the medium. Apotransferrin-stimulated E11 podocytes revealed a small but insignificant rise in GPx-4 protein, whereas this was significantly reduced by 51 % in TGF- β 1-stimulated E11 podocytes (Figure 25a). The combination of apotransferrin and TGF- β 1 had no additional effect on GPx-4 protein abundance in the E11 podocytes.

Holotransferrin is the iron-loaded form of transferrin. After releasing iron into the cell via endocytosis, empty transferrin shuttles back and is reloaded with new iron from the labile iron pool in the medium. Holotransferrin alone had no effect on GPx-4 protein content, whereas this was significantly reduced by 52 % in TGF- β 1-stimulated E11 podocytes (Figure 25b). Combination of holotransferrin and TGF- β 1 again had no additional inhibitory effect on GPx-4

protein abundance was significantly. Thus, neither the unloaded nor the iron-loaded form of transferrin had a measurable impact on GPx-4 protein abundance in the E11 podocytes.

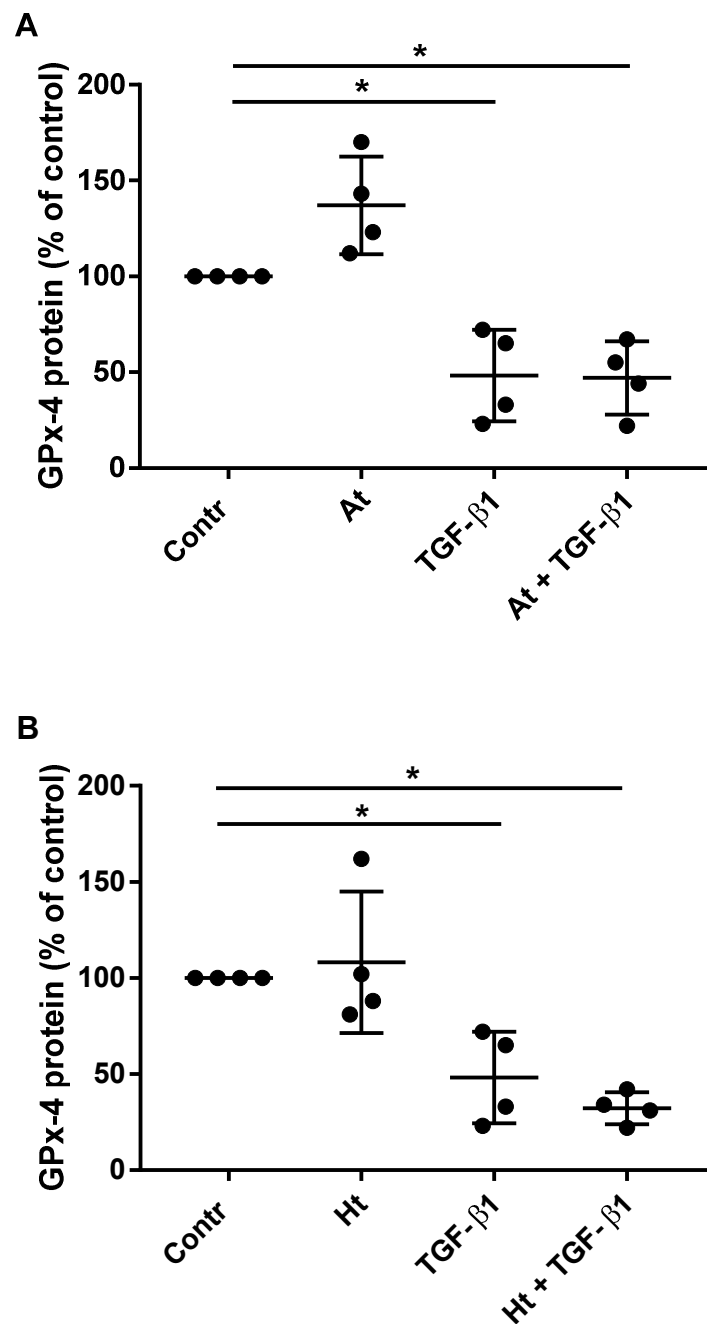


Figure 25: Impact of iron overload with or without concomitant TGF- β 1 exposure on GPx-4 protein abundance in E11 podocytes. GPx-4 protein abundance was measured in E11 podocytes stimulated with 30 ng/mL murine recombinant TGF- β 1, 30 μ M transferrin [apotransferrin (At, a) or holotransferrin (Ht, b)] or with a combination of both for 5 days. The amount of protein per sample was normalized with β -actin. Unstimulated cells served as control and were set to 100 %. Changes in GPx-4 protein abundance were calculated in percent of the corresponding control value. Means \pm SD of n=4 per group are shown. *p<0.05 as indicated

To verify whether a non-transferrin receptor-mediated iron transport plays a role in this context, we also investigated the potential role of an increased labile iron pool and

investigated alternative iron uptake pathways. To this end, E11 podocytes were stimulated for 5 days with 30 ng/mL murine recombinant TGF- β 1, 30 μ M FeNTA as an iron donor or with a combination of both. FeNTA itself had no effect on GPx-4 protein content, but this was significantly reduced (45 %) in TGF- β 1-stimulated E11 podocytes (Figure 26). The combination of FeNTA and TGF- β 1 did not surpass the inhibitory effect of TGF- β 1 alone.

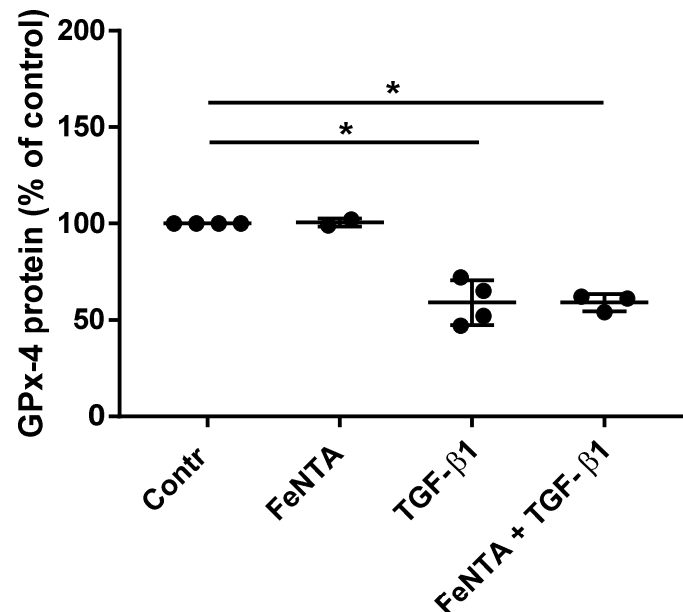


Figure 26: Impact of iron overload with or without concomitant TGF- β 1 exposure on GPx-4 protein abundance in E11 podocytes. GPx-4 protein abundance was measured in E11 podocytes stimulated with 30 ng/mL murine recombinant TGF- β 1, 30 μ M FeNTA or with a combination of both for 5 days. The amount of protein per sample was normalized with β -actin. Unstimulated cells served as control and were set to 100 %. Changes in GPx-4 protein abundance were calculated in percent of the corresponding control value. Means \pm SD of n=4 per group are shown. *p<0.05 as indicated

6.3.2.3 GPx-4 protein abundance in E11 podocytes stimulated with TGF- β 1 and iron in high-glucose medium

GPx-4 protein abundance was significantly reduced in TGF- β 1-treated E11 podocytes, whereas iron overload caused no additional reduction in the amount of GPx-4 protein. In order to activate the proposed feedback loop an additional trigger such as hyperglycemia could be required. Accordingly, E11 were cultured either in low-glucose or in high-glucose medium and part of the experiments described above repeated under these conditions. High-glucose medium itself had no effect on GPx-4 protein content while TGF- β 1 still exerted its

inhibitory effect (Figure 27). Holotransferrin again did not add to the inhibitory effect of TGF- β 1 in E11 podocytes cultured in high-glucose medium.

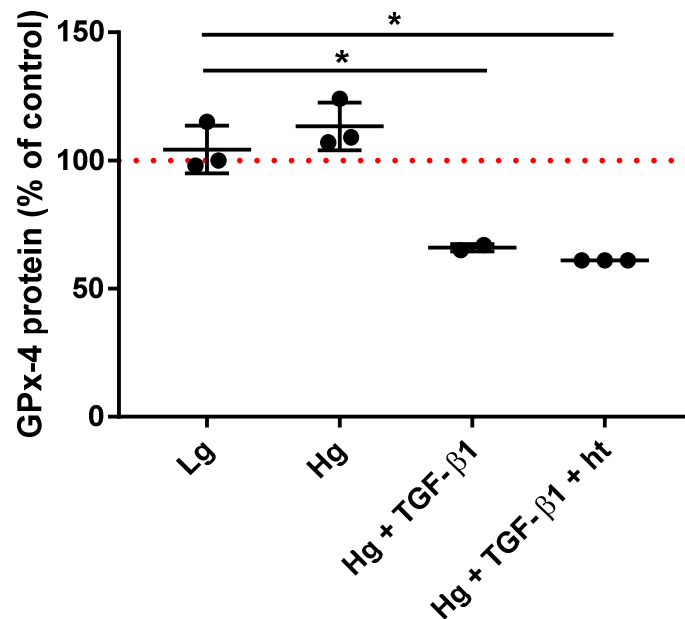


Figure 27: Impact of high glucose levels in iron- and TGF- β 1-stimulated E11 podocytes on GPx-4 protein abundance. GPx-4 protein abundance was measured in E11 podocytes cultured in low glucose medium (5 mM) or high glucose medium (30 mM) and stimulated with 30 ng/mL of murine recombinant TGF- β 1 or co-stimulated with 30 ng/mL of murine recombinant TGF- β 1 and 30 μ M holotransferrin in high glucose medium. The amount of protein per sample was normalized with β -actin. Unstimulated cells served as control and were set to 100 %. Changes in GPx-4 protein abundance were calculated in percent of the corresponding control value. Means \pm SD of n=3 per group are shown. *p<0.05 as indicated

6.3.2.4 GPx-4 activity in E11 podocytes exposed to TGF- β 1 and/or iron in high-glucose medium

As there was no difference on the GPx-4 protein level detectable, GPx-4 specific activity was measured in E11 podocytes stimulated for 3 days with 30 ng/mL murine recombinant TGF- β 1 and 30 μ M holotransferrin in high glucose medium (30 mM).

In order to verify the efficiency of the GPx-4 inhibitor RSL-3, RSL-3 (10 μ M) was added as a control. Since RSL-3 was reconstituted in DMSO, a DMSO control was included as well. The activity of GPx-4 was significantly reduced by 29% in E11 podocytes co-incubated with TGF- β 1 and holotransferrin for 3 days in high-glucose medium (Figure 28). Moreover, the activity of GPx-4 was reduced to zero in the presence of RSL-3, confirming the specificity of the

GPx-4 activity assay. The GPx-4 activity was not further inhibited in E11 podocytes co-stimulated with TGF- β 1 and holotransferrin for 3 days in high glucose medium compared to the amount of GPx-4 protein (Figure 28). In addition, there was no compensatory upregulation of the GPx-4 activity compared to the non-stimulated controls. The decrease in activity reflects almost the decrease in the amount of GPx-4 protein measured after 3 days.

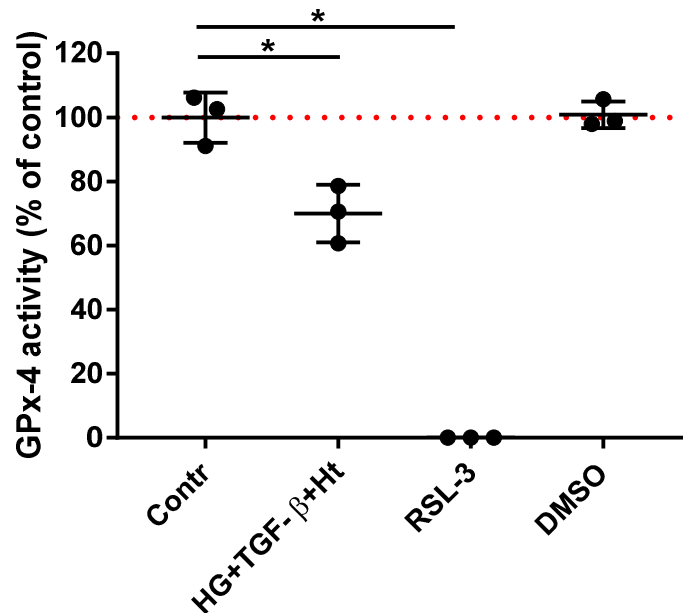


Figure 28: Impact of high glucose levels in iron- and TGF- β 1-stimulated E11 podocytes on GPx-4 activity. GPx-4 activity was measured in E11 podocytes co-stimulated with murine recombinant TGF- β 1 (30 ng/mL) and 30 μ M holotransferrin or with 10 μ M RSL-3 as an additional control stimulus in high glucose medium (30 mM). Changes in GPx-4 activity were calculated in percent of the corresponding control value. Means \pm SD of n=3 per group are shown. *p<0.05 as indicated

6.3.3 Co-culture of endothelial cells and podocytes

6.3.3.1 GPx-4 expression in E11 podocytes co-cultured with CI-muMECs

In more than two separate experiments we showed that endothelial cells respond to leptin with a significant increase in the release/activation of TGF- β 1, and that podocytes respond to TGF- β 1 with a significant decrease in GPx-4 protein abundance. Next, E11 podocytes and CI-muMECs were co-cultured in a set up mimicking the filtration barrier of the kidney. Thus, CI-muMECs were cultured as a monolayer on transwell inserts consisting of a filter with a pore size of 0.4 μ m, whereas E11 podocytes were cultured as a monolayer on the bottom of the respective wells and stimulated with 100 ng/mL murine recombinant leptin for 5 days.

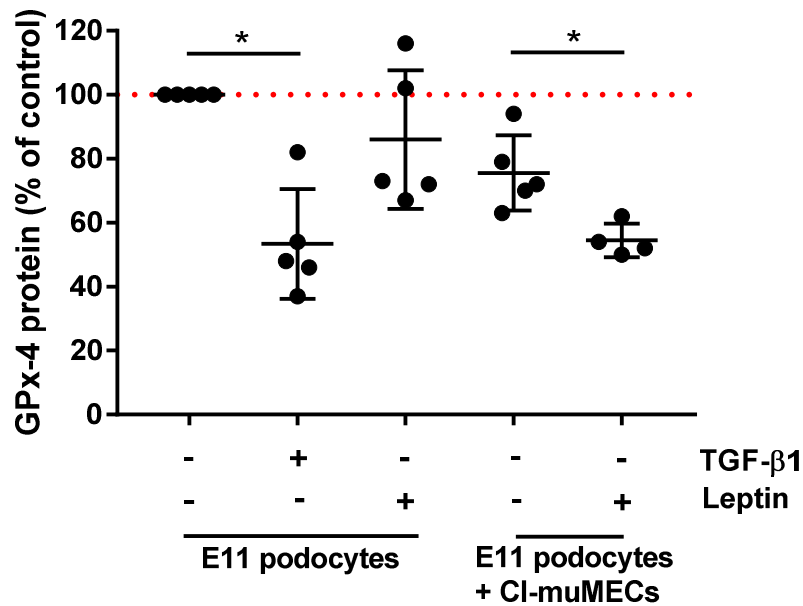


Figure 29: Effect of leptin-stimulated CI-muMECs co-cultured with E11 podocytes on GPx-4 protein abundance in E11 podocytes. GPx-4 protein abundance was determined in E11 podocytes stimulated with 30 ng/mL of murine recombinant TGF-β1 or 100 ng/mL of murine recombinant leptin, in E11 podocytes co-cultured with CI-muMECs and in E11 podocytes co-cultured with leptin-stimulated CI-muMECs. The amount of protein per sample was normalized with β-actin. Unstimulated cells served as control and were set to 100 %. Changes in GPx-4 protein abundance were calculated in percent of the corresponding control value. Means ± SD of n=4-5 per group are shown. *p<0.05 as indicated.

E11 podocytes without co-cultured CI-muMECs were stimulated with 30 ng/mL murine recombinant TGF-β1 or with 100 ng/mL murine recombinant leptin as a control stimulus. GPx-4 was significantly reduced by 47% in TGF-β1-treated E11 podocytes compared to the untreated control (Figure 29). There was no significant difference between E11 podocytes exposed to leptin and the non-stimulated controls. GPx-4 protein abundance was 24% lower in E11 podocytes co-cultured with CI-muMECs. GPx-4 protein abundance was reduced by a further 22% in E11 podocytes co-cultured with leptin-stimulated CI-muMECs.

In order to emphasize the impact of the potential paracrine TGF-β1 signaling between leptin-stimulated CI-muMECs co-cultured with E11 podocytes and the resulting decrease in GPx-4 protein abundance in E11 podocytes, GPx-4 protein abundance was compared between leptin-stimulated CI-muMECs co-cultured with E11 podocytes and non-stimulated co-cultured E11 podocytes. GPx-4 protein abundance was significantly reduced by 22% in E11 podocytes co-cultured with leptin-stimulated CI-muMECs as compared to E11 podocytes co-cultured with non-stimulated CI-muMECs (Figure 30).

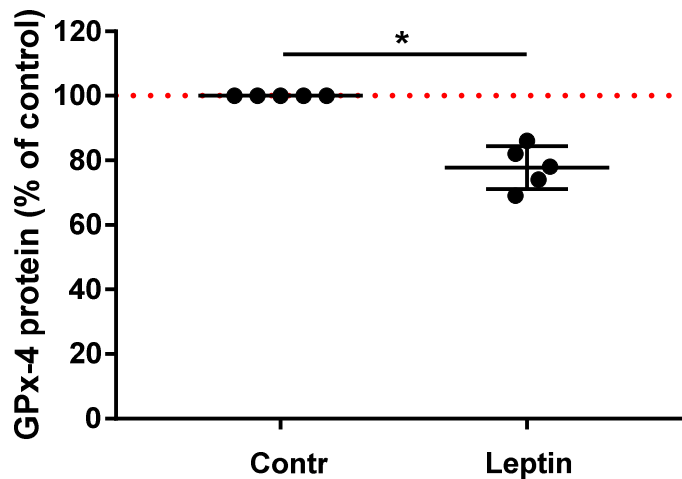


Figure 30: Effect of leptin-stimulated CI-muMECs co-cultured with E11 podocytes on GPx-4 protein abundance in E11 podocytes. GPx-4 protein abundance was determined in E11 podocytes co-cultured with CI-muMECs and in E11 podocytes co-cultured with leptin-stimulated CI-muMECs. The amount of protein per sample was normalized with β -actin. Unstimulated cells served as control and were set to 100 %. Changes in GPx-4 protein abundance were calculated in percent of the corresponding control value. Means \pm SD of n=5 per group are shown. *p<0.05 as indicated

6.3.3.2 GPx-4 expression in E11 podocytes co-cultured with gECs

Even though CI-muMECs are microvascular endothelial cells they have been isolated from the lung. As already discussed, gECs were used for further experiments as they have been isolated from the kidney and were not immortalized. According to the manufacturer these cells keep their primary cell character in low passage numbers. Thus, gECs were cultured as a monolayer on transwell inserts consisting of a filter with a pore size of 0.4 μ m, whereas E11 podocytes were cultured as a monolayer on the bottom of the respective wells and stimulated with 100 ng/mL murine recombinant leptin with or without 10 μ g/mL pan/TGF- β antibody or with 100 ng/mL murine recombinant leptin and 10 μ g/mL TGF- β I and II receptor blocker for 5 days. The TGF- β I and II receptor blocker was reconstituted in DMSO, therefore a DMSO control was included.

GPx-4 was about 10 % reduced in E11 podocytes co-cultured with leptin-stimulated gECs compared to the unstimulated co-cultured cells (Figure 31). There was no significant difference in the amount of GPx-4 protein in E11 podocytes co-cultured with leptin-stimulated gECs when the neutralizing TGF- β 1,2,3 antibody or the TGF- β I and II receptor blocker was added. As the amount of GPx-4 protein was only reduced around 10 %, it was difficult to block this effect on a significant level.

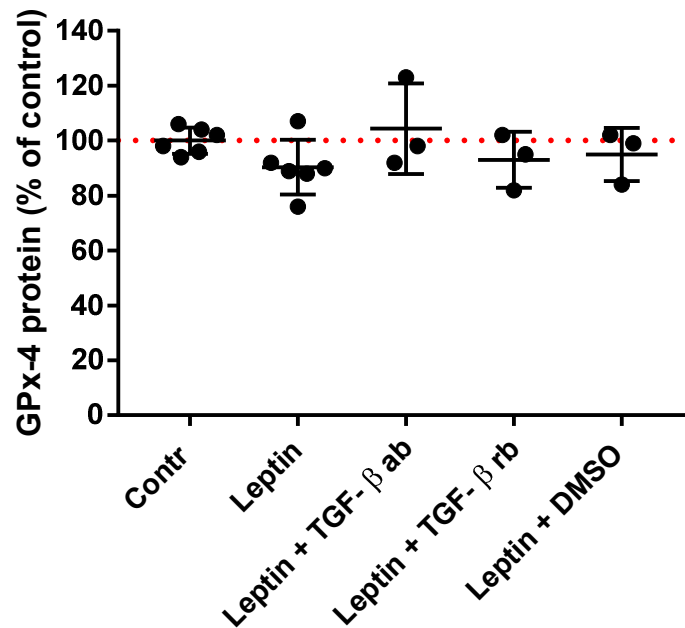


Figure 31: Impact of leptin-stimulated gECs co-cultured with E11 podocytes on GPx-4 protein abundance in E11 podocytes. GPx-4 protein abundance was determined E11 podocytes co-cultured with gECs and in E11 podocytes co-cultured with leptin-stimulated CI-muMECs or with 100 ng/mL murine recombinant leptin and 10 µg/mL TGF-β1,2,3 antibody (TGF-β ab) or with 100 ng/mL murine recombinant leptin and 10 µg/mL TGF-β I and II receptor blocker (TGF-β rb) for 5 days. A DMSO control was included. The amount of protein per sample was normalized with β-actin. Unstimulated cells served as control and were set to 100 %. Changes in GPx-4 protein abundance were calculated in percent of the corresponding control value. Means ± SD of n=3-6 per group are shown.

6.3.3.3 GPx-4 expression in primary podocytes co-cultured with gECs

E11 podocytes are immortalized podocytes, which may have lost or gained characteristic features during their cultivation. To exclude that the potential paracrine TGF-β1 signaling between endothelial cells and podocytes is not only an artefact of the cell culture, primary podocytes were used for the next experiment. The same set up as employed for the cell lines was utilized. Primary podocytes without co-cultured gECs were stimulated with 30 ng/mL murine recombinant TGF-β1 or with 100 ng/mL murine recombinant leptin as a control stimulus. The amount of GPx-4 protein was not changed in TGF-β1 or leptin-stimulated primary podocytes compared to the non-stimulated control (Figure 32). Moreover, the amount of GPx-4 protein was not changed in primary podocytes co-cultured with leptin-stimulated gECs compared to the primary podocytes co-cultured with non-stimulated gECs.

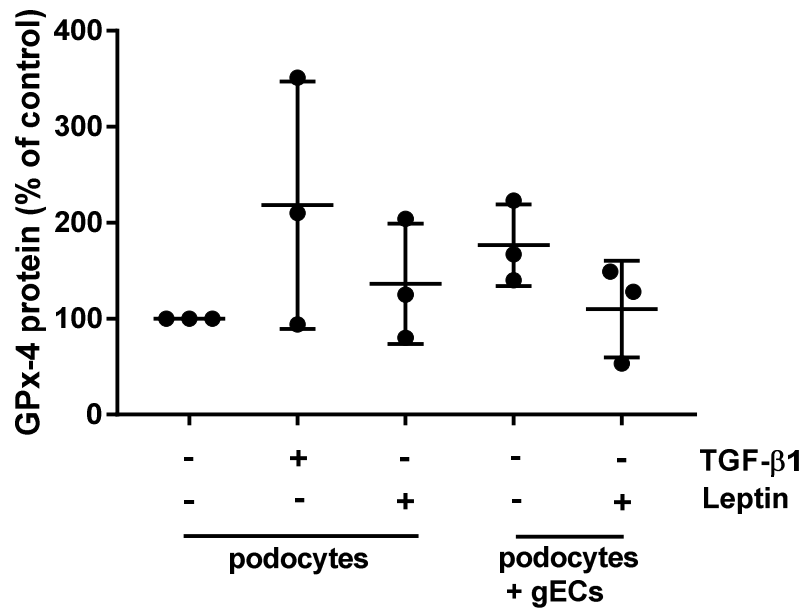


Figure 32: Effect of leptin-stimulated gECs co-cultured with primary podocytes on GPx-4 protein abundance in primary podocytes. GPx-4 protein abundance was determined in primary podocytes stimulated with 30 ng/mL of murine recombinant TGF-β1 or 100 ng/mL of murine recombinant leptin, in primary podocytes co-cultured with gECs and in primary podocytes co-cultured with leptin-stimulated gECs. The amount of protein per sample was normalized with β-actin. Unstimulated cells served as control and were set to 100 %. Changes in GPx-4 protein abundance were calculated in percent of the corresponding control value. Means ± SD of n=3 per group are shown.

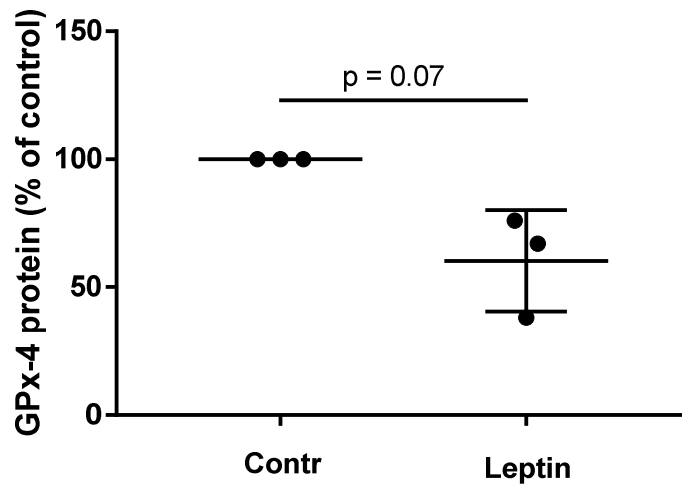


Figure 33: Effect of leptin-stimulated gECs co-cultured with primary podocytes on GPx-4 protein abundance in primary podocytes. GPx-4 protein abundance was determined in primary podocytes co-cultured with gECs and in primary podocytes co-cultured with leptin-stimulated gECs. The amount of protein per sample was normalized with β-actin. Unstimulated cells served as control and were set to 100 %. Changes in GPx-4 protein abundance were calculated in percent of the corresponding control value. Means ± SD of n=3 per group are shown.

To emphasize the potential paracrine TGF- β 1 signaling between leptin-stimulated gECs co-cultured with primary podocytes and the resulting decrease in GPx-4 protein abundance in E11 podocytes, GPx-4 protein abundance was compared between leptin-stimulated gECs co-cultured with primary podocytes and non-stimulated co-cultured primary podocytes. GPx-4 protein abundance was almost significantly reduced by 60 % in primary podocytes co-cultured with leptin-stimulated gECs when compared to the primary podocytes co-cultured with non-stimulated gECs (Figure 33).

6.4 Leptin receptor-deficient mice lacking the long leptin receptor splicing variant (Ob-Rb)

Leptin receptor-deficient mice (B6.BKS(D)-*Lep^{db}*/J) from Jackson Laboratory (Stock number 000697) are characterized by an insert of 106 bp in the long leptin receptor splice variant Ob-Rb (Chen, Charlat et al. 1996, Lee, Proenca et al. 1996). This insert has the same base pair sequence as the short leptin receptor splice variant Ob-Ra, which consists of a premature stop codon (Figure 34) (Chen, Charlat et al. 1996, Lee, Proenca et al. 1996). Thus, in db/db mice truncated leptin receptor transcript 1 (Ob-Rb) and leptin receptor 3 (Ob-Ra) are both translated into leptin receptor Ob-Ra (Chen, Charlat et al. 1996).

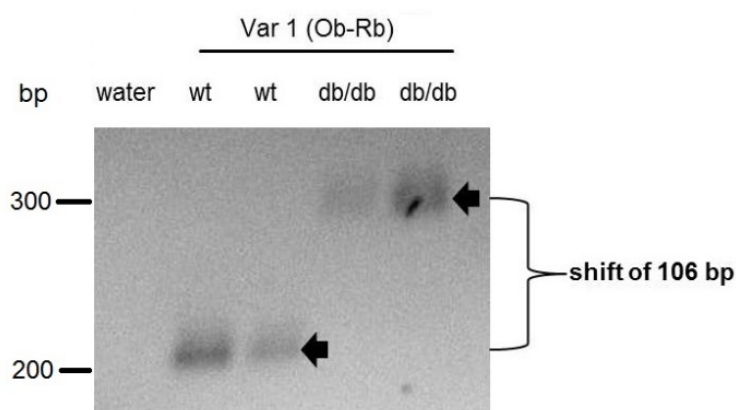


Figure 34: Exemplary image of an agarose gel showing PCR products of leptin receptor 1 (Ob-Rb) in wild-type and db/db mice (primer sequence according to Hermann Kalwa et al. Cellular Physiology (2014)).

6.5 Ex vivo data

6.5.1 Extracellular matrix expansion in the glomeruli of 32-42 weeks old *fpn*^{+/-} and db/db mice

Diabetic nephropathy is characterized by an expansion of the mesangium, which consists of mesangial cells and extracellular matrix. Glycoproteins of the extracellular matrix as well as glycoproteins on the surface of cell membranes can be visualized with a PAS (periodic acid Schiff) reaction. Thus, cryosections of kidneys from 24 and from 32-42 weeks old db/db mice, their heterozygous littermates, iron overload-simulating *fpn*^{+/-} mice and db/db/*fpn*^{+/-} mice were first incubated with Schiffs reagent and subsequently with hematoxylin as a counterstain. The amount of extracellular matrix and membranes shown as mean glomerular value in arbitrary units was not altered in heterozygous 24 weeks old db/db/*fpn*^{+/-} mice as compared to db/db mice (Figure 35).

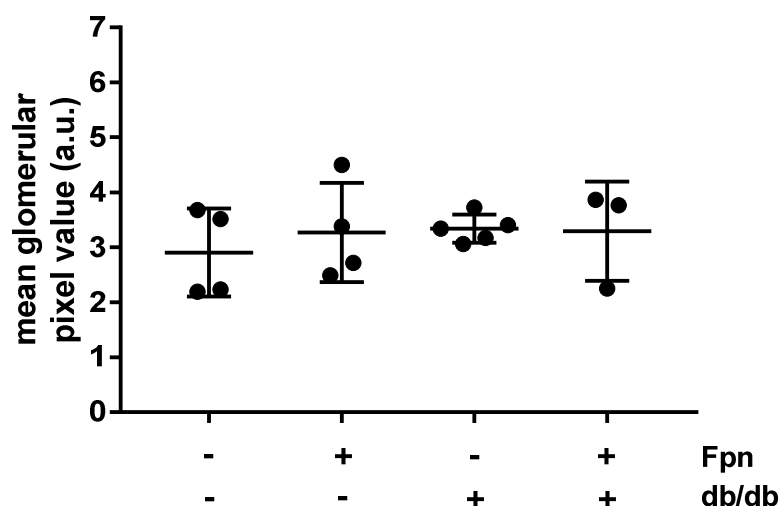


Figure 35: Impact of leptin signaling and impaired iron homeostasis on mesangial expansion and membrane thickening in 24 weeks old male mice. Extracellular matrix accumulation and membrane thickening was determined by the quantification of the PAS positive staining in cryosections of kidneys from 24 weeks old male db/db mice, their heterozygous littermates, *fpn*^{+/-} mice and db/db/*fpn*^{+/-} mice. The values obtained for the PAS staining were normalized with the area of the glomerulus and shown as a mean glomerular pixel value in arbitrary units with a standard deviation. Means \pm SD of n=3-5 per group are shown.

The amount of extracellular matrix and membranes of homozygous db/db mice was also not changed compared to their heterozygous littermates. There was also no change in the amount extracellular matrix and membranes of db/db/*fpn*^{+/-} mice detectable. Thus, an impaired iron homeostasis (systemic iron overload) as well as impaired leptin signaling did not change the amount of extracellular matrix and membranes in 24 weeks old male mice.

In 32-42 weeks old male mice the amount of extracellular matrix and membranes shown as mean glomerular value in arbitrary units was increased by 41 % albeit not significantly in heterozygous 24 weeks old *db/db/fpn^{+/-}* mice as compared to *db/db* mice (Figure 36). The amount of extracellular matrix and membranes of homozygous *db/db* mice was significantly increased by 28% as compared to their heterozygous littermates. There was no significant change in the amount of extracellular matrix and membranes of *db/db/fpn^{+/-}* mice detectable compared to the *db/db* mice. Remarkably, the trends seen in the *fpn^{+/-}* mice and the significant difference seen in the *db/db* homozygous mice seemed to be accumulated in *db/db/fpn^{+/-}* mice compared to the control mice. The amount of extracellular matrix and membranes of *db/db/fpn^{+/-}* mice was significantly increased by 72% as compared to the control mice. Both, an impaired iron homeostasis (systemic iron overload) as well as impaired leptin signaling seemed to have an impact of the amount of extracellular matrix and membranes in 32-42 weeks old male mice.

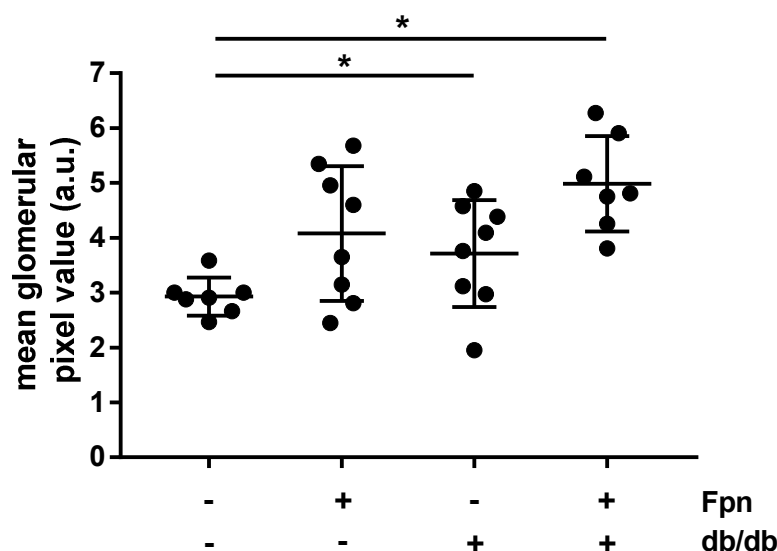


Figure 36: Impact of leptin signaling and impaired iron homeostasis on mesangial expansion and membrane thickening in 32-42 weeks old male mice. Extracellular matrix accumulation and membrane thickening was determined by the quantification of the PAS positive staining in cryosections of kidneys from 32-42 weeks old male *db/db* mice, their heterozygous littermates, *fpn^{+/-}* mice and *db/db/fpn^{+/-}* mice. The values obtained for the PAS staining were normalized with the area of the glomerulus. Means \pm SD of n=7-8 per group are shown. *p<0.05 as indicated

6.5.2 Iron accumulation in the glomeruli of 32-42 weeks old *fpn^{+/-}* mice

An impaired iron homeostasis (systemic iron overload) was associated with T2D in humans. As a consequence, epithelial cells in the liver had increased levels of stored iron. We hypothesized that epithelial cells in the kidney suffer as well from increased iron storage.

Therefore, iron in cryosections of kidneys from 24 weeks old and from 32-42 weeks old db/db mice, their heterozygous littermates, *fpn*^{+/-} mice and db/db/*fpn*^{+/-} mice was stained. DAB advanced pearls staining was applied to visualize stored iron in the glomeruli of the respective mice. The amount of stored iron in the glomeruli shown as mean DAB intensity was not altered in 24 weeks old db/db mice, *fpn*^{+/-} mice and db/db/*fpn*^{+/-} mice compared to the control mice. Thus, an impaired iron homeostasis (systemic iron overload) as well as impaired leptin signaling did not change the amount stored iron in the glomeruli of 24 weeks old male mice.

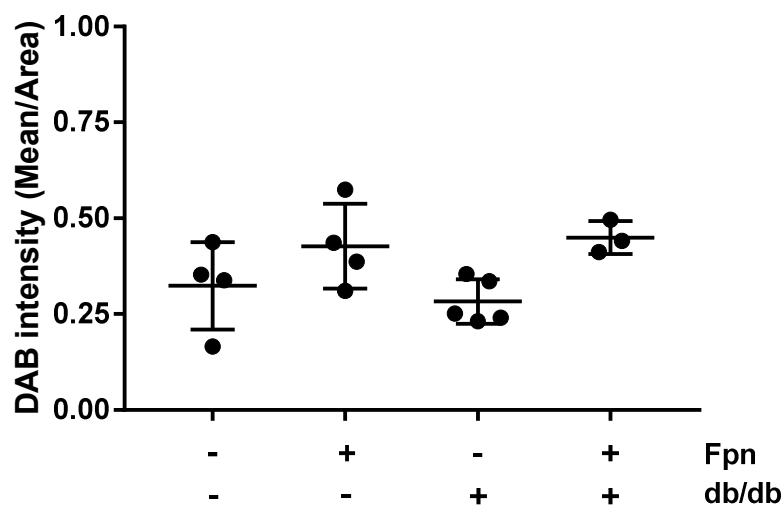


Figure 37: Impact of leptin signaling and impaired iron homeostasis on iron accumulation in the glomeruli of 24 weeks old male mice. Iron accumulation in the glomeruli was determined by the quantification of the DAB advanced pearls staining in cryosections of kidneys from 24 weeks old male db/db mice, their heterozygous littermates, *fpn*^{+/-} mice and db/db/*fpn*^{+/-} mice. The values obtained for the pearls staining were normalized with the area of the glomerulus. Means \pm SD of n=3-5 per group are shown.

In 32-42 weeks old male mice the amount of stored iron in the glomeruli shown as mean DAB intensity was significantly increased by 150 % in 24 weeks old *fpn*^{+/-} mice and by 190 % in 24 weeks old db/db/*fpn*^{+/-} mice compared to their homozygous littermates (Figure 38). Moreover, the amount of stored iron in the glomeruli of db/db mice was not altered compared to their heterozygous littermates. The iron accumulation seen in *fpn*^{+/-} mice seemed to be enhanced in db/db/*fpn*^{+/-} mice compared to the control mice. An impaired leptin signaling seemed to enhance the amount of stored iron in 32-42 weeks old male mice suffering from an impaired iron homeostasis (systemic iron overload).

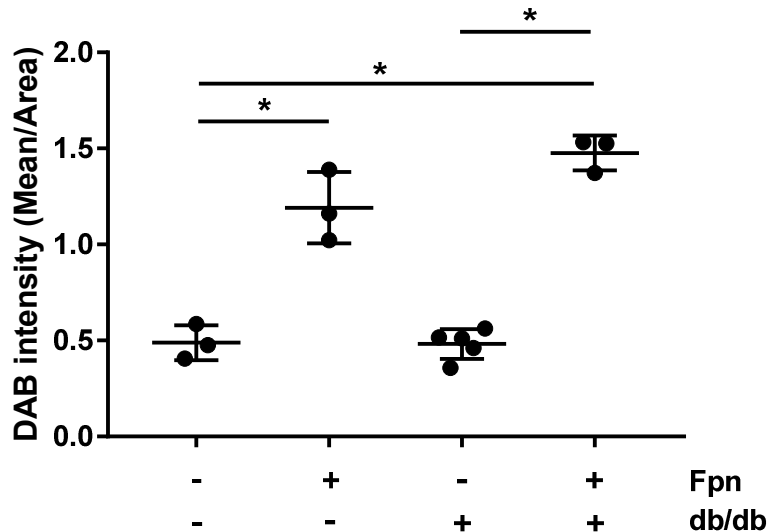


Figure 38: Impact of leptin signaling and impaired iron homeostasis on iron accumulation in the glomeruli of 32-42 weeks old male mice. Iron accumulation in the glomeruli was determined by the quantification of the DAB advanced pearls staining in cryosections of kidneys from 32-42 weeks old male db/db mice, their heterozygous littermates, *fpn*^{+/-} mice and db/db/*fpn*^{+/-} mice. The values obtained for the pearls staining were normalized with the area of the glomerulus. Means \pm SD of n=3-5 per group are shown. *p<0.05 as indicated

6.5.3 GPx-4 protein reduction in the glomeruli of 32-42 weeks old db/db mice

Reduced amounts of GPx-4 protein in the glomeruli are associated with T2D in humans. In order to test whether this observation is also true for our T2D mouse models, GPx-4 was stained in cryosections of kidneys from 24 weeks old and from 32-42 weeks old db/db mice, their heterozygous littermates, *fpn*^{+/-} mice and db/db/*fpn*^{+/-} mice.

The amount of GPx-4 protein in the glomeruli shown as GPx-4 protein (in % of control) was not altered in heterozygous 24 weeks old Fpn mice compared to their homozygous littermates (Figure 39), whereas it was significantly increased by 35 % in homozygous db/db mice compared to their heterozygous littermates. In contrast, GPx-4 protein abundance was not altered db/db/*fpn*^{+/-} mice compared to the control mice. Thus, a mildly impaired leptin signaling seemed to increase the amount of GPx-4 protein in the glomeruli of these mice. This beneficial effect was revised in the db/db/*fpn*^{+/-} mice.

The area of the synaptopodin stained glomeruli was slightly increased (p=0.05) in 24 weeks old *fpn*^{+/-} mice and in db/db/*fpn*^{+/-} mice compared to the control mice (Figure 40), whereas it was significantly increased by 32 % in db/db mice compared to *fpn*^{+/-} mice. Thus, impaired

leptin signaling at the beginning of the disease seemed to increase the size of the glomeruli of 24 weeks old male mice.

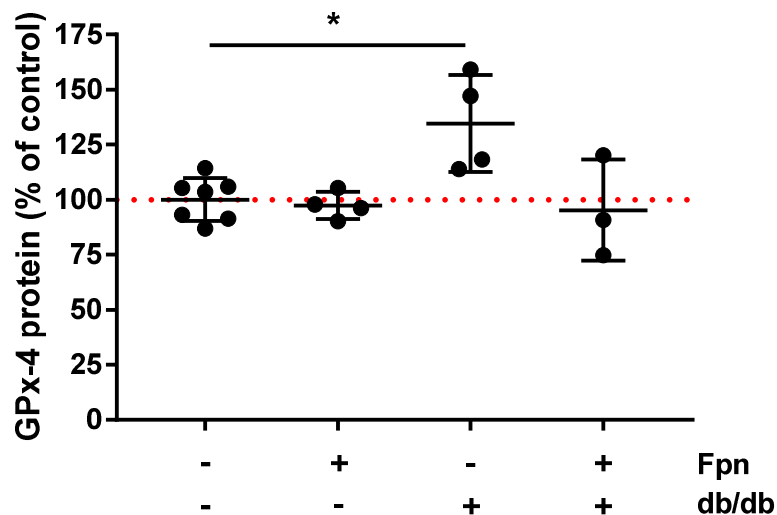


Figure 39: Impact of leptin signaling and impaired iron homeostasis on total GPx-4 protein abundance in the glomeruli of 24 weeks old male mice. Positive GPx-4 staining was quantified as mean intensities (as described in MM (section 5.1.9, page 52) from cryosections of kidneys from 24 weeks old male db/db mice, their heterozygous littermates, *fpn*^{+/-} mice and db/db/*fpn*^{+/-} mice. Means \pm SD of n=3-7 per group are shown. *p<0.05 as indicated

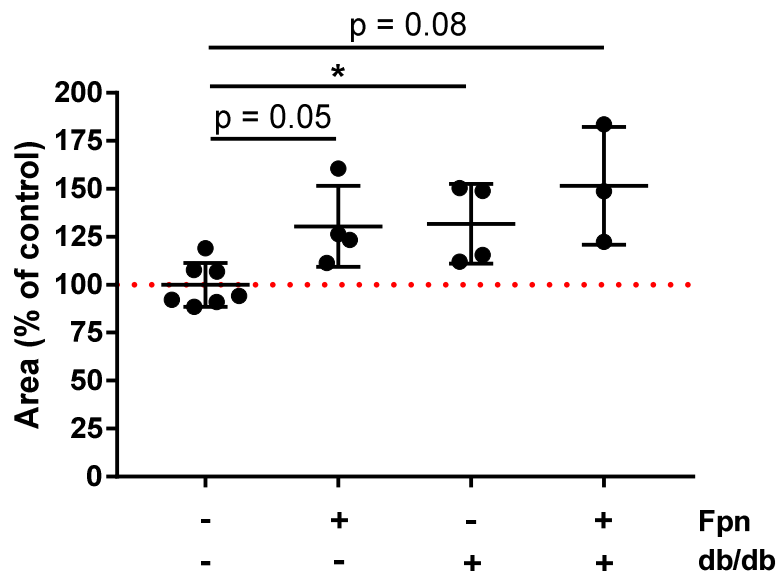


Figure 40: Impact of leptin signaling and impaired iron homeostasis on the size of the glomeruli of 24 weeks old male mice. The area of the synaptopodin stained glomeruli was determined in cryosections of kidneys from 24 weeks old male db/db mice, their heterozygous littermates, *fpn*^{+/-} mice and db/db/*fpn*^{+/-} mice. The values obtained were shown as area. Means \pm SD of n=3-7 per group are shown. *p<0.05 as indicated

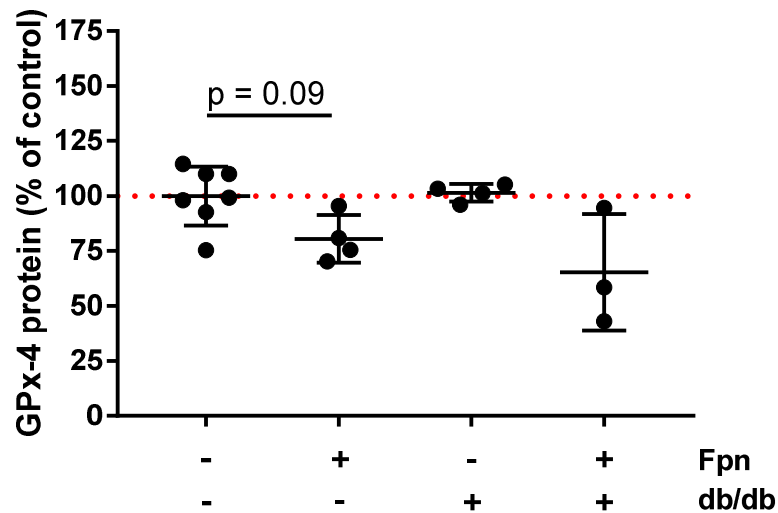


Figure 41: Impact of leptin signaling and impaired iron homeostasis on GPx-4 protein abundance in the glomeruli of 24 weeks old male mice. Positive GPx-4 staining was quantified as mean intensities (as described in MM (section 5.1.9, page 52) from cryosections of kidneys from 24 weeks old male db/db mice, their heterozygous littermates, *fpn*^{+/-} mice and db/db/*fpn*^{+/-} mice. The values obtained from the GPx-4 staining were normalized with the area of the synaptopodin stained glomerulus. Means shown as GPx-4 protein abundance/area \pm SD of n=3-7 per group are shown.

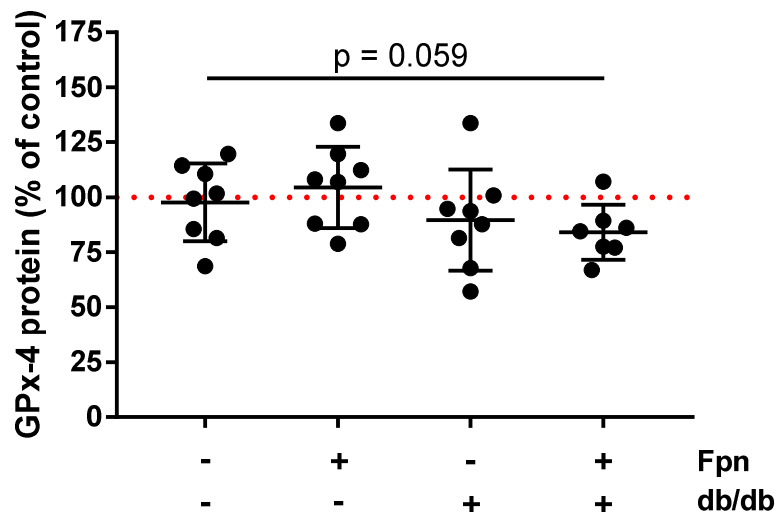


Figure 42: Impact of leptin signaling and impaired iron homeostasis on GPx-4 protein abundance in the glomeruli of 32-42 weeks old male mice. Positive GPx-4 staining was quantified as mean intensities (as described in MM (section 5.1.9, page 52) from cryosections of kidneys from 32-42 weeks old male db/db mice, their heterozygous littermates, *fpn*^{+/-} mice and db/db/*fpn*^{+/-} mice. Means \pm SD of n=7-8 per group are shown.

The amount of GPx-4 protein per area in the glomeruli was not altered in 24 weeks old *fpn*^{+/-} mice compared to their homozygous littermates (Figure 41), in db/db mice compared to their heterozygous littermates and in db/db/*fpn*^{+/-} mice compared to the control mice. Thus, an

impaired iron homeostasis (systemic iron overload) as well as impaired leptin signaling did not change the amount of GPx-4 protein abundance/area in the glomeruli of 24 weeks old male mice.

The amount of GPx-4 protein in the glomeruli was not changed in heterozygous 32-42 weeks old *fpn*^{+/-} mice compared to their homozygous littermates (Figure 42), as well as in db/db mice compared to their heterozygous littermates. In db/db/*fpn*^{+/-} mice compared to the control mice the total amount of GPx-4 was reduced by 20%. Thus, combination of leptin signaling and impaired iron homeostasis (iron overload) decreased the amount of GPx-4 protein in the glomeruli of 32-42 weeks old male mice.

Next the area of the synaptopodin stained glomeruli was compared between the respective groups of 32-42 weeks old male mice. There was no change in the total size of the glomeruli in 32-43 weeks old male *fpn*^{+/-} mice compared to their homozygous littermates (Figure 43). The size of the glomeruli in db/db mice compared to their heterozygous littermates was not changed as well.

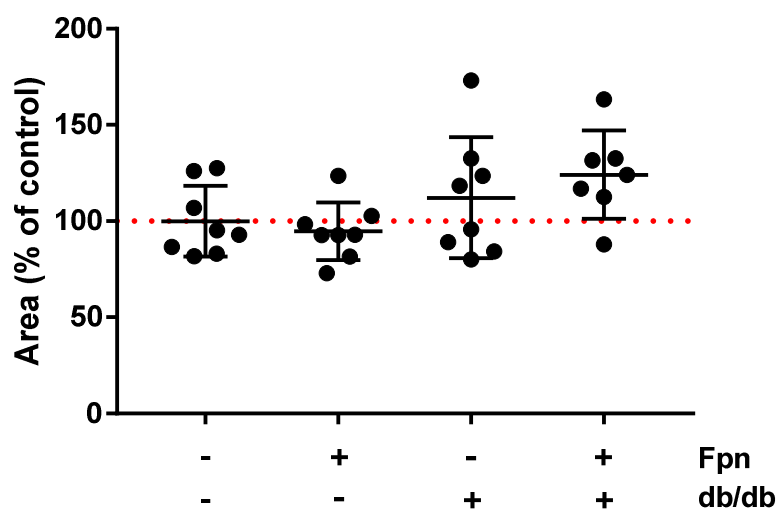


Figure 43: Impact of leptin signaling and impaired iron homeostasis on the size of the glomeruli of 32-42 weeks old male mice. The area of the glomeruli was determined in cryosections of kidneys from 32-42 weeks old male db/db mice, their heterozygous littermates, *fpn*^{+/-} mice and db/db/*fpn*^{+/-} mice. Means ± SD of n=7-8 per group are shown.

Moreover, in db/db/*fpn*^{+/-} mice the size of the glomeruli was non-significantly increased by 25 % compared to the control mice. Summarized, an impaired leptin signaling slightly changed the glomerular area of 32-42 weeks old male mice. This effect seemed to be more enhanced in the db/db/*fpn*^{+/-} mice.

In the last step the amount of GPx-4 protein per area in the synaptopodin stained glomeruli was determined and compared between the respective groups of mice at the age of 32-42

weeks. The amount of GPx-4 protein per area was not altered 32-42 weeks old *fpn*^{+/-} mice compared to their homozygous littermates (Figure 44). In contrast, the amount of GPx-4 protein per area was non-significantly reduced by 32 % in db/db mice compared to their heterozygous littermates. Moreover, the amount of GPx-4 protein per area was significantly reduced by 37 % in db/db/*fpn*^{+/-} mice compared to the respective control mice.

Summarized, an impaired leptin signaling changed the amount of GPx-4 protein abundance/area in the glomeruli of 32-42 weeks old male mice. This effect seemed to be more enhanced in the db/db/*fpn*^{+/-} mice. Thus, during the progression of the disease the combination of impaired leptin signaling and iron overload decreased the amount of GPx-4 in 32-42 weeks old male mice.

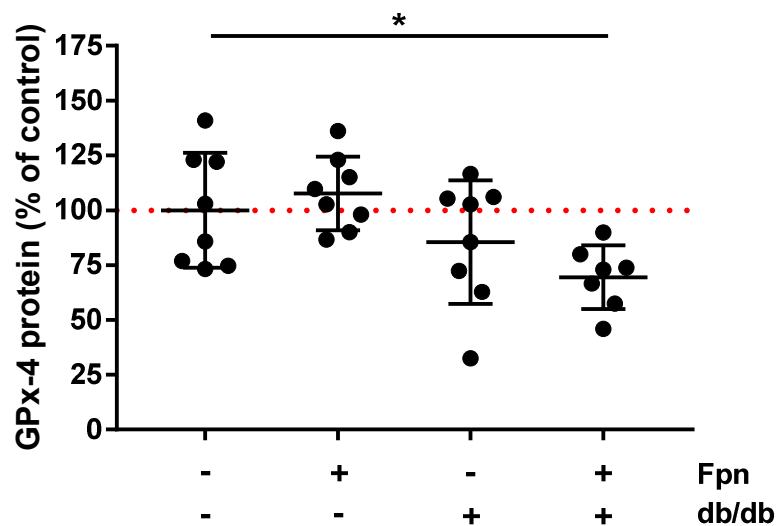


Figure 44: Impact of leptin signaling and impaired iron homeostasis on GPx-4 protein abundance in the glomeruli of 32-42 weeks old male mice. Positive GPx-4 staining was quantified as mean intensities (as described in MM (section 5.1.9, page 52) from cryosections of kidneys from 32-42 weeks old male db/db mice, their heterozygous littermates, *fpn*^{+/-} mice and db/db/*fpn*^{+/-} mice. The values obtained from the GPx-4 staining were normalized with the area of the synaptopodin stained glomerulus. Means shown as GPx-4 protein abundance/area \pm SD of n=7-8 per group are shown. *p<0.05 as indicated

6.5.4 GPx-4 protein abundance is not altered in the glomeruli of 23 weeks old ob/ob mice

In order to test whether the reduction in the amount of GPx-4 protein abundance/area in the glomeruli of 32-42 weeks old male db/db/*fpn*^{+/-} mice is mediated through the binding of the hormone leptin to the short splice variants of the leptin receptor ObRa and ObRc, ob/ob mice

have been used as a control group. Thus, GPx-4 was stained in cryosections of kidneys from 23 weeks old ob/ob mice as well as from kidneys of their heterozygous littermates.

The amount of GPx-4 protein in the glomeruli was not altered in homozygous ob/ob mice compared to their heterozygous littermates (Figure 45). Thus, in the absence of leptin, hence leptin signaling, the amount of GPx-4 protein in the glomeruli of 23 weeks old male ob/ob mice is not altered.

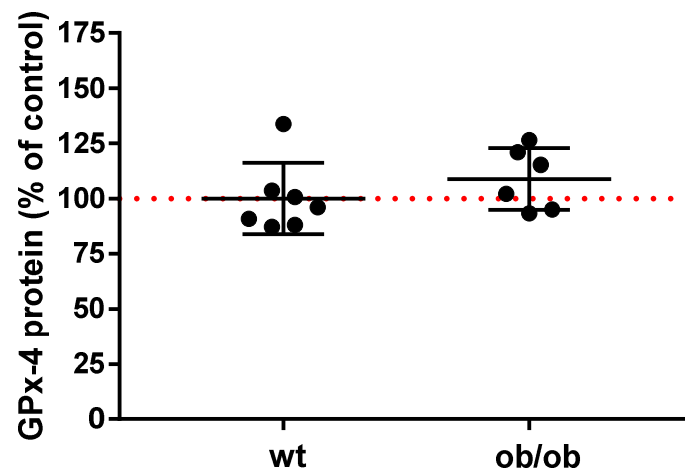


Figure 45: Impact of leptin deficiency on mean GPx-4 protein abundance in the glomeruli of 23 weeks old male mice. Positive GPx-4 staining was quantified as mean intensities (as described in MM (section 5.1.9, page 52) from cryosections of kidneys from 23 weeks old male ob/ob mice as well as from their heterozygous littermates. Means \pm SD of n=6-7 per group are shown.

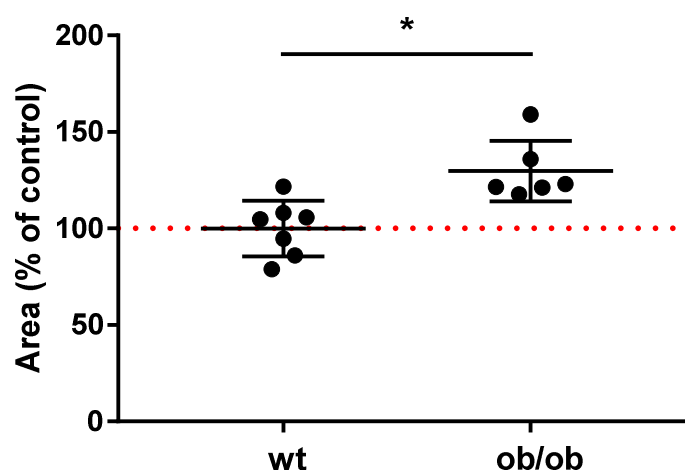


Figure 46: Impact of leptin deficiency on the size of the glomeruli of 23 weeks old male mice. The area of the synaptopodin stained glomeruli was determined in cryosections of kidneys from 23 weeks old male ob/ob mice, as well as from their heterozygous littermates. Means \pm SD of n=6-7 per group are shown. *p<0.05 as indicated

In the next step the area of the synaptopodin stained glomeruli was compared between the two groups of mice. In homozygous ob/ob mice the size of the glomeruli was significantly increased by 30 % when compared to the heterozygous control mice (Figure 46). The disease has already progressed, thus the size of the glomeruli of 23 weeks old male ob/ob mice is significantly increased.

In the last step the amount of GPx-4 protein per area in the glomeruli was determined and compared between the two groups of mice.

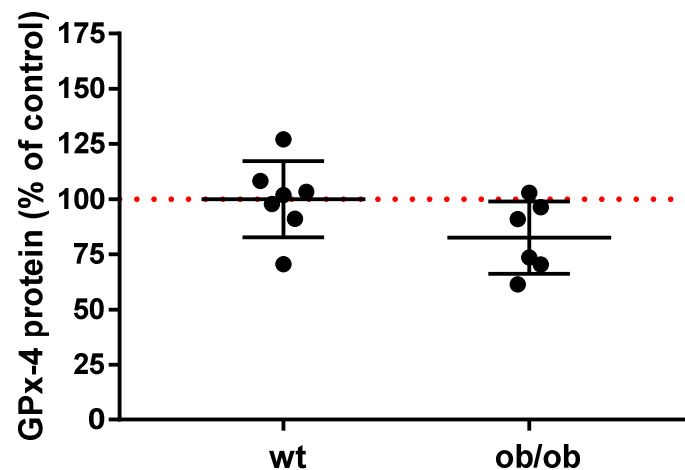


Figure 47: Impact of leptin deficiency on the size of the glomeruli of 23 weeks old male mice. Positive GPx-4 staining was quantified as mean intensities (as described in MM (section 5.1.9, page 52) from cryosections of kidneys from 23 weeks old male ob/ob mice, as well as from their heterozygous littermates. The values obtained from the GPx-4 staining were normalized with the area of the glomerulus. Means shown as GPx-4 protein abundance/area \pm SD of n=6-7 per group are shown.

The amount of GPx-4 protein per area was not significantly altered in homozygous 23 weeks old ob/ob mice compared to their heterozygous littermates (Figure 47). Thus, in the absence of leptin the amount of GPx-4 protein abundance/area was not changed in the glomeruli of 23 weeks old male mice.

7. Discussion

7.1 The source of reactive oxygen species in T2D

All cells produce ROS on a continuous basis and at a steady-state level under normal physiological conditions (Ray, Huang et al. 2012, Haas and Staels 2016). Under conditions of excessive glucose production (Tang, Luo et al. 2014), it is still unclear whether ROS cause or merely correlate with diabetic complications (Kashihara, Haruna et al. 2010). ROS play a crucial role in signal transduction processes (Fattman, Schaefer et al. 2003) such as in some ligand-receptor interactions (Ray, Huang et al. 2012). Prominent examples for such ligand-receptor interactions are the cytokines tumor necrosis factor α or interleukin-1 β (Haas and Staels 2016). In addition, ROS can activate kinases and phosphatases and therefore change the degree of phosphorylation of other proteins (Ray, Huang et al. 2012, Haas and Staels 2016). Moreover, ROS can interfere with gene expression via modulation of transcription factors (Brieger, Schiavone et al. 2012).

There is evidence for increased ROS levels in kidneys in experimental diabetes (Poulianiti, Kaltsatou et al. 2016, Cooper, El-Osta et al. 2018). There is also evidence for increased ROS in clinical diabetes (Tavafi 2013, Poulianiti, Kaltsatou et al. 2016, Cooper, El-Osta et al. 2018). Moreover, increased oxidative stress could be verified in patients with diabetes by measuring thiobarbituric acid reactive substances (TBARS) like malondialdehyde (MDA) and 4-hydroxynonenal (4-HNE) (Martín-Gallán, Carrascosa et al. 2003). MDA does not exclusively originate from breakdown of polyunsaturated fatty acids (PUFAS) (Browne and Armstrong 2000). Thus, it is only a marker for oxidative stress but does not give any information from where and how ROS emerge. Some authors claim NADPH oxidases (NOX) have an important role in the progression of diabetes as they contribute to ROS formation (Gill and Wilcox 2006). The isoform NOX-4, which is predominately expressed in the kidney cortex and produces hydrogen peroxide only, is upregulated in *in vitro* experiments using hyperglycemic conditions (Thallas-Bonke, Jandeleit-Dahm et al. 2015).

These studies provide experimental as well as clinical evidence that diabetes can be characterized by increased oxidative stress, but this phenotype is not necessarily associated with alterations in mitochondrial function (Newsholme, Haber et al. 2007, Cooper, El-Osta et al. 2018). In summary, almost all published studies have shown a uniform “over-production” of ROS in the tissues of animals and patients with diabetes (Zhang, Darshi et al. 2018). Moreover, ebselen, a pharmacologic analog to GPx-1, can improve proteinuria and limits the overall degree of diabetic nephropathy in ApoE/GPx-1 knockout mice (Chew, Yuen et al. 2010).

In hyperglycemic conditions ATP production is switched from oxidative phosphorylation to glycolysis. Superoxide dismutase (SOD) levels are not altered in people suffering from T2D (Zhang, Darshi et al. 2018). There is also no evidence that superoxide is increased in patients with T2D (Zhang, Darshi et al. 2018). Therefore, we do not assume that alternative pathways are activated. Thus, we think hyperglycemia itself is not the driving cause for developing diabetic nephropathy. Moreover, this shows us that there is no increase in ROS production. In contrast, H₂O₂ levels are increased but not at mitochondrial sides (Zhang, Darshi et al. 2018). We conclude there seems to be a problem with ROS detoxification.

7.2. Detection of leptin receptor splice variants

One overarching goal of this thesis was to show on a qualitative and on a quantitative level that the CI-muMECs as well as the gECs contain the transcripts of the leptin receptor splice variants Ob-Rb, Ob-Ra and Ob-Rc. As mentioned in chapter 3.3 the long leptin receptor splicing variant Ob-Rb is highly abundant in the hypothalamus and known to be responsible for leptin signaling causing a decrease of food intake and an increase of energy expenditure. Until today it is not known whether leptin resistance is caused by the inability of leptin to bind to its receptor Ob-Rb or an impaired transport via the blood-brain barrier. In peripheral tissues, the short splice variants Ob-Ra and Ob-Rc are highly abundant (Goto, Kaneko et al. 2016). We could confirm that in CI-muMECs the amount of Ob-Ra transcript is 3.3-fold higher compared to the Ob-Rb transcript, and in gECs the amount of Ob-Ra is 1.4-fold higher compared to Ob-Rb. Even though it was long time believed that only Ob-Rb is able to transmit a signal downstream, more and more publications claim that also the short leptin receptor splice variants are able to transmit a signal downstream (Goto, Kaneko et al. 2016). Thus, high leptin concentrations as detected in patients with T2D should lead to increased downstream signaling in these cells. It needs to be determined which leptin receptor splice variant is responsible for leptin signaling in other organs as the brain, such as e.g. the kidney.

7.3. Cell culture

7.3.1 TGF- β 1 mRNA expression and active TGF- β 1 in the supernatant of leptin-stimulated endothelial cells

Leptin levels are five times higher in obese people (40 ng/mL leptin) compared to healthy individuals (8 ng/mL leptin) (Li, Shen et al. 2013). We could show, that endothelial cells contain transcripts of the leptin receptor. Moreover, it was published that gECs release TGF- β 1 in co-culture with in the presence of epithelial cells (proximal tubular epithelial cells) (Zhao, Zhao et al. 2014). Furthermore, leptin induces hepatic fibrosis most likely through the action of TGF- β 1 (Honda, Ikejima et al. 2002). In addition, it was shown that gECs respond to leptin with an increased secretion of TGF- β 1 (Wolf, Chen et al. 2002). Thus, we investigated whether CI-muMECS and gECs respond to leptin binding.

CI-muMECs did not respond to leptin stimulation on the transcriptional level. We could not detect an increase of TGF- β 1 transcripts in leptin-stimulated CI-muMECs compared to non-stimulated controls. Thus, we assumed a potential role in TGF- β 1 processing in response to leptin-stimulation. Indeed, we measured a significant 1.6-fold increase of activated TGF- β 1 in the cell culture medium of leptin-stimulated CI-muMECs (100 ng/mL) compared to the non-stimulated controls. We could confirm this result analyzing the cell culture medium of leptin-stimulated gECs. In this case, we measured a significant 1.24-fold increase of activated TGF- β 1 in the cell culture medium of leptin-stimulated gECs (100 ng/mL) compared to the non-stimulated controls. The observed different fold-changes between CI-muMECs (1.24) and gECs (1.6) can be explained by different background levels of naïve TGF- β 1 in the FCS of the respective medium. To avoid such differences naïve TGF- β 1 could be depleted using TGF- β 1 antibody coupled magnetic beads before incubating the endothelial cells with the respective medium. It is not known, which leptin receptor splicing variant is responsible for the observed signaling. We can only predict at this point that one of the small splice variants is involved resulting in JAK/STAT signaling, even though it is not confirmed that the short splice variants are able to signal via this signaling pathway (Han, Isono et al. 2001). Consequently, phosphorylated STAT 1,3 heterodimers might translocate to the nucleus activating gene transcription. Potential candidate genes might be metalloproteases, inter alia metalloprotease 9 (MMP9) (Travis and Sheppard 2014). Furthermore, leptin has the potential to induce ROS in endothelial cells (Adya, Tan et al. 2015). ROS on the other hand can cleave both, TGF- β 1 and MMP9 resulting in active TGF- β 1 and active MMP9. Besides ROS or changes in the pH, MMP9 is one of the factors that can cleave TGF- β 1 resulting in active TGF- β 1 as well (Liu and Desai 2015). People suffering from T2D have high circulating leptin

levels. Thus, we assume leptin increases the release/activation of TGF- β 1 from the matrix of glomerular endothelial cells in these people. Moreover, TGF- β 1 reduces podocyte adhesion to the glomerular basal membrane via downregulation of α 3 β 1 integrin (Wolf, Chen et al. 2002, Wolf 2004, Vallon and Komers 2011). It might induce epithelial to mesenchymal transition of podocytes by attenuating epithelial markers and by acquisition of mesenchymal markers resulting in podocyte depletion (Miyazono 2009). Moreover, TGF- β 1 impairs the architecture of slit-diaphragm (Vallon and Komers 2011), alters the perm-selectivity of podocytes and increases podocyte apoptosis (Wolf, Chen et al. 2002, Vallon and Komers 2011).

7.3.2. GPx-1 and GPx-4 protein abundance in leptin-stimulated or TGF- β 1-stimulated E11 podocytes

A podocyte loss was observed in kidney biopsies from people with T2D suffering from diabetic nephropathy as well as in mouse models mimicking the human disease (Susztak, Raff et al. 2006). It is not known whether podocyte loss occurs early at the stage of microalbuminuria or late at the stage of ESRD. It is also unknown whether podocyte foot process enfacement causing podocyte detachment and hence podocyte loss into the urine (Vogelmann, Nelson et al. 2003) is responsible for this loss of podocytes or whether podocytes simply die from a regulated or a non-regulated form of cell death. Some authors claim podocytes detach from the GBM during the progression of the disease (Petermann, Krofft et al. 2003). The only available data was generated in an experimental membranous nephropathy set-up, not reflecting the pathophysiological conditions observed in diabetic nephropathy in humans or mouse models mimicking the human disease. In line with the genome wide association studies (Zhang, Darshi et al. 2018) we assume that podocyte loss occurs early at the stage of microalbuminuria (Schiffer, Susztak et al. 2005) and is caused by a regulated cell death termed ferroptosis. Therefore, we came up with the hypothesis that an inadequate detoxification of hydrogen peroxide as well as lipid hydroperoxides causes irreversible damage to the podocytes, which ends with their ferroptotic cell death and therefore with a loss of these cells. For this reason, the amount of GPx-1 and especially GPx-4 protein was analyzed in E11 podocytes after exposure to either leptin or TGF- β 1. Leptin itself had no impact on GPx-1 or GPx-4 protein abundance. Moreover, the amount of GPx-1 protein was not altered after TGF- β 1 stimulation. Contrary to our findings, it was published that TGF- β 1 can induce GPx-1 in colon cancer cells (Huang, Fang et al. 2012). Furthermore, in TGF- β 1-stimulated E11 podocytes the amount of GPx-4 protein was

significantly reduced in a dose-dependent as well as in a time-dependent manner. These findings are in line with publications showing that TGF- β 1 can suppress the antioxidant defense by inducing redox imbalances (Liu and Desai 2015). The kinetics of primary podocytes seemed to be different as short-time (24-48 hours) exposure to TGF- β 1 as the GPx-4 protein content was not changed. The response of primary podocytes might be delayed a few days, compared to the E11 podocytes, because other naturally occurring signaling pathways might interfere with the observed TGF- β 1 signaling. Thus, the time of future experiments should be prolonged a few days to receive a similar downregulation of the amount of GPx-4 protein obtained from TGF- β 1-stimulated E11 podocytes.

7.3.3. GPx-4 protein abundance in E11 podocytes exposed to TGF- β 1 and/or iron overload

Ferroptosis is characterized by a reduction of GPx-4 activity and/or protein abundance, an accumulation of lipid peroxides and excess iron. The source of iron remains unknown. Some authors described ferroptosis as an autophagic cell death of ferritin (Gao, Monian et al. 2016). They concluded that this is the reason for a dramatic increase of the labile iron pool. More iron causes more Fenton reaction (Lee, Choi et al. 2015). Thus, more lipid peroxides are generated. In order to test this hypothesis iron donors were added to the pre-existing set-up. The iron donors apotransferrin and holotransferrin seemed to have no additional effect on the downregulation of GPx-4 protein abundance in TGF- β 1-stimulated E11 podocytes. The iron donor FeNTA (Lee, Choi et al. 2015) added to TGF- β 1-stimulated E11 podocytes did also not change the amount of GPx-4 protein in E11 podocytes. Thus, hyperglycemic conditions might be necessary to initiate the self-reinforcing feedback loop.

7.3.4. GPx-4 protein abundance in E11 podocytes exposed to TGF- β 1 and/or iron overload in high-glucose medium

Even though we believe that hyperglycemia is not the primary course for developing diabetic nephropathy (Falkevall, Mehlem et al. 2017), we have to consider that podocytes are more susceptible to high glucose concentrations, as their regulation of glucose uptake is different compared to other cells types and can be triggered by the glucose concentration or by mechanical stress (Lewko, Bryl et al. 2005). Thus, we hypothesized that in addition to the exposure to TGF- β 1 and an iron donor, hyperglycemic conditions (30 mM glucose) are

necessary to initiate the feedback loop. Therefore, E11 podocytes were exposed to TGF- β 1 and holotransferrin under hyperglycemic conditions. Remarkably, we could not detect a further downregulation of GPx-4 protein, compared to the E11 podocytes cultured with normal glucose (5 mM glucose). Moreover, we assumed that iron has an indirect influence on GPx-4, not by causing a stronger reduction of the GPx-4 protein amount but rather by inhibiting the GPx-4 activity through this increased glutathione consumption. Thus, GPx-4-specific activity was measured in E11 podocytes treated with TGF- β 1 and holotransferrin under hyperglycemic conditions for 3 days. Indeed, we could show that GPx-4 activity is reduced by 29% in these cells compared to the control group. This effect was similar to the observed reduction on the protein level. We therefore conclude that the overall reduction of GPx-4 activity is due to the reduction of GPx-4 protein. In the cell culture system GPx can be blocked with erastin. Erastin blocks system Xc, which is an antiporter transporting glutamate outside the cell and cystine inside the cell (Yang, SriRamaratnam et al. 2014, Conrad and Friedmann Angeli 2015, Shah, Shchepinov et al. 2018). Cystine is then converted to cysteine and used for synthesizing glutathione. Besides its ability to unspecifically block the activity of all GPx, GPx-4 can be specifically and directly inhibited by the Ras small molecule like inhibitor 3 (RSL-3) (Yang, SriRamaratnam et al. 2014, Shah, Shchepinov et al. 2018). We could show that RSL-3 is a potent GPx-4 inhibitor which inhibits the activity of GPx-4 by 100 % *in vitro* mimicking the *in vivo* situation of patients suffering from T2D. Clinical studies have shown that patients suffering from T2D exhibit significantly less GPx-4 enzyme and a subsequent accumulation of HNE-adducts in their hearts compared to healthy individuals (Katunga, Gudimella et al. 2015).

7.3.5. GPx-4 expression in podocytes co-cultured with endothelial cells

Similar to the situation in the kidney, endothelial cells and podocytes were co-cultivated as described in chapter 6.3.3. We could confirm that GPx-4 protein abundance was significantly reduced in leptin-stimulated E11 podocytes co-cultured with CI-muMECs. The amount of GPx-4 protein was not changed in leptin-stimulated gECs co-cultured with E11 podocytes and co-cultured with primary podocytes. As already discussed in chapter 7.2.4. it is likely that our cell-culture system did not cover all the characteristics which emerge in the pathophysiological state of diabetic nephropathy in humans and in the respective mouse model. It is likely that the simultaneous action of a reduction of GPx-4 protein/activity, excess iron and hyperglycemic conditions is needed. The last point was missing in our co-culture model. Oxidative stress from glucose metabolism (Latunde-Dada 2017) can trigger the feedback loop. As cells constantly metabolize glucose, the glucose in the medium drops

constantly as well. Thus, these cells were only exposed to high glucose concentrations for a short period of time. Therefore, it is likely that hyperglycemia needed to activate and drive the feedback loop was not contributing to the programmed cell death ferroptosis. Glucose consumption experiments are necessary to quantify the amount of consumed glucose per day. In a next step, the amount of metabolized glucose can be added to the co-culture system on a daily basis to ensure constant hyperglycemic conditions. In addition, it might be necessary to prolong the time the cells are co-cultured.

7.4. Leptin receptor-deficient mice lacking the long leptin receptor splicing variant (Ob-Rb)

Even though mouse models of diabetes reflect most of the features of human diabetes, they do not cover all characteristics. During the development and the progression of diabetic nephropathy in mice characteristics such as glomerular hyperfiltration, increased albuminuria and specific histopathologic changes as GBM thickening and expansion of the mesangium are similar to human diabetic nephropathy, whereas diabetic nephropathy in mice never proceeds to ESRD (Breyer, Bottinger et al. 2005). As already discussed in chapter 6.4 db/db mice carry a point mutation in the long leptin receptor splice variant Ob-Rb causing a premature termination of the translation of this splice variant. Moreover, the premature termination of leptin receptor splice variant Ob-Rb leads to the translation of the short splice variant Ob-Ra.

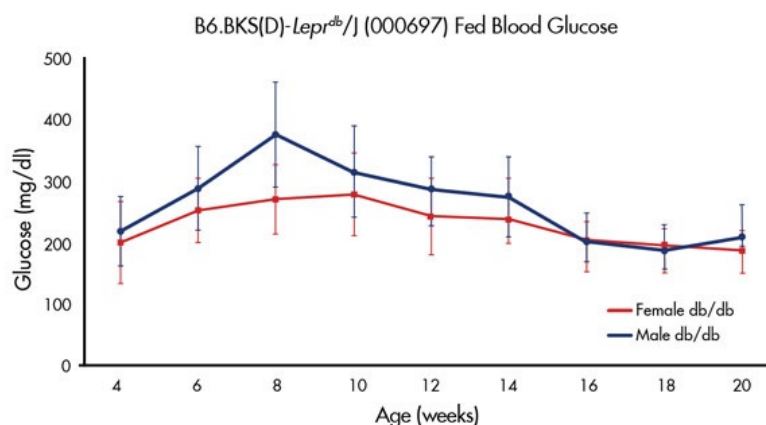


Figure 47: Blood glucose in B6.BKS(D)-Lepr^{db}/J mice. Graph was supplied from Jackson Laboratory

According to our hypothesis, leptin resistance in the brain caused by an impaired leptin transport via the blood-brain-barrier does not imply that leptin signaling in the periphery such as the kidney is impaired. It is likely that leptin binds to the short splice variants causing a

downstream signaling leading to an increased release/activation of TGF- β 1. Furthermore, we think that this effect is more pronounced in db/db mice as truncated transcript Ob-Rb as well as transcript Ob-Ra are both translated into Ob-Ra. The point mutation was first introduced in the BKS mouse strain and then several times backcrossed to the B6 mouse strain. The original mouse strain develops a severe diabetic phenotype with more severe kidney damage. The reason might be the glucose level, as male B6.BKS(D)-Lepr^{db}/J mice are only transiently hyperglycemic. Hyperglycemia increases until 8 weeks of age and drops back to normal level at 12 weeks of age (Figure 47). For this reason, we assume that ferroptosis inter alia podocyte damage is less severe compared to the B6 mouse strain.

7.5. Ex vivo experiments

7.5.1. Extracellular matrix expansion in the glomeruli of 32-42 weeks old *fpn*^{+/-} and db/db mice

Characteristic histopathologic changes of diabetic nephropathy as the expansion of the mesangium were previously described in db/db mice (Sharma, McCue et al. 2003). Thus, we quantified the amount of extracellular matrix in 24 and 32-42 weeks old db/db mice. We could not detect a significant accumulation of extracellular matrix in 24 weeks old db/db mice, in *fpn*^{+/-} mice or in db/db/*fpn*^{+/-} mice compared to the wildtype littermates. In 32-42 weeks old db/db mice, we could detect a significant accumulation of extracellular matrix compared to the wildtype littermates. This effect was more pronounced in the db/db/*fpn*^{+/-} mice. Thus, both iron as well as leptin signaling have a detrimental effect on the kidneys during the progression of the disease, as both contribute to the expansion of the mesangium, a histologic phenotype of diabetic nephropathy (Brosius, Alpers et al. 2009).

7.5.2. Iron accumulation in the glomeruli of 32-42 weeks old *fpn*^{+/-} mice

Previous published data revealed that T2D is associated with a systemic iron overload (Lee, Choi et al. 2015, Altamura, Kopf et al. 2017) that leads to more ROS formation (Lee, Choi et al. 2015, Handa, Morgan-Stevenson et al. 2016). For the first time it was shown that epithelial cells in the liver of db/db mice have a significant higher iron content, compared to their wild-type littermates (Altamura, Kopf et al. 2017). Thus, we investigated whether this is also true for epithelial cells in the kidney. Unfortunately, we could not discriminate between iron-positive podocytes and iron-positive endothelial or mesangial cells and therefore we quantified the amount of iron in the whole glomeruli of the respective mice. There was no iron

accumulation in 24 weeks old *fpn*^{+/-} mice as well as in *db/db/fpn*^{+/-} mice detectable. In 32-42 weeks old *fpn*^{+/-} mice the amount of iron was significantly increased compared to their wildtype littermates. This effect was more pronounced in *db/db/fpn*^{+/-} mice. It was reported that iron has the ability to form complexes with low molecular weight molecules such as glutathione (Fanzani and Poli 2017). This can be crucial, as glutathione is depleted in many diseases (Bertrand 2017). In case of a glutathione depletion below a certain threshold the labile iron pool could be suddenly increased.

7.5.3. GPx-4 protein reduction in the glomeruli of 32-42 weeks old db/db mice

As already discussed there is evidence for increased ROS in kidneys in experimental diabetes, but the data of the activity or the protein abundance of the antioxidative enzymes SOD and catalase are contradictory (Poulianiti, Kaltsatou et al. 2016). Some studies claim the activity or the protein abundance of SOD or catalase is decreased (Fattman, Schaefer et al. 2003), some claim the activity or the protein abundance of SOD or catalase is increased (Thallas-Bonke, Jandeleit-Dahm et al. 2015) in the respective mouse or rat model mimicking diabetes. Until today, there is also no convincing data about the GPx-4 protein abundance or the GPx-4 activity in the glomeruli of mice suffering from diabetes available. As already published by Tanja Wiedenmann (Wiedenmann, Dietrich et al. 2018) GPx-1 and GPx-4 protein abundance are significantly reduced in the glomeruli of people with T1D as well as in the glomeruli of people with T2D. We investigated, whether GPx-4 protein abundance is reduced to the same degree in our mouse model for T2D. If so, the *db/db* mice in combination with the systemic iron overload could be used to identify the underlying mechanism responsible for the progression of the disease.

In 24 weeks old *db/db* mice the amount of GPx-4 protein was significantly increased compared to their wildtype littermates (chapter 6.5.3). In all other groups the amount of GPx-4 protein abundance was not altered. Moreover, the area of the synaptopodin stained glomeruli was significantly increased in the *db/db* mice as well as in the *db/db/fpn*^{+/-} mice. To get a more exact comparable value, the values obtained from the GPx-4 staining were normalized with the area of synaptopodin stained glomeruli. Neither leptin signaling, nor excess iron changed the amount of GPx-4 protein in 24 weeks old mice compared to their wild-type littermates. The action of both excess iron and leptin signalling significantly reduced the amount of GPx-4 protein. To conclude, the increase in the amount of GPx-4 protein in *db/db* mice was mainly due to the increased size of the glomeruli, as quantified normalized data showed no difference. The amount of GPx-4 protein abundance was even further

decreased after normalization which substantiates that this effect is not due to the increased size of the glomeruli.

In 32-42 weeks old db/db mice as well as in db/db/*fpn*^{+/-} mice the amount of GPx-4 protein was slightly decreased compared to their wild-type littermates. Furthermore, the area of the synaptopodin stained glomeruli was slightly increased in the db/db mice as well as in the db/db/*fpn*^{+/-} mice. Excess iron did not change the amount of GPx-4 protein in this aged group of mice comparing normalized GPx-4 values, whereas the amount of GPx-4 protein was slightly decreased in the db/db mice. In contrast, the amount of GPx-4 protein abundance was significantly reduced in the db/db/*fpn*^{+/-} mice. To conclude, the action of both excess iron and leptin signalling is needed to reduce the amount of GPx-4 protein abundance. One can speculate that this effect is more pronounced in the BKS db/db mouse strain, as hyperglycemia is only transient in B6 db/db mice. As already discussed hyperglycemia is a potential candidate that triggers the feedback loop described above.

GPx-1 knockout mice have no severe phenotype, whereas GPx-4 knockout mice do not survive more than two weeks. This shows us that other redox enzymes such as other GPx isoforms or catalases can compensate for the loss of GPx-1 but not the loss of GPx-4 (Yang, SriRamaratnam et al. 2014). In the mammalian system there seems to be no effective redundant mechanism available (Brigelius-Flohe and Maiorino 2013).

In order to prove that leptin signalling via the short leptin receptor splice variants Ob-Ra or Ob-Rc, rather than the absence of leptin signalling via the long leptin receptor splice variant Ob-Rb is responsible for the downregulation of GPx-4 protein abundance in the db/db mice, we used the leptin deficient ob/ob mice. Thus, we quantified the amount of GPx-4 protein in the synaptopodin positive stained glomeruli of the respective mice. The amount of GPx-4 protein was not changed compared to their wild-type littermates. In contrast, the area of the synaptopodin stained glomeruli was significantly increased in ob/ob mice compared to their wildtype littermates. The amount of GPx-4 protein was not changed in ob/ob mice compared to their wildtype littermates using normalized GPx-4 values. To conclude, leptin-deficiency does not change the amount of GPx-4 protein abundance in the glomeruli of these mice.

As the difference between db/db mice and ob/ob mice emerges from the impaired leptin signalling, we conclude that this is detrimental for the progression of diabetic kidney disease. We could show that leptin signalling via the short splice variants of the leptin receptor leads to a downregulation of GPx-4 protein abundance in the glomeruli. This substantiate the hypothesis that there is no problem with ROS production but rather with ROS detoxification (Chew, Yuen et al. 2010).

7.6. Outlook

7.6.1. *In vivo* activation of the feedback loop

Glutathione depletion is associated with different neurodegenerative diseases such as Alzheimer's disease, Parkinson's disease and Huntington's disease (Bertrand 2017). A decrease in GSH levels was also observed in patients with T1D (Martín-Gallán, Carrascosa et al. 2003). The reason, why GSH levels are decreased in these patients is not known. One reason could be that GSH depletion inhibits the apoptotic program (Cao and Dixon 2016). Furthermore, it was suggested that increased TGF- β 1 is responsible for GSH depletion in fibrotic diseases such as cystic fibrosis, chronic obstructive pulmonary diseases, acute respiratory distress syndrome and chronic liver diseases (Liu and Desai 2015). Moreover, it was shown that despite the direct impact of TGF- β 1 signalling, an additional dysregulation of glutathione synthesis might be the reason for a low glutathione pool (Cao and Dixon 2016).

Moreover, lysosomes contain a quite large labile iron pool, as they are involved in iron import, iron storage and iron recycling (Doll and Conrad 2017). Followed by a significant reduction of the amount of GPx-4 protein, an accumulation of lipid peroxides might have an impact on the permeability of the lysosomal membranes releasing iron into the cytoplasm. This might result in a significant depletion of the glutathione pool, as Fenton reaction occurs more often. Preliminary results generated in cooperation with Prof. Bernhard Spengler (Justus-Liebig-University Gießen, Institute of Anorganic and Analytic Chemistry) showed that the PE lysoform 18:0 accumulates in TGF- β 1 and iron treated E11 podocytes cultured in high-glucose medium or in RSL-3 treated E11 podocytes similar to the experiments performed in chapter 3.6.2.4. The amount of the PE lysoform was defined by the ratio of lyso PE (18:00) to PE (38:4) and lyso PE (18:00) to PE (40:6). These results are in line with published data showing an accumulation of these lysophospholipids after peroxidation of PUFAs (Else and Kraffe 2015). Further experiments are needed to reliably quantify these lysoforms. Surprisingly, only one research group connected the accumulation of these lysoforms to a loss of GPx-4 protein (Toppo, Flohe et al. 2009) and no research group connected these results to ferroptotic cell death. In a next step, the amount of PC, PE and cardiolipin lysoforms will be analyzed in tissue of db/db mice, *fpn*^{+/-} mice and in tissue of db/db/*fpn*^{+/-} mice. According to our hypothesis these lysoforms should accumulate in our mouse models mimicking diabetic nephropathy of T2D.

7.6.2 Quantification of TGF- β 1 in mouse models of T2D

TGF- β plays a key function in diabetic nephropathy (Lee, Guh et al. 2004). Endothelial cells respond to leptin via an increase/release of activated TGF- β 1 (Chapter 6.3.1 and 6.3.3). Moreover, podocytes respond to TGF- β 1 with a subsequent downregulation of the amount of GPx-4 protein abundance (Chapter 6.3.2). Next, our *in vitro* data needs to be confirmed *ex vivo*. It was already published that db/db mice contain more glomerular TGF- β 1 (Sharma, McCue et al. 2003). As already discussed the amount of active TGF- β 1 should be increased in the db/db mice and even further increased db/db/*fpn*^{+/-} mice. TGF- β 1 not only has a direct effect on the amount of GPx-4 protein abundance. It also has a direct effect on the composition of the GBM, as it stimulates the α 3 chain of type IV collagen, whereas it inhibits the level of the α 5 chain. The GBM consists in large parts of type IV collagen (Chen, Kasama et al. 2004). In contrast, it was published that TGF- β 1 activates hepcidin mRNA expression in hepatocytes (Chen, Feng et al. 2016). This is contradictory to our hypothesis as hepcidin levels were found to be significantly reduced in patients suffering from diabetes (Altamura, Kopf et al. 2017). Moreover, it was published that TGF- β 1 is a key factor regulating fibrosis. In addition, it is debated whether TGF- β 1 is able to induce epithelial to mesenchymal transition (EMT) (Loeffler and Wolf 2015) or endothelial to mesenchymal transition (endoMT) in the kidney (Zeisberg, Potenta et al. 2008).

The mechanism by which TGF- β 1 reduces GPx-4 protein abundance is not known. TGF- β 1 binding to the podocytes might lead to Smad 2/3 phosphorylation (Miyazono 2009, Liu and Desai 2015). This could then activate the proteasome resulting in an increased degradation of the protein GPx-4. Inactivation or a reduction of GPx-4 protein seems to be enough to induce ferroptosis (Gao, Monian et al. 2016).

7.6.3 Obesity and overfeeding might drive the pathophysiological changes in the kidney

As already discussed in chapter 7.4 leptin signaling in peripheral tissue might be the reason for the paracrine TGF- β 1 signaling causing the reduction of GPx-4 protein abundance in the podocytes resulting in the programmed cell death termed ferroptosis. Besides leptin signaling in peripheral tissue such as the kidney, excess free iron is needed to drive the pathophysiological changes in the kidney contributing to an early podocyte loss. Increased signaling via mammalian target of rapamycin (mTOR) caused by excess nutrients is

suspected to be the reason for increased phosphorylation of Akt resulting in the downregulation of hepcidin expression in the liver. Thus, constantly active ferroportin implements a systemic iron overload leading to an iron accumulation in the podocytes. One of the key characteristics of an obese phenotype during the progression of the metabolic syndrome is the development of insulin resistance. Interestingly, insulin binding to the insulin receptor activates PDK1, which phosphorylates Akt (Dupont and Scaramuzzi 2016). Moreover, mTOR plays a key role in insulin signaling (Hale and Coward 2013). Furthermore, hyperglycemic conditions are needed in order to activate the feedback loop. Podocytes are able to sense and respond to increased insulin levels as they contain glucose transporter 1 and 4, which contribute to insulin-induced glucose uptake (Coward, Welsh et al. 2005). In addition, overall glucose concentration and mechanical stress can modulate glucose transport into the podocytes sensitizing them to hyperglycemic conditions (Lewko, Bryl et al. 2005).

8.1. References

- Adya, R., et al. (2015). "Differential effects of leptin and adiponectin in endothelial angiogenesis." J Diabetes Res **2015**: 648239.
- Alberti, K. G. and P. Z. Zimmet (1998). "Definition, diagnosis and classification of diabetes mellitus and its complications. Part 1: diagnosis and classification of diabetes mellitus provisional report of a WHO consultation." Diabet Med **15**(7): 539-553.
- Altamura, S., et al. (2014). "Resistance of ferroportin to hepcidin binding causes exocrine pancreatic failure and fatal iron overload." Cell Metab **20**(2): 359-367.
- Altamura, S., et al. (2017). "Uncoupled iron homeostasis in type 2 diabetes mellitus." J Mol Med (Berl) **95**(12): 1387-1398.
- Arosio, P. and S. Levi (2010). "Cytosolic and mitochondrial ferritins in the regulation of cellular iron homeostasis and oxidative damage." Biochim Biophys Acta **1800**(8): 783-792.
- Ballermann, B. J. (2007). "Contribution of the endothelium to the glomerular permselectivity barrier in health and disease." Nephron Physiol **106**(2): p19-25.
- Barisoni, L., et al. (2000). "Podocyte cell cycle regulation and proliferation in collapsing glomerulopathies." Kidney Int **58**(1): 137-143.
- Bertrand, R. L. (2017). "Iron accumulation, glutathione depletion, and lipid peroxidation must occur simultaneously during ferroptosis and are mutually amplifying events." Med Hypotheses **101**: 69-74.
- Bogdan, A. R., et al. (2016). "Regulators of Iron Homeostasis: New Players in Metabolism, Cell Death, and Disease." Trends Biochem Sci **41**(3): 274-286.
- Breyer, M. D., et al. (2005). "Mouse models of diabetic nephropathy." J Am Soc Nephrol **16**(1): 27-45.
- Brieger, K., et al. (2012). "Reactive oxygen species: from health to disease." Swiss Med Wkly **142**: w13659.
- Brigelius-Flohe, R. and M. Maiorino (2013). "Glutathione peroxidases." Biochim Biophys Acta **1830**(5): 3289-3303.
- Brosius, F. C., 3rd, et al. (2009). "Mouse models of diabetic nephropathy." J Am Soc Nephrol **20**(12): 2503-2512.
- Browne, R. W. and D. Armstrong (2000). "HPLC analysis of lipid-derived polyunsaturated fatty acid peroxidation products in oxidatively modified human plasma." Clin Chem **46**(6 Pt 1): 829-836.

Brownlee, M. (2001). "Biochemistry and molecular cell biology of diabetic complications." Nature **414**(6865): 813-820.

Brownlee, M. (2005). "The pathobiology of diabetic complications: a unifying mechanism." Diabetes **54**(6): 1615-1625.

Burk, R. F., et al. (2011). "Glutathione peroxidase-3 produced by the kidney binds to a population of basement membranes in the gastrointestinal tract and in other tissues." **301**(1): G32-G38.

Cai, Z. and L. J. Yan (2013). "Protein Oxidative Modifications: Beneficial Roles in Disease and Health." J Biochem Pharmacol Res **1**(1): 15-26.

Cao, J. Y. and S. J. Dixon (2016). "Mechanisms of ferroptosis." Cell Mol Life Sci **73**(11-12): 2195-2209.

Cattaruzza, M. and M. Hecker (2008). "Protein carbonylation and decarboxylation: a new twist to the complex response of vascular cells to oxidative stress." Circ Res **102**(3): 273-274.

Chen, H., et al. (1996). "Evidence that the diabetes gene encodes the leptin receptor: identification of a mutation in the leptin receptor gene in db/db mice." Cell **84**(3): 491-495.

Chen, S., et al. (2016). "Transforming Growth Factor beta1 (TGF-beta1) Activates Hepcidin mRNA Expression in Hepatocytes." J Biol Chem **291**(25): 13160-13174.

Chen, S., et al. (2004). "Podocyte-derived vascular endothelial growth factor mediates the stimulation of alpha3(IV) collagen production by transforming growth factor-beta1 in mouse podocytes." Diabetes **53**(11): 2939-2949.

Chew, P., et al. (2010). "Antiatherosclerotic and renoprotective effects of ebselen in the diabetic apolipoprotein E/GPx1-double knockout mouse." Diabetes **59**(12): 3198-3207.

Conrad, M. and J. P. Friedmann Angeli (2015). "Glutathione peroxidase 4 (Gpx4) and ferroptosis: what's so special about it?" Mol Cell Oncol **2**(3): e995047.

Cooper, M. E., et al. (2018). "Metabolic Karma-The Atherogenic Legacy of Diabetes: The 2017 Edwin Bierman Award Lecture." Diabetes **67**(5): 785-790.

Coward, R. J., et al. (2005). "The human glomerular podocyte is a novel target for insulin action." Diabetes **54**(11): 3095-3102.

Cozza, G., et al. (2017). "Glutathione peroxidase 4-catalyzed reduction of lipid hydroperoxides in membranes: The polar head of membrane phospholipids binds the enzyme and addresses the fatty acid hydroperoxide group toward the redox center." Free Radic Biol Med **112**: 1-11.

Creighton Mitchell, T. and D. A. McClain (2014). "Diabetes and hemochromatosis." Curr Diab Rep **14**(5): 488.

Dam, J., et al. (2015). Leptin Receptors and Mechanism of Action. Leptin: 15-24.

De Matteis, R., et al. (2007). "Localization of leptin receptor splice variants in mouse peripheral tissues by immunohistochemistry." Proceedings of the Nutrition Society **57**(3): 441-448.

de Mello, N. P., et al. (2019). "Insulin and Autophagy in Neurodegeneration." Front Neurosci **13**: 491.

Deen, W. M., et al. (2001). "Structural determinants of glomerular permeability." Am J Physiol Renal Physiol **281**(4): F579-596.

Dintsios, C. M., et al. (2018). "Quantified patient preferences for lifestyle intervention programs for diabetes prevention-a protocol for a systematic review." Syst Rev **7**(1): 214.

Disse, E., et al. (2014). "Greater Weight Loss with the Omega Loop Bypass Compared to the Roux-en-Y Gastric Bypass: a Comparative Study." **24**(6): 841-846.

Dixon, S. J. and B. R. Stockwell (2014). "The role of iron and reactive oxygen species in cell death." Nat Chem Biol **10**(1): 9-17.

Doll, S. and M. Conrad (2017). "Iron and ferroptosis: A still ill-defined liaison." IUBMB Life **69**(6): 423-434.

Dupont, J. and R. J. Scaramuzzi (2016). "Insulin signalling and glucose transport in the ovary and ovarian function during the ovarian cycle." Biochem J **473**(11): 1483-1501.

Else, P. L. and E. Kraffe (2015). "Docosahexaenoic and arachidonic acid peroxidation: It's a within molecule cascade." Biochim Biophys Acta **1848**(2): 417-421.

Enculescu, M., et al. (2017). "Modelling Systemic Iron Regulation during Dietary Iron Overload and Acute Inflammation: Role of Hepcidin-Independent Mechanisms." PLoS Comput Biol **13**(1): e1005322.

Falkevall, A., et al. (2017). "Reducing VEGF-B Signaling Ameliorates Renal Lipotoxicity and Protects against Diabetic Kidney Disease." Cell Metab **25**(3): 713-726.

Fang, W., et al. (2010). "Functional and physical interaction between the selenium-binding protein 1 (SBP1) and the glutathione peroxidase 1 selenoprotein." Carcinogenesis **31**(8): 1360-1366.

Fanzani, A. and M. Poli (2017). "Iron, Oxidative Damage and Ferroptosis in Rhabdomyosarcoma." Int J Mol Sci **18**(8).

Fattman, C. L., et al. (2003). "Extracellular superoxide dismutase in biology and medicine." Free Radic Biol Med **35**(3): 236-256.

Fei, H., et al. (1997). "Anatomic localization of alternatively spliced leptin receptors (Ob-R) in mouse brain and other tissues." Proc Natl Acad Sci U S A **94**(13): 7001-7005.

Forbes, J. M. and M. E. Cooper (2013). "Mechanisms of diabetic complications." Physiol Rev **93**(1): 137-188.

Freedman, B. I., et al. (2007). "Genetic factors in diabetic nephropathy." Clin J Am Soc Nephrol **2**(6): 1306-1316.

Friedman, J. M. and J. L. Halaas (1998). "Leptin and the regulation of body weight in mammals." Nature **395**(6704): 763-770.

Friedmann Angeli, J. P., et al. (2014). "Inactivation of the ferroptosis regulator Gpx4 triggers acute renal failure in mice." Nat Cell Biol **16**(12): 1180-1191.

Furukawa, T., et al. (1991). "Morphometric study of glomerular slit diaphragms fixed by rapid-freezing and freeze-substitution." Kidney Int **40**(4): 621-624.

Gao, M., et al. (2016). "Ferroptosis is an autophagic cell death process." Cell Res **26**(9): 1021-1032.

Giacco, F. and M. Brownlee (2010). "Oxidative stress and diabetic complications." Circ Res **107**(9): 1058-1070.

Gill, P. S. and C. S. Wilcox (2006). "NADPH oxidases in the kidney." Antioxid Redox Signal **8**(9-10): 1597-1607.

Goto, K., et al. (2016). "Leptin deficiency down-regulates IL-23 production in glomerular podocytes resulting in an attenuated immune response in nephrotoxic serum nephritis." Int Immunol **28**(4): 197-208.

Haas, J. T. and B. Staels (2016). "An oxidative stress paradox: time for a conceptual change?" Diabetologia **59**(12): 2514-2517.

Hale, L. J. and R. J. Coward (2013). "The insulin receptor and the kidney." Curr Opin Nephrol Hypertens **22**(1): 100-106.

Han, D. C., et al. (2001). "Leptin stimulates type I collagen production in db/db mesangial cells: glucose uptake and TGF-beta type II receptor expression." Kidney Int **59**(4): 1315-1323.

Handa, P., et al. (2016). "Iron overload results in hepatic oxidative stress, immune cell activation, and hepatocellular ballooning injury, leading to nonalcoholic steatohepatitis in genetically obese mice." Am J Physiol Gastrointest Liver Physiol **310**(2): G117-127.

Haraldsson, B. and J. Nystrom (2012). "The glomerular endothelium: new insights on function and structure." Curr Opin Nephrol Hypertens **21**(3): 258-263.

Haraldsson, B., et al. (2008). "Properties of the glomerular barrier and mechanisms of proteinuria." Physiol Rev **88**(2): 451-487.

Hoggard, N., et al. (1997). "Localization of leptin receptor mRNA splice variants in murine peripheral tissues by RT-PCR and in situ hybridization." Biochem Biophys Res Commun **232**(2): 383-387.

Honda, H., et al. (2002). "Leptin is required for fibrogenic responses induced by thioacetamide in the murine liver." Hepatology **36**(1): 12-21.

Huang, Y., et al. (2012). "Transforming growth factor-beta1 induces glutathione peroxidase-1 and protects from H₂O₂-induced cell death in colon cancer cells via the Smad2/ERK1/2/HIF-1alpha pathway." Int J Mol Med **29**(5): 906-912.

Jung, H., et al. (2016). "Rapid and efficient identification of the mouse leptin receptor mutation (C57BL/KsJ-db/db) by tetra-primer amplification refractory mutation system-polymerase chain reaction (ARMS-PCR) analysis." Lab Anim Res **32**(1): 70-73.

Kalapos, M. P. (2008). "The tandem of free radicals and methylglyoxal." Chem Biol Interact **171**(3): 251-271.

Kanwar, Y. S., et al. (2011). "A glimpse of various pathogenetic mechanisms of diabetic nephropathy." Annu Rev Pathol **6**: 395-423.

Kashihara, N., et al. (2010). "Oxidative stress in diabetic nephropathy." Curr Med Chem **17**(34): 4256-4269.

Katsuya, K., et al. (2006). "An improved method for primary culture of rat podocytes." Kidney Int **69**(11): 2101-2106.

Katunga, L. A., et al. (2015). "Obesity in a model of gpx4 haploinsufficiency uncovers a causal role for lipid-derived aldehydes in human metabolic disease and cardiomyopathy." Mol Metab **4**(6): 493-506.

Kemna, E. H., et al. (2008). "Hepcidin: from discovery to differential diagnosis." Haematologica **93**(1): 90-97.

Koster, I., et al. (2011). "Direct costs of diabetes mellitus in Germany - CoDiM 2000-2007." Exp Clin Endocrinol Diabetes **119**(6): 377-385.

Krttil, J., et al. (2007). "Culture methods of glomerular podocytes." Kidney Blood Press Res **30**(3): 162-174.

Latunde-Dada, G. O. (2017). "Ferroptosis: Role of lipid peroxidation, iron and ferritinophagy." Biochim Biophys Acta Gen Subj **1861**(8): 1893-1900.

Lee, C. I., et al. (2004). "Leptin and connective tissue growth factor in advanced glycation end-product-induced effects in NRK-49F cells." J Cell Biochem **93**(5): 940-950.

Lee, G. H., et al. (1996). "Abnormal splicing of the leptin receptor in diabetic mice." Nature **379**(6566): 632-635.

Lee, H. J., et al. (2015). "Effect of excess iron on oxidative stress and gluconeogenesis through hepcidin during mitochondrial dysfunction." J Nutr Biochem **26**(12): 1414-1423.

Lewko, B., et al. (2005). "Mechanical stress and glucose concentration modulate glucose transport in cultured rat podocytes." Nephrol Dial Transplant **20**(2): 306-311.

Li, Z., et al. (2013). "Phenotypic effects of an induced mutation of the ObRa isoform of the leptin receptor." Molecular Metabolism **2**(4): 364-375.

Li, Z., et al. (2013). "The role of leptin on the organization and expression of cytoskeleton elements in nucleus pulposus cells." J Orthop Res **31**(6): 847-857.

Liu, Q., et al. (2009). "Role of iron deficiency and overload in the pathogenesis of diabetes and diabetic complications." Curr Med Chem **16**(1): 113-129.

Liu, R. M. and L. P. Desai (2015). "Reciprocal regulation of TGF-beta and reactive oxygen species: A perverse cycle for fibrosis." Redox Biol **6**: 565-577.

Loeffler, I. and G. Wolf (2015). "Epithelial-to-Mesenchymal Transition in Diabetic Nephropathy: Fact or Fiction?" Cells **4**(4): 631-652.

Lubos, E., et al. (2011). "Glutathione peroxidase-1 in health and disease: from molecular mechanisms to therapeutic opportunities." Antioxid Redox Signal **15**(7): 1957-1997.

Maggard, M. A., et al. (2005). "Meta-analysis: surgical treatment of obesity." Ann Intern Med **142**(7): 547-559.

Makita, Z., et al. (1991). "Advanced glycosylation end products in patients with diabetic nephropathy." N Engl J Med **325**(12): 836-842.

Martín-Gallán, P., et al. (2003). "Biomarkers of diabetes-associated oxidative stress and antioxidant status in young diabetic patients with or without subclinical complications." Free Radical Biology and Medicine **34**(12): 1563-1574.

Mbanya, J. C., et al. (2017). "Recombinant Human Insulin in Global Diabetes Management - Focus on Clinical Efficacy." Eur Endocrinol **13**(1): 21-25.

Miyazono, K. (2009). "Transforming growth factor-beta signaling in epithelial-mesenchymal transition and progression of cancer." Proc Jpn Acad Ser B Phys Biol Sci **85**(8): 314-323.

Moller, I. M., et al. (2011). "Protein carbonylation and metal-catalyzed protein oxidation in a cellular perspective." J Proteomics **74**(11): 2228-2242.

Muckenthaler, M. U., et al. (2017). "A Red Carpet for Iron Metabolism." Cell **168**(3): 344-361.

Najafian, B., et al. (2011). "Pathology of human diabetic nephropathy." Contrib Nephrol **170**: 36-47.

Neves, J., et al. (2017). "Disruption of the Hecpudin/Ferroportin Regulatory System Causes Pulmonary Iron Overload and Restrictive Lung Disease." EBioMedicine **20**: 230-239.

Newsholme, P., et al. (2007). "Diabetes associated cell stress and dysfunction: role of mitochondrial and non-mitochondrial ROS production and activity." J Physiol **583**(Pt 1): 9-24.

Ni, L., et al. (2012). "Podocyte culture: tricks of the trade." Nephrology (Carlton) **17**(6): 525-531.

Nigro, C., et al. (2017). "Methylglyoxal-Glyoxalase 1 Balance: The Root of Vascular Damage." Int J Mol Sci **18**(1).

Pagtalunan, M. E., et al. (1997). "Podocyte loss and progressive glomerular injury in type II diabetes." J Clin Invest **99**(2): 342-348.

Pavenstadt, H., et al. (2003). "Cell biology of the glomerular podocyte." Physiol Rev **83**(1): 253-307.

Petermann, A. T., et al. (2003). "Podocytes that detach in experimental membranous nephropathy are viable." Kidney Int **64**(4): 1222-1231.

Peters, V., et al. (2017). "Allosteric inhibition of carnosinase (CN1) by inducing a conformational shift." J Enzyme Inhib Med Chem **32**(1): 1102-1110.

Poulianiti, K. P., et al. (2016). "Systemic Redox Imbalance in Chronic Kidney Disease: A Systematic Review." Oxid Med Cell Longev **2016**: 8598253.

Ray, P. D., et al. (2012). "Reactive oxygen species (ROS) homeostasis and redox regulation in cellular signaling." Cell Signal **24**(5): 981-990.

Reidy, K., et al. (2014). "Molecular mechanisms of diabetic kidney disease." J Clin Invest **124**(6): 2333-2340.

Riserus, U., et al. (2009). "Dietary fats and prevention of type 2 diabetes." Prog Lipid Res **48**(1): 44-51.

Risérus, U., et al. (2009). "Dietary fats and prevention of type 2 diabetes." Prog Lipid Res **48**(1): 44-51.

Ritz, E. (2006). "Diabetic nephropathy." Saudi J Kidney Dis Transpl **17**(4): 481-490.

Rops, A. L., et al. (2004). "Isolation and characterization of conditionally immortalized mouse glomerular endothelial cell lines." Kidney Int **66**(6): 2193-2201.

Roza, A. M., et al. (1994). "Hydroxyethyl starch deferoxamine, a novel iron chelator, delays diabetes in BB rats." J Lab Clin Med **123**(4): 556-560.

Saberzadeh-Ardestani, B., et al. (2018). "Type 1 Diabetes Mellitus: Cellular and Molecular Pathophysiology at A Glance." Cell J **20**(3): 294-301.

Sachdeva, R., et al. (2019). "Methylglyoxal evokes acute Ca(2+) transients in distinct cell types and increases agonist-evoked Ca(2+) entry in endothelial cells via CRAC channels." Cell Calcium **78**: 66-75.

Schiffer, M., et al. (2001). "Apoptosis in podocytes induced by TGF-beta and Smad7." J Clin Invest **108**(6): 807-816.

Schiffer, M., et al. (2005). "Localization of the GLUT8 glucose transporter in murine kidney and regulation in vivo in nondiabetic and diabetic conditions." Am J Physiol Renal Physiol **289**(1): F186-193.

Scott, R. P. and S. E. Quaggin (2015). "Review series: The cell biology of renal filtration." J Cell Biol **209**(2): 199-210.

Shah, R., et al. (2018). "Resolving the Role of Lipoxygenases in the Initiation and Execution of Ferroptosis." ACS Cent Sci **4**(3): 387-396.

Shankland, S. J., et al. (2007). "Podocytes in culture: past, present, and future." Kidney Int **72**(1): 26-36.

Sharma, K., et al. (2003). "Diabetic kidney disease in the db/db mouse." Am J Physiol Renal Physiol **284**(6): F1138-1144.

Sjostrom, L., et al. (2004). "Lifestyle, diabetes, and cardiovascular risk factors 10 years after bariatric surgery." N Engl J Med **351**(26): 2683-2693.

Song, J., et al. (2014). "Unglycosylated recombinant human glutathione peroxidase 3 mutant from Escherichia coli is active as a monomer." Sci Rep **4**: 6698.

Steinbicker, A. U. and M. U. Muckenthaler (2013). "Out of balance--systemic iron homeostasis in iron-related disorders." Nutrients **5**(8): 3034-3061.

Susztak, K., et al. (2006). "Glucose-induced reactive oxygen species cause apoptosis of podocytes and podocyte depletion at the onset of diabetic nephropathy." Diabetes **55**(1): 225-233.

Swaminathan, S., et al. (2007). "The role of iron in diabetes and its complications." Diabetes Care **30**(7): 1926-1933.

Takebe, G., et al. (2002). "A comparative study on the hydroperoxide and thiol specificity of the glutathione peroxidase family and selenoprotein P." J Biol Chem **277**(43): 41254-41258.

Tang, X., et al. (2014). "Mitochondria, endothelial cell function, and vascular diseases." Front Physiol **5**: 175.

Tavafi, M. (2013). "Diabetic nephropathy and antioxidants." J Nephropathol **2**(1): 20-27.

Thallas-Bonke, V., et al. (2015). "Nox-4 and progressive kidney disease." Curr Opin Nephrol Hypertens **24**(1): 74-80.

Thallas-Bonke, V., et al. (2008). "Inhibition of NADPH oxidase prevents advanced glycation end product-mediated damage in diabetic nephropathy through a protein kinase C- α -dependent pathway." Diabetes **57**(2): 460-469.

Toppo, S., et al. (2009). "Catalytic mechanisms and specificities of glutathione peroxidases: variations of a basic scheme." Biochim Biophys Acta **1790**(11): 1486-1500.

Travis, M. A. and D. Sheppard (2014). "TGF- β Activation and Function in Immunity." **32**(1): 51-82.

UK Prospective Diabetes Study Group (1998). "Tight blood pressure control and risk of macrovascular and microvascular complications in type 2 diabetes: UKPDS 38. ." Bmj **317**(7160): 703-713.

Ursini, F., et al. (1985). "The selenoenzyme phospholipid hydroperoxide glutathione peroxidase." Biochim Biophys Acta **839**(1): 62-70.

Vallon, V. and R. Komers (2011). "Pathophysiology of the diabetic kidney." Compr Physiol **1**(3): 1175-1232.

Vogelmann, S. U., et al. (2003). "Urinary excretion of viable podocytes in health and renal disease." Am J Physiol Renal Physiol **285**(1): F40-48.

Wagner, A. H., et al. (2009). "Upregulation of glutathione peroxidase offsets stretch-induced proatherogenic gene expression in human endothelial cells." Arterioscler Thromb Vasc Biol **29**(11): 1894-1901.

Wiedenmann, T., et al. (2018). "Modulation of glutathione peroxidase activity by age-dependent carbonylation in glomeruli of diabetic mice." J Diabetes Complications **32**(2): 130-138.

Wolf, G. (2004). "New insights into the pathophysiology of diabetic nephropathy: from haemodynamics to molecular pathology." Eur J Clin Invest **34**(12): 785-796.

Wolf, G., et al. (2002). "Leptin and renal disease." Am J Kidney Dis **39**(1): 1-11.

Yang, W. S., et al. (2014). "Regulation of ferroptotic cancer cell death by GPX4." Cell **156**(1-2): 317-331.

Zeisberg, E. M., et al. (2008). "Fibroblasts in kidney fibrosis emerge via endothelial-to-mesenchymal transition." J Am Soc Nephrol **19**(12): 2282-2287.

Zhang, G., et al. (2018). "The Warburg Effect in Diabetic Kidney Disease." Semin Nephrol **38**(2): 111-120.

Zhao, Y., et al. (2014). "Isolation and epithelial co-culture of mouse renal peritubular endothelial cells." BMC Cell Biol **15**: 40.

Additional sources:

Rossing, Peter. Clinical pathology of nephropathy [internet]. 2015 Sep 23; Diapedia 71040851172 rev. no. 10. Available from: <https://doi.org/10.14496/dia.71040851172.10> (abgerufen am 6.05.2017)

wbanimalhospital.com/wp-content/uploads/2014/05/Kidney3.jpg (abgerufen am 28.02.2016)

Acknowledgments

At first, I would like to thank Prof. Markus Hecker for the opportunity to write my Ph.D. thesis under his supervision and especially for reviewing my thesis. I would like to thank PD Dr. Andreas Wagner for supporting me all the way through the end, especially at difficult times during the project. I appreciated that I could take his time and talk to him anytime I needed help or when I had the feeling to discuss some important issues. He offered me such interesting topics of investigation and gave me the freedom to establish, develop, shape and finalize the project. I would also like to thank Prof. Marc Freichel for the input and the discussions at my TAC meetings and for reviewing my thesis. Special thanks to our cooperation partner Prof. Martina Muckenthaler and Dr. Sandro Altamura for the supply of kidneys from various mouse strains and for the help to stain iron in the respective kidney slides. In addition, I like to thank Prof. Martina Muckenthaler, supporting me with helpful questions at my TAC meetings and for being part of the thesis defense committee. I like to thank our cooperation partner Prof. Fulvio Ursini for analyzing GPx-4 specific activity in our samples and our cooperation partner Prof. Bernhard Spengler for quantifying phospholipid lysoforms in our samples. I like to thank Dr. Thomas Fleming and Prof. Viola Nordström for the input of ideas shaping important parts of my working hypothesis. Of course, I like to thank Prof. Hans-Peter Hammes and Prof. Jens Kroll for the organization of the first and the second round of GRK1874, including the various spring and autumn schools. I also like to thank the DDG (Deutsche Diabetes Gesellschaft) for the funding of consumables subsequent to the funding of the GRK1874/2.

I like to thank Franziska Mohr and Lena Schwenker for the help, especially during the final phase of my Ph.D. All the stainings and the quantification of the stainings would not have been possible without the continuous help and the reliable work of Franziska Mohr and Lena Schwenker. Apart from that I would like to thank the colleges and former colleges in the lab Dr. Sebastian Lont, Prisca Friede, Nadine Heselmaier, Yvonne Feuchter, Dr. Eda Demirel, Dr. Anja and at HIBIGS Dr. Alexa Lauer who supported me with technical and theoretical knowledge, helpful discussions and who finally became friends.

In particular, I would like to thank my family for supporting and motivating me the whole time of my Ph.D. thesis. Special thanks to my lovely girlfriend Rebecca Hoffmann who always encouraged me to give my best and to stay focused on my thesis.